PGE mineralization at the Allard stock: Implications for the porphyry to epithermal transition, La Plata Mountains, Colorado.

by

Erin Sloane Summerlin

A thesis submitted to the Graduate Faculty of
Auburn University
in partial fulfillment of the
requirements for the Degree of
Master of Science

Auburn, Alabama
May 4th, 2014

Keywords: Porphyry, PGE-Copper, Alkaline,
Colorado, Tellurides

Approved by

James A. Saunders, Chair, Professor of Geology and Geography
Willis E. Hames, Professor of Geology and Geography
Haibo Zou, Associate Professor of Geology and Geography

Abstract

Geochemical and petrographic studies on the Allard stock, which hosts a porphyry Cu-Ag-Au-Te-PGE deposit in the La Plata Mountains of southwestern Colorado, suggest mantle sources for both metals and sulfur. Microprobe analysis of ores verifies the PGE host mineral phase(s) as Pd±Pt±Bi-tellurides and Ag±Pd tellurides, and a possible previously unidentified mineral with a suggested formula of $PdTe_2$. The La Plata mining district, named after the laccolithic La Plata mountains, lies ~20 km northwest of Durango, Colorado, at the southwestern-most part of the Colorado Mineral Belt. Intrusion of Cretaceous laccolithic diorite-monzonite porphyries from igneous activity that propagated inward from the flat-slab subuction of the Farallon plate during the Laramide Orogeny (70-80 Ma) caused domal uplift of strata and contact metamorphosed the surrounding country rocks. Younger alkaline stocks appear to have initiated the ore-forming processes in the district by providing fluids and reopening existing faults. One of these alkaline porphyry stocks, The Allard stock (~67 Ma), hosts both massive, stockwork, and disseminated chalcopyrite and pyrite, Ag-Au tellurides, and PGEs.

Sulfur isotope values for the Allard stock range from -7.8 to +1‰ $\delta^{34}S_{(VCDT)}$, indicating a magmatic source with a minor ^{32}S-enriched component of contamination apparently derived from the country rocks. Copper isotope values range from +0.965 to +2.700‰ $\delta^{65}Cu$, within the range for typical porphyry coppers. Lead isotope data suggests a mantle source for lead from sulfides in the stock mineralization. Due to the ~1

km of topographic relief, the transition between porphyry and epithermal styles of mineralization is well exposed and amenable to sampling in the La Plata district. Mineralization in the district includes porphyry mineralization (the Allard stock) as well as contact-metamorphic Au-bearing sulfides, limestone replacement (skarn) with sulfides and tellurides, Au-bearing pyrite, mixed sulfides with free Au, chalcocite veins, ruby silver veins, and Au-Ag-telluride deposits. Because of their close spatial association, hydrothermal fluids that mineralized the Allard stock porphyry are likely coeval or analogous to fluids that mineralized the Au-Ag-tellurides in the epithermal deposits and perhaps even the skarn deposits. Geochemically, the porphyry and epithermal ores in the La Plata district are extremely similar (Au, Ag, Te). Therefore the migration of fluids from the mantle source, to the porphyry regime, and finally to the epithermal environment seems a likely model for ore deposition in the La Plata district.

Acknowledgments

I am greatly appreciative to the wonderful family, friends, and colleagues that have loved and supported me throughout the completion of my MS degree. Michael Mason, my office mate and fellow student of Dr. Saunders, carried many heavy rocks, double checked my math, and was an Excel formula master, to him I am very grateful. My advisor, Dr. Saunders, was unbelievably patient and encouraging during the entirety of my MS project, and even before I chose to come to Auburn. Without his wealth of knowledge and guidance, this thesis would not have been possible. I would also like to thank the National Science Foundation who funded Dr. Saunder's grant, NSF grant #1004381370012000, which in turn provided me with graduate research assistant funding for my second year at Auburn and helped to fund some of my fieldwork and travel expenses for sulfur and microprobe analyses. I am also very thankful to the Society of Economic Geologists, the Southeastern Section of the Geological Society of America, and the Colorado Scientific Society for finding my grant proposals worthy enough to fund. Thank you also to Dr. Willis E. Hames, Dr. Haibo Zou, and Dr. Robert B. Cook for providing editing and advice.

Table of Contents

List of Tables

List of Figures

List of Abbreviations

AT	Allard Tunnel
BSE	Backscatter Electron
CH	Copper Hill Glory Hole
COMB	Colorado Mineral Belt
EDS	Energy-dispersive X-ray Spectroscopy
ICP-MS	Inductively Coupled Plasma Mass Spectrometry
LMI	Layered Mafic Intrusion
PGE	Platinum Group Element

1. INTRODUCTION

Two important and distinct classes of hydrothermal metallic ores are often found in close proximity to one another other: (1) Typical porphyry ore deposits are adjacent to or hosted by an igneous intrusion, form between <600 – 300° C at between 2-5 km below the surface, and contain metals such as copper (Cu), molybdenum (Mo), gold (Au), and tungsten (W) or tin (Sn). Certain classes of porphyries may also anomalously include silver (Ag), tellurium (Te), and platinum group elements (PGEs), and (2) Epithermal ore deposits, which fall into two main classes: high sulfidation and low sulfidation systems. The epithermal environment is above or more distal to intrusive bodies, is near surface (>1.5 km) and cooler (<300° C), and typically contains Au-Cu- lead (Pb), and zinc (Zn). Epithermal deposit types are classified by proximity to the intrusion (high sulfidation is more proximal) and by mineral assemblage (Hedenquist and Lowenstern, 1994). Both porphyry and epithermal ore deposit types occur in the La Plata Mountains of southwestern Colorado (Fig. 1).

Understanding the probable genetic connection between ore-forming processes in both setting types is an area of current research called the "porphyry to epithermal transition." Discerning the source(s) of fluids, metals, ligands, and other constituents that interplay to create these ore deposits is crucial for constructing genetic models for ore-forming processes. PGEs include the six transition metals ruthenium (Ru), rhodium (Rh),

palladium (Pd), osmium (Os), iridium (Ir), and platinum (Pt). These economically valuable elements are primarily used for their catalytical properties, mainly in catalytic converters in the transportation industry. Due to their economic importance and their anomalous occurrence, understanding PGE mineralization in the Allard Stock is one focus of this study.

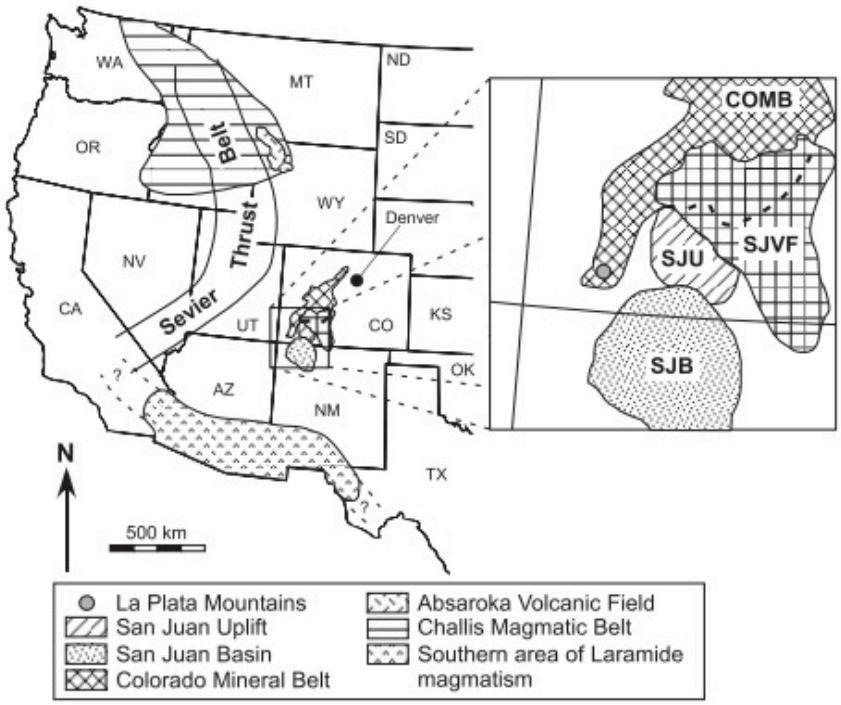

Fig. 1. Location map of the La Plata Mountains in Southwestern Colorado, USA in association with the southern extent of the Colorado Mineral Belt, (Wegert and Parker, 2011).

Discerning where ore-forming species originate, how they travel, and how they precipitate to make ores involves determination of their sources, source material, and the geochemical processes controlling transportation and ore phase formation. Porphyry deposits are high temperature (>700°C to <250°C), low-grade stockwork ores within

associated sub-volcanic porphyritic intrusive bodies and surrounding country rock. In contrast, epithermal deposits are shallow (<1 km deep) disseminated, stockwork, or vein deposits that were hydrothermally formed. Delineating the connection and transition between the two regimes is a necessity for fully characterizing ore deposits and formation on the "district" scale. Further, PGE occurrence in the Allard stock porphyry mineralization is both anomalous and perhaps economically significant because PGEs are typically associated with mafic igneous rocks, rather than alkaline (felsic) rocks.

PGE and Te deposits deemed economically viable typically occur in layered mafic intrusions (LMIs) and therefore originate via magmatism. Interestingly, along with tellurium, PGEs may also occur in a distinctly alkaline subclass of copper porphyry deposits. Famous LMI's include South Africa's Bushveld complex, USA's Stillwater complex and the Duluth Gabbro, Canada's Sudbury LMI, and Russia's Noril'sk LMI (Naldrett, 1999; Cabri, 2002; Arndt et al., 2005; Barnes and Lightfoot, 2005; and Cawthorn et al., 2005). In the U.S., mining for PGEs is planned for in the Duluth Gabbro (as byproducts of Cu-Ni ores) and are produced at the Stillwater Complex. Utah's Bingham copper mine may also begin production of PGEs as byproducts in the near future. Exploration for more "nontraditional" PGE sources will become more important as the traditional (LMI) sources are progressively mined out.

PGEs have a high value because of their uses in industry and due to their low crustal abundance, which is a function of their siderophile nature. Most chondritic meteorites contain ~100-600 ppb of PGEs, indicating that PGEs are likely enriched in the outer core rather than in Earth's crust (Anders and Grevesse, 1989). Although the US produces some PGEs currently, it imports roughly 75% of the PGE's used in domestic

industry. In light of this statistic, exploring alternative sources for PGE deposits has become of interest. Hydrothermal systems as conduits and sources for PGE deposits could provide alternative exploration targets for PGE-Te production. Te is used in the creation of Cd-Te films for photovoltaic solar cells and as an additive to steel, copper, and lead alloys. These hydrothermal systems are most commonly associated with hypabyssal alkaline porphyry intrusions, and associated ores are within a subclass of porphyry copper deposits and may be transitional to "subepithermal" (LeFort et al., 2011) and also epithermal ores (Saunders and May, 1986; Mutschler et al., 1997). Alkaline intrusions hosting these ores may have been enriched in PGE's via deeper and earlier magmatic processes affecting the area; however, PGEs are integrated into epigenetic hydrothermal sulfide minerals that originated at the same time as their emplacement and crystallization (Werle, 1983; Werle et al., 1984; Eliopoulos and Economou-Eliopoulos, 1991; Mutschler et al., 1997).

Porphyry deposits supply about 60% of the world's copper as well as significant amounts of silver and gold. In addition, Te, Se, Re are concentrated locally in some Cu deposits and these deposits will likely provide most of the world's Te, Se, and Re in the future. Recent research on porphyry Cu deposits has been extensive (Sillitoe, 2000, 2005, 2010; Richards 2003, 2009, 2011; John et al. 2010). Porphyry Cu deposits and systems consist of Cu-rich stocks or intrusions that are surrounded by large volumes of hydrothermally altered rock. Porphyry Cu deposits may include spatially associated deposits such as epithermal, skarn, carbonate replacement, and sediment hosted base and precious metal deposits (Sillitoe, 2010). The formation of porphyry Cu systems usually occurs in subduction-related environments and may be the result of the intrusions of calc-

alkaline or even alkaline magmas, as in the case of the Allard stock. Te, Se, Re, PGMs, Ag, As, W, U, and Zn are byproducts recovered from porphyry Cu deposits (Silitoe, 1983) and both Te and Pd±Pt are enriched in the Allard stock. In the La Plata district, bismuth minerals are quite abundant and occur within mineralization in porphyry, epithermal, and skarn-type deposits as Bi-tellurides. John and Taylor (2014, in press) comment on the Te connection between porphyry and epithermal environments by stating that "Many Au-rich epithermal deposits with significant Te concentrations may be post-porphyry ores, thus reflecting the late-stage events in an evolving porphyry-epithermal magmatic-hydrothermal system most consistently of an alkaline nature." The La Plata district hosts Au-Te epithermal mineralization in close spatial association with Cu-Ag-Au-Te-PGE porphyry mineralization and is therefore a prime location for investigating the porphyry to epithermal transition resulting from a single or coeval magmatic-hydrothermal system(s).

Geochemically, PGE's can be both calcophile and siderophile, and they can make relatively strong aqueous hydrosulfide and chloride complexes (Gammons and Bloom, 1993). Te should also have a strong affinity for dissolved H_2S (Saunders and May, 1986; Zhang and Spry, 1994) and combines with noble metals such as Au, Ag, and PGEs to form ore minerals of economic value. Investigating the porphyry-related hydrothermal occurrences of PGE and Te mineralization, as well as characterizing the porphyry to epithermal transition for ore deposits, could provide the data to develop models for new mineral resource occurrence and characterization in the US and worldwide. For example, the USGS is currently developing a model for "alkalic" noble metal deposits, like those in the proposed research area. Both porphyry and epithermal ore deposits are exposed in

the La Plata district due to the high (~ 1 km) topographic relief of the La Plata Mountains.

2. PREVIOUS WORK

History of the La Plata Mining District

Background information discussed below on the La Plata District (also previously named the California District) history, geology and ore deposits comes largely from the definitive published research on the area, USGS Professional Paper 219 by Edwin B. Eckel (1949). The La Plata Mountains lie in southwestern Colorado between the San Juan Mountains and the Colorado Plateau, roughly 12-32 km southwest of Durango, Colorado (Eckel, 1949). Mining in the 310 km^2 La Plata District began sometime in the 18^{th} century when Spanish explorers visited the La Plata Mountains. However, no documented record of mining in the area exists before 1861 when placer gold was found near Durango, Colorado along the Animus River. Mining in the district officially began in 1873 when placer gold was discovered along the La Plata River, which runs through the center of the district. Despite unrest with the Ute Indian tribes in the area, prospecting and mining continued to thrive well into the 1930s, and by 1900, more than 200-patented mining claims existed in the La Plata district, along with nine milling sites.

Production in the district from 1878-1937 is shown in Table 1. Production in the district prior to 1900 was comparatively small due to unsuccessful milling attempts and intermittent production efforts. Despite milling site difficulties, the remote location and rugged terrain, and character of deposits, the district took an upturn in both new discoveries and production after the early 1900s. Mining activity persisted until 1937,

due to the discovery and exploitations of a few small but high grade deposits (Neglected, Red Arrow, Gold King, Incas, and May Day/Idaho), which yielded more than two-thirds ($1,000,000) of the district's total production. Exploratory work continues in the district today, with the only known recently small-scale producing mines are Red Arrow and May Day/Idaho.

Geology of the La Plata District

The La Plata mountains lie at the southwestern end of the Colorado Mineral Belt (COMB) and have >1 km of topographic relief. The mountains, characterized by a domal structure, were created by the uplift of sedimentary rocks via the intrusion of numerous igneous stocks, dikes, and sills. The areal stratigraphy comprises Devonian through Upper Cretaceous strata, and beds dip away from central high areas. The central part of the mountains is nearly encircled by a steeply dipping horseshoe-shaped hinge fold (Fig. 2), however dips on both sides of the fold are relatively horizontal. Large displacement faults cut the outer part of the dome, and there are numerous faults and fractures within the main dome. Both porphyritic and nonporphyritic igneous rocks occur in the district, however they vary widely in both composition and form. Diorite-monzonite porphyry, the most common porphyry in the district, occurs as contemporaneous sills, stocks, and dikes that intruded into the overlying strata. Generally younger than the porphyry, the nonporphyritic rocks (syenite, monzonite, and diorite) occur as irregular stocks associated with many dikes.

Table 1: Historical Production in the La Plata District from Eckel, (1949.)

			Silver			Copper			Lead			
Year	Ore Treated (short tons)	Lode Gold	Fine Ounces	Average price per ounce ($)	Value ($)	Pounds	Average price per pound ($)	Value ($)	Pounds	Average price per pound ($)	Value ($)	Total Value ($)
1878	--	1000	1934	1.15	2224	--	--	--	--	--	--	3224
1879	--	2500	3867	1.12	4331	--	--	--	--	--	--	6831
1880	--	5000	7734	1.15	8894	--	--	--	--	--	--	13894
1881	--	5000	7734	1.13	8739	--	--	--	--	--	--	13739
1882	--	10000	23203	1.14	26541	--	--	--	--	--	--	36451
1883	--	13000	3867	1.11	4292	--	--	--	--	--	--	17292
1884	--	500	4641	1.11	5152	--	--	--	--	--	--	5652
1885	--	5000	5000	1.07	5350	--	--	--	--	--	--	10350
1886	--	10225	4671	0.99	4625	--	--	--	100000	0.046	4600	19449
1887	--	12473	7126	0.98	6983	--	--	--	42210	0.045	1899	21355
1888	--	3574	2294	0.94	2156	--	--	--	--	--	--	5730
1889	--	4465	1118	0.94	1051	--	--	--	--	--	--	5516
1890	--	3729	2011	1.05	2112	--	--	--	--	--	--	5841
1891	--	23054	3207	0.99	3175	--	--	--	--	--	--	26229
1892	--	34881	3335	0.87	2901	--	--	--	--	--	--	37782
1893	--	37872	4928	0.78	3844	--	--	--	--	--	--	41716
1894	--	114264	417465	0.63	263003	--	--	--	--	--	--	377267
1895	--	3682	99	0.65	64	--	--	--	--	--	--	3746
1896	--	10741	41	0.68	28	--	--	--	--	--	--	10769
1897	--	36944	1514	0.6	908	420	0.12	50	857	0.035	31	37933
1898	--	38653	5219	0.59	3079	2586	0.124	318	8407	0.038	319	42369
1899	--	41092	3389	0.6	2033	211	0.171	36	3176	0.045	143	43304
1900	--	24927	7187	0.62	4456	350	0.166	58	14500	0.044	683	30079
1901	--	30819	5588	0.6	3353	132	0.167	22	6197	0.043	266	34460
1902	--	127182	7416	0.53	3930	3143	0.122	383	2156	0.041	88	131583
1903	--	145331	7716	0.54	4167	810	0.137	111	3017	0.042	127	149736
1904	3792	130200	31086	0.58	18030	1473	0.128	189	2177	0.043	94	148513
1905	5662	254007	93258	0.61	56887	2923	0.156	456	610	0.047	29	311379
1906	7757	304633	121721	0.68	82770	445	0.193	86	2228	0.057	127	387616
1907	7812	413034	217579	0.66	143602	708	0.2	142	340	0.053	18	556796

Table 1 Continued: Historical Production in the La Plata District from Eckel, (1949.)

			Silver			Copper			Lead			
Year	Ore Treated (short tons)	Lode Gold	Fine Ounces	Average price per ounce ($)	Value ($)	Pounds	Average price per pound ($)	Value ($)	Pounds	Average price per pound ($)	Value ($)	Total Value ($)
1914	5083	126498	60244	0.553	33315	26038	0.133	3463	11410	0.039	445	163721
1915	2966	72024	46472	0.507	23561	4114	0.175	720	23532	0.047	1106	97411
1916	1688	33055	29380	0.658	19332	15142	0.246	3725	6667	0.069	460	56572
1917	1772	27952	15512	0.824	12782	28333	0.273	7735	3745	0.086	322	48791
1918	300	7378	6415	1	6415	668	0.247	165	3000	0.071	213	14171
1919	405	5966	6075	1.12	6804	167	0.186	31	2283	0.053	121	12922
1920	717	11020	10578	1.09	11530	--	--	--	937	0.08	75	22625
1921	1279	45181	20327	1	20327	--	--	--	3734	0.045	168	65676
1922	791	32261	10656	1	10656	--	--	--	--	--		42917
1923	838	15905	17138	0.82	14053	816	0.147	120	1800	0.07	126	30204
1924	1295	23502	11597	0.67	7770	488	0.13	64	387	0.08	32	31367
1925	905	24074	22831	0.694	15845	--	--	--	2000	0.087	174	40093
1926	119	6472	2681	0.624	1673	--	--	--	--	--		8145
1927	613	23103	8912	0.567	5053	--	--	--	--	--		28156
1928	8120	47433	24193	0.585	14153	97	0.144	14	63000	0.058	3654	65254
1929	19970	116511	83107	0.533	44296	--	--	--	71000	0.063	4473	65280
1930	272	8482	2969	0.385	1143	--	--	--	600	0.05	30	9655
1931	404	12752	2317	0.29	672	--	--	--	190	0.041	7	13431
1932	3041	30397	6968	0.282	1965	--	--	--	7000	0.03	210	32571
1933	7822	43958	14889	0.35	5211	200	0.064	13	9700	0.037	359	49541
1934	14430	116344	17523	0.646	11328	600	0.08	48	7900	0.037	292	128012
1935	11666	85876	17490	0.718	12571	--	--	--	23400	0.04	936	99383
1936	13331	97923	14465	0.774	11203	2000	0.092	186	13300	0.046	612	109922
1937	18161	143311	34242	0.773	26486	2000	0.121	242	257000	0.059	15163	185202
Total	--	4368792	2018947	--	1287328	283894	--	45590	715183	--		5641711

These nonporphyritic stocks pervasively metamorphosed the sedimentary strata within the center of the district. Sedimentary strata within the district, including sequence and description, are described in Table 2.

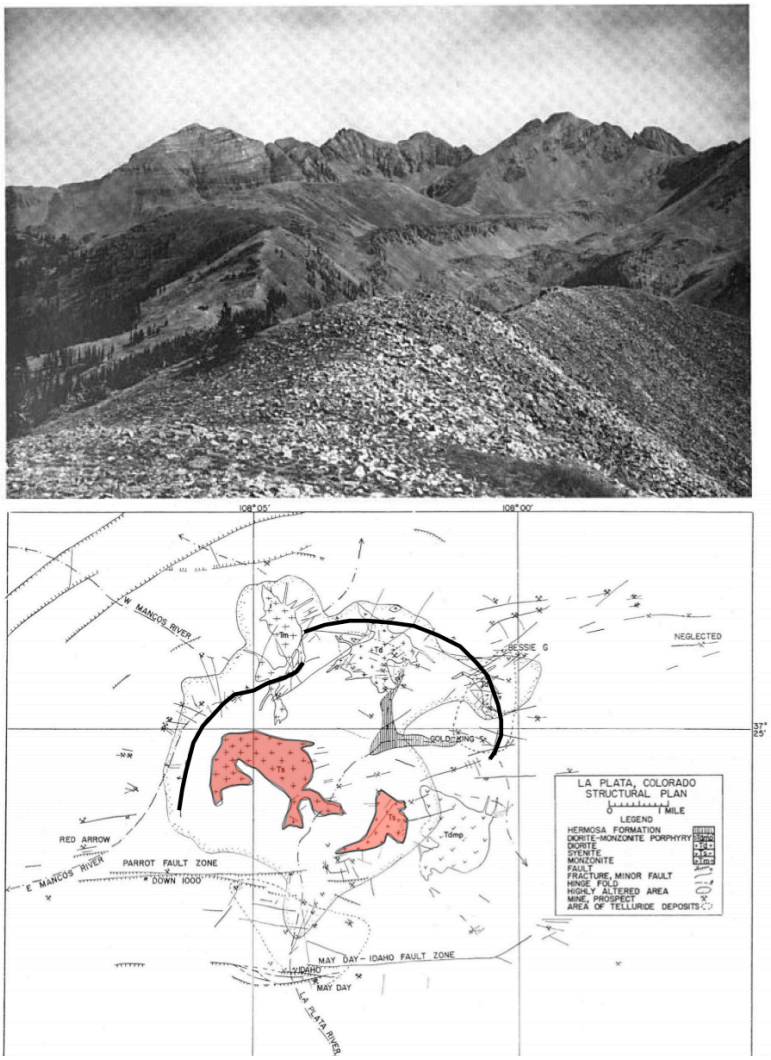

Fig. 2. Photograph (top) of a portion of the hinge fold creating the domal structure of the La Plata Mountains. From Eckel (1949) and a structure map (bottom) of the La Plata district, showing the hinge fold outlined in black and the Allard stock outlined in red, from Wisser (1960).

Table 2: Stratigraphy in the La Plata District

Age	Formation	Name in local use	Thickness (m)	Description
Upper Cretaceous	Mancos Shale	Mancos Shale	366	Soft dark-gray to black carbonaceous shale with thin lenses and concretions of impure limestone. Only the lower part is exposed within the La Plata district.
	Dakota Sandstone	Dakota Sandstone	30-46	Gray or brown sandstone with variable conglomerate at or near base. Carbonaceous shale partings and coal at several horizons. Forms cliffs. Should be favorable to ore, but little of it occurs in the mineralized area.
Upper Jurassic	Morrison Formation	McElmo Formation	122-190	Alternating friable fine-grained yellowish-brown to gray sandstones and variegated shales with one or more lenses of conglomerate near top. Largely altered to dense light-colored quartzite and hornfels in central part of district. Generally unfavorable to ore deposits.
	Junction Creek Sandstone	Upper La Plata Sandstone	49-152	Massive friable white sandstone, distinctly crossbedded. Altered to hard white to brown quartzite in central part on the district. Contains much ore in several places.
	Wanakah Formation	Middle La Plata Shale	8-38	Alternating pink to red sandy marls with lenses of friable white or light-colored sandstone. Similar to Morrison formation where metamorphosed. Generally unfavorable to ore deposits.
		La Plata Limestone	0-8	Medium-gray to black massive un-fossiliferous limestone. Locally replaced by pyrite or by telluride minerals. Largely altered to contact-metamorphic minerals in central part of district. Contains much ore in several places.
	Entrada Sandstone	Lower La Plata Sandstone	30-50	Similar to Junction Creek sandstone.
	Unconformity			
Jurassic and Upper Triassic	Dolores Formation	Dolores Formation "Red Beds"	152-229	Salmon-pink to bright-red mudstones and fine-grained mudstones. Several beds and lenses of limestone-shingle conglomerate and of light-gray slabby mudstone at or near base. Where metamorphosed it has same character as shale from Morrison formation. Limestone conglomerate beds altered to contact-metamorphic minerals in places. Generally unfavorable to ore deposits.
Permian	Cutler Formation	Cutler Formation "Red Beds"	457-671	Alternating dull-red arkosic sandstones, conglomerates, limy shales, and mudstones. Similar to Morrison where metamorphosed. Nodules of limestone, unaltered in places but elsewhere represented by garnet, epidote, etc. Favorable to ore deposits where rocks are silicified.
	Rico Formation	Rico Formation	30-91	Dull-red shale, sandstone, and thin beds of sandy fossiliferous limestones. Similar to Morrison where metamorphosed. Contains ore deposits in places.
Pennsylvanian	Hermosa Formation	Hermosa Formation	854±	Alternating green to gray and occasionally dull-red arkosic sandstone, shale, fossiliferous limestone, and gypsum. Only the upper 500 ft is exposed within the La Plata district. Favorability to ore deposits not known.
	Molas Formation		0-23 (?)	Red limy shale. May not be present beneath La Plata district.
	Unconformity			
Mississippian	Leadville Limestone		18 (?)	Fossiliferous massive to laminated limestone.
Upper Devonian	Ouray Limestone		23 (?)	Fossiliferous limestone, sandy limestone, and quartzite.
	Elbert Formation		0-40 (?)	Shale, Limestone, and sandstone.
	Unconformity			
Upper Cambrian	Ignacio Quartzite		15-30 (?)	Massive to thin-bedded quartzite, with some conglomerate at base.
	Unconformity			
Precambrian	(?)		(?)	Thought to be similar to basement rocks along the Animus River and in the Needle Mountains. Evidence points to granite and hornblendite, but volcanics, schists, and gneisses could also be present.

Table 2: Modified stratigraphy of the La Plata district, from Eckel (1949).

Precambrian basement rock is not exposed in the district, but its existence and character are inferred from outcrops in the nearby Needle Mountains. The intrusion of porphyritic bodies into the district is the main cause for the uplift of the La Plata dome, but the nonporphyritic stocks crosscut the stratigraphy and preexisting sills without disturbing them. Contacts between the stocks and enclosing sedimentary strata include are sharply defined, brecciated, or exhibit gradational contacts.

The La Plata dome is the most noticeable structure in the district and is roughly 24 km in diameter and it grades into the flank of the more regional San Juan uplift. The La Plata dome is asymmetrical due to its superimposition upon the 5° regional dip of the San Juan Mountains. The horseshoe-shaped hinge fold encircles the central part of the mountains and there are several large faults on the south, northern, and northwestern margins of the dome, initiated by the intrusion of the porphyries prior to metamorphism. Short, small displacement discontinuous faults, many of which trend east or radiate from the dome center, occurred during the doming event. With the emplacement of the nonporphyritic stocks, these older small faults were reopened and new similar faults were formed. These later faults are the location of many of the district's mineral deposits, as they provided convenient conduits for mineralizing fluids. The ore-bearing fractures tend to be concentrated along the hinge fold, where beds dip 25° to 60°, and where shearing and brecciation is most common.

Ore Deposits of the La Plata District

As mentioned earlier, most of the district's deposits are associated with faults. District faults are either "barren" or "ore-bearing." Generally, the barren faults are much

older and exhibit larger displacement, and are situated in the northwestern and southern margins of the dome. Ore-bearing faults tend to concentrate towards the center of the dome, although in general these fractures are widely distributed. The relationship of the minor ore-bearing or mineralized faults to the larger barren faults suggests that most of the smaller faults formed prior to the intrusion of the nonporphyritic rocks, and after the porphyry emplacement and faulting associated with the domal uplift. When renewed faulting occurred after the intrusion of the nonporphyritc stocks, due to the crustal readjustment at the end of igneous activity, reopened and new fractures became prime sites for ore-bearing solutions to precipitate ore.

Gold and silver constituted more than 98% of the district's metal production and the district is best known for its veins and replacement deposits of Au±Ag-bearing tellurides. The district also contains disseminated PGE-bearing chalcopyrite, gold with sulfides in contact-metamorphic deposits and Au-bearing pyrite in veins, replacement bodies, and breccia bodies, mixed sulfides with silver and free gold, chalcocite veins, ruby silver veins, and gold placers. The following section describes the ore deposits and mines focused on for this study.

Allard Tunnel (AT)

The Allard tunnel, located near an upper tributary to Bedrock Creek, at approximately 3124 m elevation, intercepts a deposit within a mineralized section of the syenite porphyry. Allard Mining Company drove the tunnel on an unpatented claim in 1921 in order to explore the disseminated copper deposits in the area, however no ore was produced (Eckel, 1949). According to Eckel (1949) mineralization in the vicinity of

the Allard tunnel extends at least 457 m westward and 122-152 m vertically from the tunnel. Disseminated chalcopyrite, cupiferous pyrite (Cu, Au), and ruby silver veins occur in the vicinity of the Allard tunnel.

Copper Hill Glory Hole (CH)

Located on the ridge separating Bedrock and Boren Creeks, at relatively the same elevation as the Allard tunnel is the Copper Hill glory hole. The Copper Hill glory hole exploited the only known PGE-bearing ore body within the district. The most obvious feature of this deposit is the glory hole that is 15-23 m at its widest and is 9-15 m deep. A ~183 m tunnel is also present within the workings. Copper Hill is situated along the border of the syenite porphyry (the Allard stock) and the metamorphosed sediments. Mineralization occurs as veins containing chalcopyrite, magnetite, and hematite in a metamorphosed augite-orthoclase-rich rock.

Cumberland (CB)

This Au-Ag-Te low sulfidation epithermal deposit lies in the eastern part of the Cumberland Basin, along the western slope of Cumberland Mountain, in the basin below the San Juan Mountains lookout and the notch leading to the Bessie G mine. The workings range from 3511-3764 m and the mine exists predominantly within the Cutler and Delores Formation red beds. Discovered in 1878, Cumberland was worked intermittently until 1937, with periods of activity that lead to the existence of a 30-stamp mill, a power plant, and machine shop in the Cumberland Basin. The vein, striking N 60° to 80° E, has been partially worked through a vertical range of 302 m, with four levels and at least two known portals.

Bessie G (BG)

Originally named the Egyptian Queen when opened around 1880, the Bessie G mine is a high grade low sulfidation epithermal gold telluride deposit located near the divide between Columbus Basin and Heffernan Gulch, at an elevation of 3065 m. This patented claim has been worked several times and production records indicate that roughly 500 kg of gold, and of silver, have been produced from Bessie G since 1887 (Saunders and May, 1986). With two portals and an upper and lower level, Bessie G follows an Au-rich quartz vein within the silicified redbeds of the Dolores formation that is cut by a complex irregular sills and dikes of diorite porphyry. Both a shear zone and breccia zone exist in places along the vein, where roscoelite (V-rich mustovite), and native gold are locally visible.

May Day/ Idaho (MD)

The May Day and Idaho Ag-Au-Te limestone replacement (skarn) and vein deposit mines, located at the mouth of the La Plata river canyon, are responsible for more than half of the reported total production in the La Plata District, through 1949. Production numbers at that time for Idaho and May Day are 1359.7 kg Au and 10857.9 kg Ag, and 2123.8 kg Au and 21516.8 kg of Ag respectively. These mines are located at comparatively low elevations and are more easily accessible than other mines in the district. Due to abundant faulting (the May Day/Idaho fault system), veining is common at this location, and porphyry dikes contact sedimentary units (calcareous) to form the limestone replacement bodies and veins. The major eastward-trending reverse faults were important in localizing ore here, however a series of northward-trending, steeply dipping

normal faults with adequate displacement contain the principal ore bodies mined at May Day/Idaho.

Bedrock Gulch: A Detailed Report

Lonsdale (1921) completed a graduate thesis on the La Plata District, specifically on the Bedrock Gulch area, where the Allard Stock is located. Lonsdale's main focus was to bridge gaps in existing data on the district as a whole, but ended up concentrating on only the geology and ore deposits of Bedrock Gulch. The small mining town of La Plata was located at the mouth of Bedrock Gulch, three miles from May Day and the Rio Grande Southern Railroad spur servicing May Day (Lonsdale, 1921). The area experienced periods of intermittent exploration and production, but once the deposit at May Day was discovered, renewed exploration occurred, and the town of La Plata grew (Lonsdale 1921). During this period of resurgence, the deposits on Bedrock Gulch were prospected and developed, with the result that roughly 3,000 tons of copper ore were shipped to Durango, CO to be smelted (presumably from Copper Hill). Lonsdale (1921) reported no significant ore production (no copper bodies were really developed, and no significant Au or Ag was economically produced) by the Allard Mining Company at Allard tunnel.

Lonsdale (1921) describes the contact-metamorphism and "baking" of the Dolores Formation in Bedrock Gulch, which is silicified, grey, and more competent and dense, as compared to the un-metamorphosed characteristic "redbeds" seen in other parts of the district. The author discusses the "brilliantly white" quartzite of the metamorphosed La Plata sandstone in the vicinity of Bedrock Gulch, also due to intrusion of igneous bodies

(the Allard stock). Lonsdale (1921) reports three different types of igneous rocks in the vicinity of the gulch, however the geologic map from Eckel (1949) does not go as deeply into detail. Lonsdale (1921) cited petrographic and geochemical data for a diorite-monzonite porphyry, an augite-syenite, and a diorite in Bedrock Gulch.

Two types of deposits, a disseminated low-grade copper ore, and lead-silver-bismuth enriched veins (within the Black Rock Claim), are reported to occur within Bedrock Gulch (Lonsdale, 1921). The Pb-Ag-Bi veins are apparently not found elsewhere within the district and Eckel (1949) does not mention them. Lonsdale (1921) also states that throughout Bedrock Gulch, there are copper-bearing ores similar to those at Copper Hill, specifically within the exposures of syenite and diorite-monzonite porphyry in the gulch. A small occurrence of chalcocite and several veins of cuprite are also noted to be in Bedrock Gulch. Lonsdale (1921) suggests that the diorite may be the most likely source of ore forming fluids, but offers no evidence to corroborate that idea. He does affirm that "geologic conditions are favorable for continuity of depth and size of ore bodies" in Bedrock Gulch (Lonsdale, 1921).

Recent Study

After a ~30-year gap in publications on the La Plata District, several studies conducted research that built upon the extensive USGS Professional Paper by Eckel (1949). Werle et al. (1984) updated geochemical data on the Allard Stock and detailed the evolution of the stock and its mineralization in seven major stages. Werle et al. (1984) discussed how the Allard stock's mineralization is unlike the typical calc-alkaline copper porphyry mineralization characteristic of the western United States and Canada. They

compared it to the alkaline suite porphyry copper deposits of British Columbia (Barr et al. 1976), as opposed to the calc-alkaline porphyry coppers in western North America. Werle et al. (1984) also studied the trace element geochemistry of the Allard Stock, noted the extensive K-metasomatism of the syenites, and formulated a genetic model of the Allard Stock mineralization. Werle et al. (1983) also mapped the Allard stock in greater detail (Fig. 3) than previously published Eckel (1949).

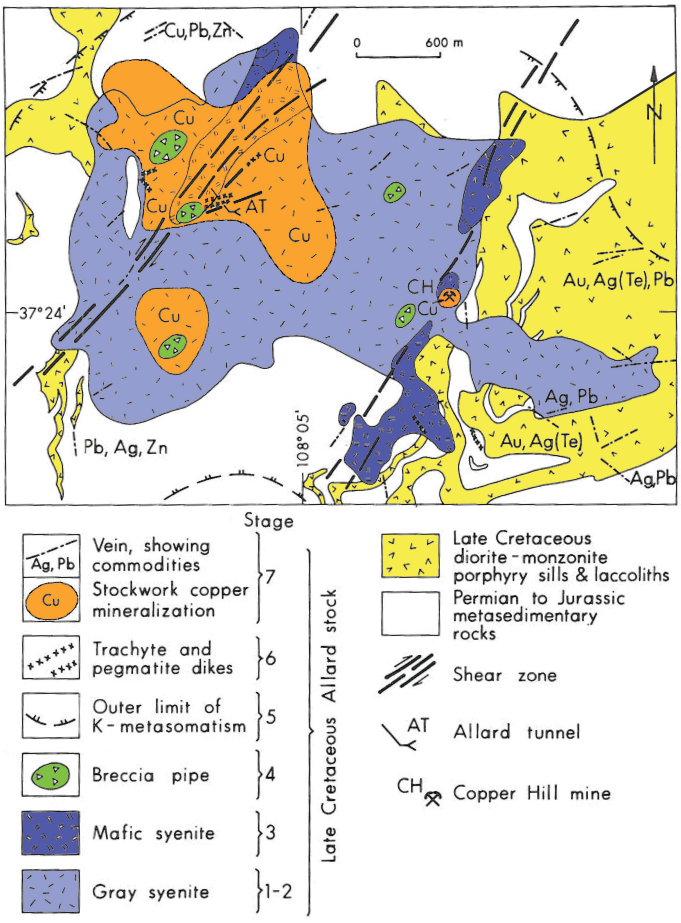

Fig. 3. Detailed geologic map of the Allard stock, modified from Werle et al. (1983) and adapted from Ft. Lewis College student Goncalves' senior thesis (2010)

The following intrusive event descriptions are quoted directly from Werle et al. (1983).

Stage 1

The bulk of the Allard stock is made up of its earliest intrusive units, a composite group of hydrothermally altered grey syenite plutons. Locally well-developed phenocryst lineations and occasional occulsions of Precambrian basement rocks demonstrate the intrusive nature of these plutons. Wall rocks show little evidence of lateral displacement adjacent to these plutons, suggesting that the intrusives made room for themselves by lifting roof rocks vertically . . . rather than by shouldering aside wall rocks. The grey syenites are seriate porphyritic to equigranular rocks composed of alkali feldspar and plagioclase (oligoclase) with minor biotite, hornblende, quartz, and accessory apatite, sphene, zircon, allanite, garnet, and opaques. Two magmatic feldspars are usually present: (1) an earlier, larger grained, microperthitic, often Carlsbad-twinned variety with an orthoclase structure as indicated by the X-ray method of Wright (1968); and (2) a later interstitial, less pertthitic variety with an orthoclase or anomalous structure.

Stage 2

After their emplacement the gray syenites were hydrothermally argillized. Plagioclase, and to a lesser extent, orthoclase were replaced by fine-grained aggregates of kaolinite and sericite, and mafic minerals were altered to chlorite. Argillic alteration extends over 1000 m beyond the limits of the stock.

Stage 3

Intrusive plutons of mafic syenite were emplaced along two northeast-treanding shear zones cutting the altered grey syenites. Mafic syenites constitute about 15% of the Allard stock, at its present level of exposure, and are typically hypidiomorphic-heterogranular to porphyritic rocks composed of varying amounts of orthoclase, plagioclase, augite, hornblende, and biotite, with trace amounts of apatite, sphene, and opaques. A small body of chemically distinct layered mafic syenite is exposed in the glory hole of the Copper Hill mine. These cumulate rocks exhibit fine-scale rhymithic layering consisting of (1) layers composed of 0.1 mm cumulus aegirine-augite, magnetite, apatite, zircon, and sphene together with intercumulus alkali feldspar; some aegerine-augite ezhibits adcumulate overgrowths that have produced crescumulate crystals up to 2 mm long; and (2) layers of cumulus plagioclase (An_{25-35}), aegerine-augite, apatite, zircon, and sphene in a matrix of intercumulus alkali feldspar. Sulfides, predominantly chalcopyrite, are found interstitial to the cumulus crystals in both types of layers. Locally the layered rocks are cut by veinlets, or mottled by patches of deuteric(?) garnet, calcite, biotite, albite, hematite, and sulfides. With the exception of the Copper Hill rocks, most of the stage 3 syenites are the only rocks from the Allard stock that have Ab/Or/Q ratios plotting close to the thermal

minimum on the Ab-Or liquidus surface. In the vicinity of the Allard tunnel, inclusions of stage 3 mafic syenite, some of which show distinct layering, occur in stage 5 pink syenite.

Stage 4

Violent escape of volatiles locally formed shattered cylindrical or elliptical prisms of rock within the stock, and fragments of the shattered rock were rotated and carried upward, producing intrusive breccia pipes. The matrix of these breccias tanges from fine-grained high sanidine to finely comminuted rock fragments. The compositional and textural similarities between sanidine in the fine-grained breccia matrix, the widespread replacement sanidine elsewhere in the stock, and sanidine in mineralized veins suggest a close temporal relationship between breccia pipe formation (stage 4), K-metasomatism (stage 5), and mineralization (stage 7).

Stage 5

Intense K-metasomatism profoundly altered the composition of the older stock units and the wall rocks adjacent to the stock. Introduced sanidine replaced argillized feldspars in the gray syenite and formed a network of replacement veins in both stage 1 and stage 3 syenites. Replacement sanidine is not as abundant in stage 3 mafic syenites as it is in argillized stage 1 gray syenites, suggesting that the agrillized feldspars were more succeptible to replacement. The extensive K-metasomatism at Allard is comparable to the potassic fenite halos associated with some carbonatite-alkaline complexes, but is more extensive than the K-metasomatic zones in most calc-alkaline porphyry copper deposits. Dikes of pink syenite, consisting largely of equigranular alkali feldspar, and dikes of pink porphyritic syenite were emplaced during stage 5. These dikes contain up to 15% interstitial calcite, which appears to have crystallized simultaneously with alkali feldspar.

Stage 6

Emplacement of trachyte and pegmatite dikes marks the transition from magmatic to pneumatolitic activity. Trachyte dikes, best exposed in the south-central part of the stock, consist of plagioclase phenocrysts in a groundmass of high sanidine laths with a trachytoid texture. Pegmatite dikes are common in the vicinity of the Allard tunnel where they fill tension fractures resulting from right lateral movement on a northeast-trending shear zone. Pegmatite dikes range in thickness from a few centimeters to 2 m and have exposed strike lengths of up to 50 m. Two types of pegmatites have been recognized: older syenite pegmatites and younger mafic pegmatites. The syenite pegmatites consist predominantly of orthoclase, with subordinate plagioclase, augite, calcite, and quartz. The mafic pegmatites consist of intergrown dark green augite, orthoclase, calcite, and quartz. Some of the mafic pegmatites are symmetrically zoned with borders of augite, followed inward by orthoclase zones surrounding a core of quartz, chalcedony,

tremolite(?), and calcite. Sulfides, dominantly chalcopyrite with subordinate pyrite and bornite, occur as coarse interstitial masses and fracture fillings in all of the pegmatite dikes. The mafic pegmatites are the only acmite-normative (peralkaline) rocks of the Allard stock.

Stage 7

Hydrothermal solutions deposited metallic minerals, sanidine, quartz, calcite, and fluorite as veinlets and disseminated replacement masses throughout the stock, locally producing significant volumes of stockwork mineralization containing more than 0.1% copper. A generalized paragenetic sequence for the hypogene opaque minerals is (1) iron oxides (magnetite and hematite); followed by (2) pyrite (continuing through all the later stages) and arsenopyrite; followed by (3) chalcopyrite, enargite, sphalerite, bornite, and chalcocite; followed by (4) marcasite and galena. At the copper Hill mine, trace amounts of domeykite and tennanite formed before chalcopyrite. The gangue minerals in order of formation is (1) sanidine, (2) minor quartz, and (3) calcite and fluorite. The following sequence of vein types is also apparent: (1) iron oxide – pyrite – copper sulfarsenite – copper sulfide – calcite – quartz veins; (2) calcite – quartz – sphalerite – galena – chalcopyrite – pyrite veins; (3) fluorite – quartz – pyrite – chalcopyrite – marcasite veins. Small base metal sulfide veins and mantos and quartz – pyrite – fluorite – telluride veins that occur peripheral to the stock may have formed at the same time as vein types (2) and (3) within the stock. The amount of replacement and vein calcite introduced during stage 7 ranges from 2 to 12 vol. %. That over 6 km^2 of rock was affected by carbonatization indicates a significant source of CO_2 at depth.

Trace element chemistry shows volatile enrichment and anomalous concentrations of barium, rubidium, and strontium, as well as high amounts of arsenic, tellurium, and bismuth (Werle et al., 1983). The stock is enriched with up to 10% CO_2, which occurs as extensive calcitic alteration of both feldspars and mafic mineral species. Fluid inclusion studies indicate a CO_2-saturated fluid phase was present during crystallization of rocks in stages 4, 5, and 6, as well as during early vein formation. The most important finding from Werle et al. (1983), other than their genetic model and geochemical analyses, are the sulfur isotope values cited. The authors do not go into detail about the sulfur isotopes but do report, "The Allard sulfides have an average $\delta^{34}S$ of -6.5‰ (range -4.7 to -7.9)." They comment that other alkaline suite porphyry copper systems have similar values (i.e.

Shasket Creek, WA, Goose Lake, MT, Copper Mountain, BC, Galore Creek BC). A comparison of the geochemical data obtained from Werle et al. (1983) with the data gathered by this study is discussed further in the Geochemistry section of this thesis.

Saunders and May (1986) published data on the Bessie G mine, described in the above ore deposits section. Saunders (1986) proposed that the Cu-Au-Te-PGE enriched Allard stock was actually genetically related to the epithermal mineralization, although the authors mainly focused on the Bessie G vein for his PhD research. The authors state, "The close spatial and temporal association between the gold telluride mineralization at the Bessie G deposit with Tertiary alkalic stocks suggests that they are genetically related." Saunders and May (1986) go on to propose the idea that Bessie G is underlain by a syenite or monzonite stock at depth, and this stock provided precious metals and tellurium to the epithermal system, which produced the high grade bonanza gold deposit.

The Allard stock is enriched in Au, Ag, and Te, and Saunders and May (1986) postulate that a similarly enriched stock could perhaps underlie Bessie G. Gold telluride mineralization is considered the latest hydrothermal event in the district, due to crosscutting relationships between the ore-bearing veins and the district's youngest intrusive bodies. Alkalic rocks are associated with other gold telluride deposits in Colorado, such as the Cripple Creek district. The Allard stock is enriched in Au, Ag, Te, Bi, Ba, Pt, and Pd (Werle et al. 1984) and Bessie G has a very similar elemental suite associated with its mineralization. Saunders and May (1986) cite that Bessie G contains a maximum of 80 ppb Pt+Pd. Comparing mineralization at Bessie G to the Allard stock thus leads to a comparison of the La Plata district's epithermal and porphyry mineralization, and to the porphyry to epithermal transition in general. Saunders (1986,

1991) and Saunders and Bookstrom (1998) also proposed a genetic link between deeper porphyry-style ores and shallower Au-Ag-Te epithermal mineralization.

In 1992, the US Bureau of Mines conducted a Mineral Appraisal of the San Juan National Forrest, including the La Plata mining district, and published the report in the Mineral Land Assessment Open File Report 2-92 (Neubert et al., 1992). In their report on the Allard stock, the MLA cites that the Allard stock has been drilled numerous times by several different mining companies. No drill holes apparently contained high enough grade or tonnage to make mining the Allard stock economically profitable, however the report cites that the Bedrock Creek copper mineralization offers a inferred exposed 200 million ton resource grading 0.4% copper, 60 ppb gold, 7 ppm silver, and 5 ppb PGEs. If the drill holes are representative of the subsurface, then the inferred resource would be 300 million tons grading 0.34% copper, and with similar precious metal contents as seen at the surface. At Copper Hill, a resource of 30,000 tons also exists, with 1.45% copper and 0.42 oz/ton silver and unknown amount of gold and PGEs. This report concludes that large-scale mining of the Allard stock could occur if copper prices rose about $2.50/lb (currently the price of copper fluctuates around $3.00/lb) or if exploration efforts revealed larger tonnages or higher grades of ore (Neubert et al. 1992).

Schiowitz et al. (2008) completed stream sediment geochemistry for 41 samples from the La Plata district in their GIS analysis of the district. They created a GIS geodatabase complete with geology, structural features, mine locations, sample locations, and watersheds within the district. Spatial analysis was done in order to help visualize the relationships between geology, structure, and geochemistry. An “exploration model” was

created (Table 3), detailing the favorable situations for gold occurrence, and they mapped the geochemical concentrations, as shown in figure 4.

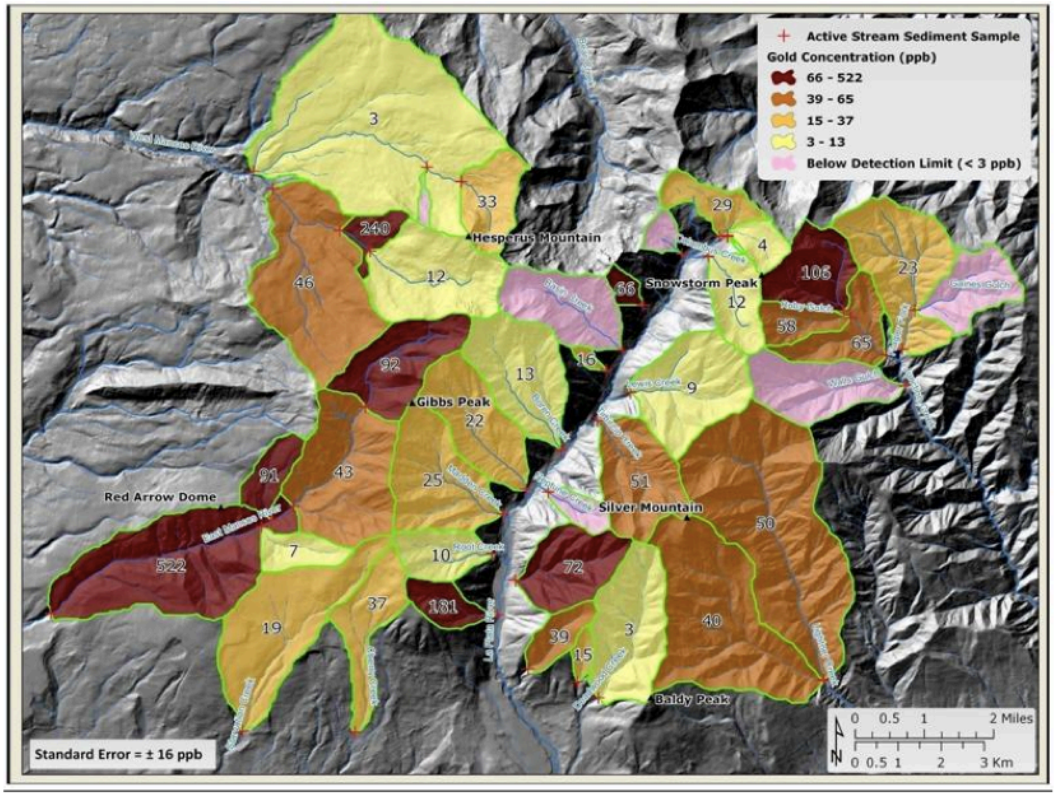

Fig. 4. Map showing stream sediment geochemistry for drainage basins in the La Platas, highlighting the gold geochemical basins with concentrations in ppb (Schiowitz et al., 2008)

Table 3: Possible exploration model from Schiowitz et al., (2008).

Commodity of Interest	Gold
Generic Model Types	Polymetallics Veins/Alkalic Intrusion
Favorable Host Rocks	Wanakah Formation, Entrada Sandstone, and Junction Creek Sandstone, hornfels aureole
Favorable Structures	Quartz veins, vein stockworks, breccias, and second order structures adjacent to major faults
Geochemical Signature	Au, As, Ag, Ba, Hg, Sb, Se, Pb, Zn, Te
Ore Minerals	Au-Ag tellurides and free gold

Laramide Orogeny and Flat Slab Subduction Influence on COMB Ore Deposits

The Laramide orogeny began in the Late Cretaceous (70-80 Ma) and continued well into the Eocene (33-55 Ma). During this event, the Farallon/Proto-Pacific plate collided with the North American plate and active subduction and mountain building occurred. In Colorado, the Laramide orogeny began during the Late Campanian (~72 Ma) as the Late Cretaceous sea underwent its final regression from the Western Interior; orogeny began in Colorado before marine deposition ended, in the southwest and northeast respectively (Tweto, 1980). Uplifts and consequent subsidence (structural basin development) accompanied the Laramide orogeny in Colorado, and major erosion of Laramide features took place during the Oligocene tectonic quiescence in the area. Development of the Rio Grande Rift triggered rejuvenation of these uplifts via block-faulting (Tweto, 1979).

Prior to the start of the Laramide orogeny, major shear zone systems formed in the

Precambrian, accompanied by deformation including deep-seated folding and plastic flow and shallower brittle deformation and retrograde metamorphism. This northeast-trending shear system was recognized as a precursor and structural controlling mechanism for the COMB (Tweto and Sims, 1963). As the Laramide orogeny persisted, it provided an opportune tectonomagmatic setting for intrusive events, which sourced the metals and hydrothermal fluids responsible for the COMB ore deposits. Without the structural set up of the COMB in the Precambrian, the Laramide intrusions and associated mineralization would not have formed what we now know as the northeast-trending COMB (Tweto and Sims 1963; Tweto, 1980).

Flat-slab subduction associated with the Laramide orogeny led to a fertile lithospheric mantle via mantle devolitization reactions (Fig. 5). This fertile mantle became enriched in volatile ore-forming species such as water, CO_2, sulfur, and metals/metalloids (Saunders and Brueseke, 2011). As the flat-slab subducts, it sinks and experiences increasing temperatures and pressures (increasing metamorphism), followed by melting, and then devolitization (Saunders and Bruseke, 2011). Metals/metalloids can be either fluxed into the overlying asthenospheric wedge or into the lithospheric mantle, however the key inference is that they are driven off into whatever type of mantle overlies the subduction zone. In the western USA, the flat-slab subduction of the Laramide orogeny caused volatiles to flux from the Farallon Plate into the North American lithosphere (English et al., 2003; Humphreys et al., 2003, Crossey et al., 2009).

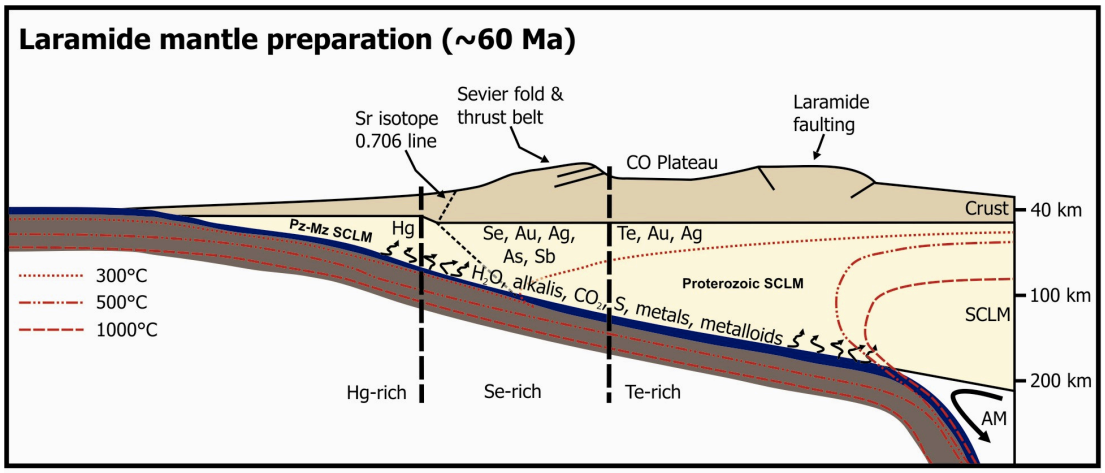

Fig. 5. Figure based on concepts in Saunders and Bruseke (2011) showing Laramide flat-slab subduction and lithospheric mantle devolitization. The Allard stock falls within the Colorado Plateau's Te-rich zone enriched with the metals Te-Au-Ag sourced from the subducted slab.

Richards (2009) discusses "postsubduction" magmatisim and Cu-Au porphyry and Cu epithermal deposits as products of remelted subduction-modified lithosphere. In this case, the enriched postsubdicition lithospheric mantel can partially melt. This partial melting can be triggered by a number of tectonomagmatic processes. Richards (2009) gives evidence that these types of deposits are predominantly associated with alkaline rocks, as are the "synsubduction" versions of this process (i.e. the intrusion of the Allard stock). Furthermore, magmatism becomes progressively alkalic (K-rich) deeper and farther from the trench (Saunders personal communication 2014). In reference to the Laramide events and the COMB, intrusions appear to get younger from the southwest to the northeast (with some of the oldest being the La Plata intrusives). In opposition, once the Rio Grande Rift initiated, new tetonomagmatic events and magmatism became progressively older from the northeast to the southwest (Art Bookstrom, personal communication to Saunders).

Mutschler et al. (1997a,b) and Kelley and Ludington (2002) note the alkaline nature of the Allard stock in the La Plata district in their overview papers concerning alkaline magmatism and Au-Te mineralization throughout Colorado. Several types of productive gold deposits (79 Ma to 26 Ma) in the Rocky Mountains (porphyry Cu-precious metal systems ± PGEs, transitional types, and Au-Ag epithermal systems) exhibit a close spatial, temporal, and genetic association with alkaline igneous rocks. These alkalic rocks apparently represent mantle melts that fractionated in crustal level magma chambers. Coeval calc-alkaline rocks, which formed from crustal melting and magma mixing, also occur with these alkaline stocks in many locations (Mutschler et al. 1997a,b). Porphyry Cu>Ag>Au ± PGE deposits (Allard Stock - CO, Goose Lake Stock – MT, Cerillos district – NM) occur in or adjacent to shoshonitic syenite stocks and mineralization occurs as stockworks, disseminations, veins, pegmatite dikes and segregations, endoskarns, exoscarns, and local immiscible sulfide concentrations.

These deposits usually contain high sulfur abundances and precious metals are byproducts or coproducts of copper production. In Brittish Columbia, deposits of this nature are being actively mined, although they occur in Mesozoic accreted terranes (Schroeter et al., 1989; Mutschler et al., 1997a,b). Epithermal gold deposits associated with alkaline rocks, as discussed by Mutschler et al. (1997a,b) occur throughout the Rocky Mountains, and the Bessie G mine fit the criteria, as does the Cripple Creek district, and the Boulder County telluride camps (Saunders, 1991). Kelley and Ludington (2002) note the formation of alkaline igneous rocks and associated hydrothermal ore deposits as falling into two distinct time periods – (1) during the (70-40 Ma) Laramide orogeny (deposits restricted to the COMB) and then later more widespread mineralization

associated with alkalic igneous bodies (35-27 Ma) during the transitional period from compressional to extensional regimes. The most important factor in these gold deposits' formation seems to be the opportune near-surface emplacement of volatile-rich, relatively oxidized alkaline magmas, that source from subduction-modified subcontinental lithosphere, as evidenced by Sr and Pb isotope compositions (data for the La Plata Mountains is unavailable).

Mostly all alkaline-related gold deposits have five characteristics, that are typical of economic alkaline-related ore deposits around the world: (1) they occur in areas of multiple episodes of intrusive activity (with or without prior calc-alkaline activity); (2) they contain evidence of magmatic-hydrothermal activity such as breccia pipes and stockworks; (3) mineralization and the hydrothermal system came late in the evolution of the igneous body; (4) alteration assemblages are potassic (K-feldspar, sericite, and biotote); (5) consistent paragenesis can be seen in veins (early base-metal sulfides, then gold or Au-bearing tellurides) (Mutschler and Mooney, 1993; Richards 1995; Jensen and Barton 2000). Figure 6 shows a grade tonnage plot for alkaline-related gold deposits as discussed in Kelley and Ludington (2002). It should be noted that although Au-Cu alkaline related deposits have been isolated as a class, most of their fundamental characteristics are basically the same of calc-alkaline influenced deposits. Only the occurrence of roscoelite (V-bearing muscovite), anomalous high Te and F contents, pervasive potassic alteration, and deficiency of quartz as a gangue mineral are the truly distinctive characteristics of these deposits (Bonham, 1988; Jensen and Barton, 2000; Silitoe, 2002), albeit none exhibit all of these attributes.

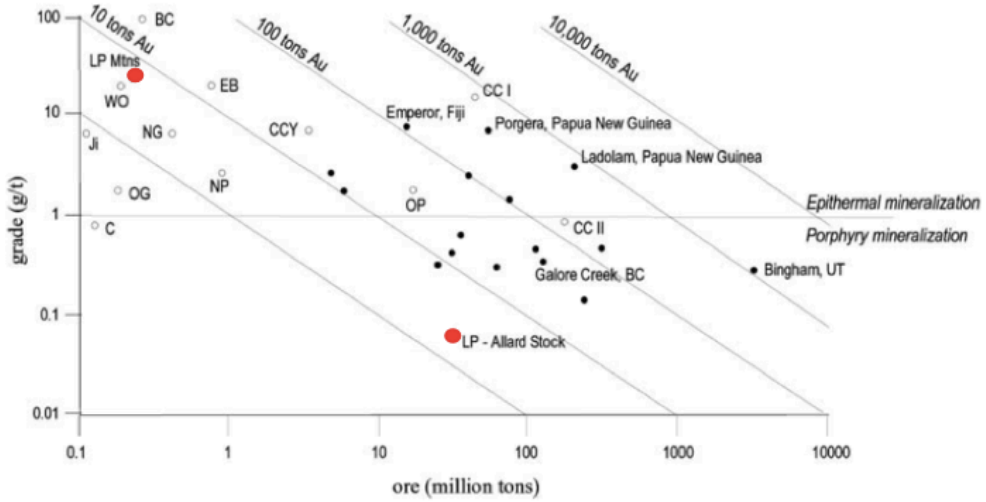

Fig. 6. Grade tonnage plot for alkaline-related gold deposits, from Jensen and Barton (2000). Dashed contours indicate total gold in deposit. Cripple Creek and the La Plata district have each been plotted as two points. The point labeled LP Mtns represents historic production from high-grade epithermal veins. The point labeled LP ± Allard Stock represents the porphyry-style Cu±Au±PGE deposit. Cripple Creek is plotted as CC I and CC II, high grade vein systems and low-grade ``disseminated'' deposits, respectively most districts include all gold produced, including that which is in vein, breccia, porphyry, skarn, or placer deposits. Because most of the deposits are incompletely explored, the data shown on this plot are not suitable for use as a predictive model. (From Kelly and Ludington, 2002).

Alkaline-hosted PGE Porphyry Deposits

Alkaline porphyry deposits (Fig. 7) constitute a significant global resource due to their large size. As previously stated, the Allard stock hosts anomalous PGEs, most notably at the Copper Hill deposit. The Allard stock is part of a distinct Cu±Au±PGE±Te subclass of porphyry deposits that are known worldwide. Most deposits of this type are located in Eastern Europe, such as Bulgaria's Elatsite and Chelopech and Serbia's Bor and Madjanpek, which occur in the Srednogorie zone. The Srednogorie zone is an east-west striking belt consisting of a Late Cretaceous subduction/island arc system that hosts both porphyry and epithermal deposits associated with sub-alkaline igneous rocks.

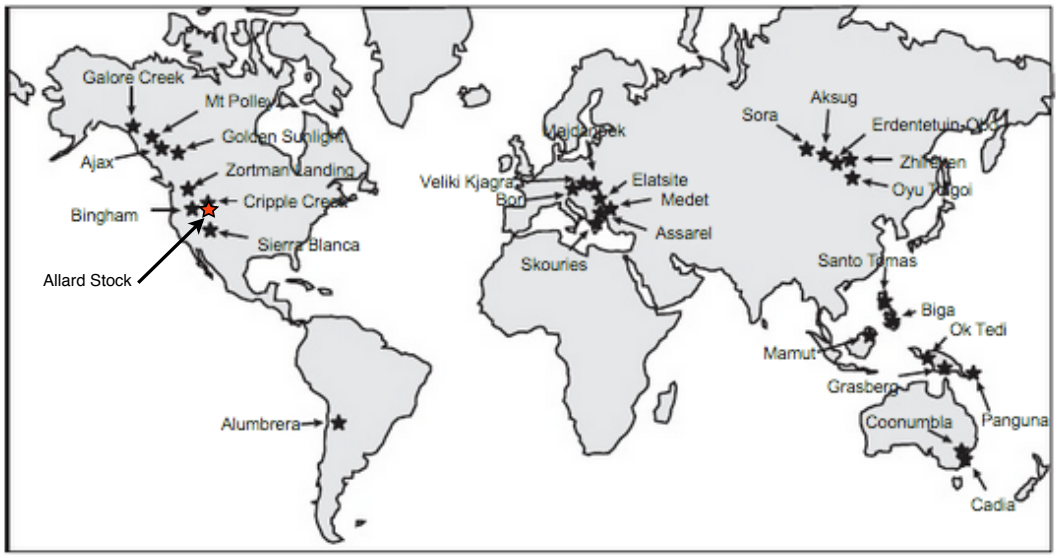

Fig. 7. Location map of alkalic porphyry Cu ± Mo ± Au ± Pt ± Pd ore deposits. Modified from Economou-Eliopolous (2005).

The Skouries alkaline porphyry Cu-Au-PGE-Te deposit in northern Greece exhibits strongly fractured and intensely altered country rocks due to hydrothermal fluids which additionally caused silicification, potassic, phyllic, and propylitic alteration associated with a 18 Ma monzonitic-trachytic mineralized stock (Elipolous and Economou-Elipolous, 1991). Porphyry mineralization includes chalcopyrite, pyrite, bornite, and chalcocite in veins, disseminations, and stockworks. Sulfides contain includions of native gold and electrum and the geochemical signature is characterized by PGEs with Cu, Au, Ag, B, Bi, Co, Se, and Te. Barium and Sr contents are also high while Rb is low. Palladium concentrations range from less than 2 to 480 ppb. Ruthenium content ranges from 8 to 41 ppb, Pt from 2 to 10 ppb, and Te up to 2700 ppb (Elipolous and Economou-Elipolous, 1991; Economou-Elipolous, 2005). PGEs occur in merenskyite [$(Pd,Pt)Te_2$] and a (Pt,Pd,Bi)Te phase (michenerite?) within chalcopyrite and bornite, or enclosed by electrum and hessite (Ag_2Te) inclusions in chalcopyrite (Economou-Elipolous, 2005). Of the seven alkaline-hosted Cu-Au porphyry deposits in British

Columbia, Galore Creek, Mt. Polley, Afton/Ajax and Mt. Milligan are known to contain significant PGEs (Thompson et al., 2001, Economou-Elipoulos, 2005; LeFort et al., 2011), and locally are also enriched in Te such as Mt. Milligan (LeFort et al., 2011). The youngest (183 Ma) and most well studied of the British Columbia deposits is Mt. Milligan, which contains PGE tellurides, base-metal sulfides, arsenides, antimonides and various Au-Ag-Te-Bi minerals with PGE contents up to 6.4 ppm (Thompson et al., 2001; LeFort et al., 2011). LeFort et al. (2011) hypothesize that the Cu-Au-PGE-Te veinlets are transitional ("subepithermal") between the porphyry and epithermal environments, although no epithermal mineralization is present there, unlike in the La Plata district.

The common link between these porphyry Cu-Au±PGE±Te deposits aside from their similar mineralization is their alkaline nature. While alkaline magmas can form in virtually every tectonomagmatic setting, many are associated with subduction and/or areas that have been affected by past subuduction. In the aforementioned deposits, the magmas were all noted to have sourced from previously metasomatized, subduction-affected mantle (Thompson et al., 2001; Economou-Eliopoulos, 2005; Auge et al., 2005). The Allard stock was emplaced in such a tectonomagmatic setting, which affected southwestern Colorado during the Laramide and throughout the Cenozoic (Jones et al., 2011). The alkaline chemistry of the magmas is a key characteristic that influences PGE enrichment in these deposits, evidenced by the geochemistry of both the Allard stock and the porphyry deposits listed above. John and Taylor (2014, in press) plotted the grade-tonnage for PGMs in porphyry Cu and Mo deposits (Fig. 8). Note that the Allard stock is estimated to contain a resource of ~200 million tons with a Pt+Pd content of 72.3 ppb.

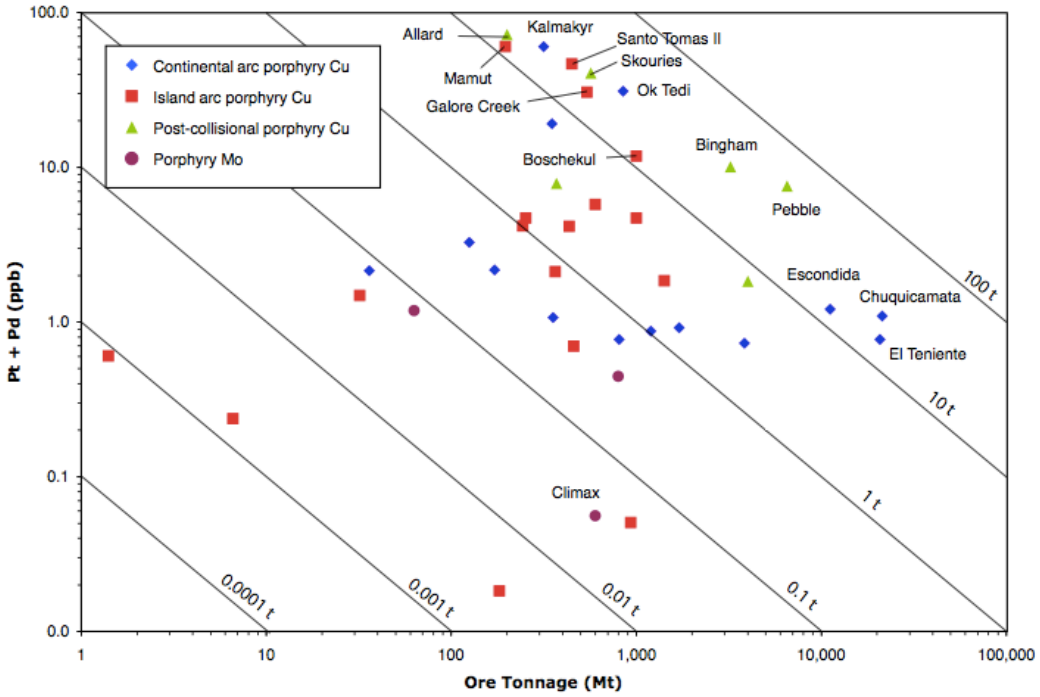

Fig. 8. Plot of Pt+Pd (ppb) grade and ore-tonnage (million tons) from John and Taylor (2014). The Allard stock plots the highest grade for the post-collisonal porphyry copper deposits on the plot. A tonnage of 200 Mt is shown for the Allard stock, as reported by Neubert et al. (1992).

PGE-Copper Association in Other Deposit Types

PGEs can be associated with copper in other types of precious metal deposits. For example, a Cu-Ag-Au mine in the Revais Creek district of Montana produced roughly 300 ounces of platinum metals during its lifetime (Mertie, 1969). This deposit, named the Green Mountain mine, shows a similar mineral assemblage to that of Copper Hill, including the supergene minerals chrysocolla and malachite. The tenor of Pd and Pt at this mine was ~3.0 g/t for each. In Nevada, the Boss mine in the Yellow Pine district also produced Cu, Au, and PGEs. Ore minerals consisted of chalcopyrite, limonite, chrysocolla, bornite, chalcocite, malachite, and cuprite, however the mineralization was hosted in a quartz vein. Bismuth was apparently part of the system as well, similar to the situation at the Allard stock.

The Boss mine reported a tenor of 14.6 oz/ton Pt and 64.2 oz/ton Pd (Mertie, 1969). In addition, supergene PGE deposits occur associated with Cu-Ni sulfide deposits. The Key West deposit, in the Copper King/Bunkerville mining district in Nevada, contains chalcopyrite, pyrite, pyrrhotite, millerite, pentlandatie, and magnetite. Pt and Pd exists as sulfarsenides [mainly Irarsite (Ir, Pt, Rh, Ru)AsS] and tellurides, however secondary PGE-bearing phases consist of Pd-oxides ± Te-Bi, Pd-Cu-rich oxides, and Pd-Fe-rich oxides. Key West averaged roughly 871 ppm Pt, 2612 ppb Pd, and 496 ppm Au (Suarez et al., 2012). Clearly there is an important association of Pt and Pd with Cu, Au, Te, and Bi, and they are likely transported together in chloride- or hydroxide- complexes (Wood, 1992). Bi-tellurides commonly occur in gold skarns (Meinert, 1992), which gives further evidence of a magmatic hydrothermal source for Bi and Te, and by extension

PGEs. The PGEs in the Allard stock occur as Pt ± Pd bismuth-tellurides with or without Ag.

Porphyry to Epithermal Transition

Historically, two schools of thought concerning precious metal sources in hydrothermal ores exist, where the metals are either (1) leached from the surrounding rocks or (2) are sourced directly from the magmas. The Hedenquist and Lowenstern (1994) model links epithermal precious metal deposits to porphyry systems indicating that magmatic fluids are important contributors to epithermal hydrothermal systems (Fig. 9). Magmas provide the heat source needed to sustain hydrothermal systems throughout their lifespans. Perhaps magmas also provide water, metals, ligands, and other species to these hydrothermal systems. Due to their close spatial association, there are chemical and physical connections between ore-forming fluid processes in porphyry and epithermal environments and the transition zone between them (Gammons and Williams-Jones, 1997).

Studies on active hydrothermal systems experimentally show that magmas do contribute such components to hydrothermal systems, however as distance from the intrusion increases, evidence of a connection becomes weaker. Modeling experiments show that metals and ligands can be entirely mobilized from magmas (Hedenquist and Lowenstern, 1994). Au, Sn, Mo, PGEs and other siderophile elements have low crustal abundances relative to the Earth's mantle and core, however Fe-Ni sulfides in the mantle contain these metals. During partial melting, these sulfides can contribute metals into the

melt, which then ascends to the crust. Once extruded, these basaltic magmas (the ocean floor) are altered and then subducted, providing abundant Cl^-, H_2O, alkali-group elements, oxidized S, Zn and Cu, thereby enriching the subducted mantle wedge.

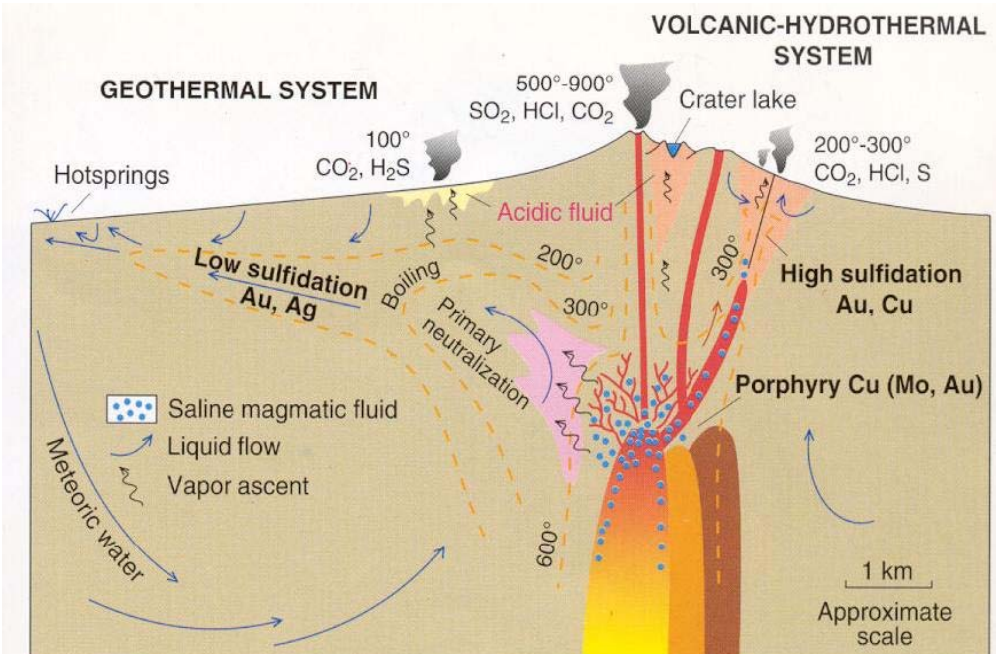

Fig. 9. Illustration of the "porphyry-epithermal" transition and possible associated deposit types, modified from Hedenquist and Lowenstern (1994).

Ligands that transport ore metals can include chloride, bisulfide, and hydroxyacids, and are dependent on fluid composition. Fluid inclusion studies of minerals in ore deposits that formed at 700-800° C have recently shown that hypersaline brines can contain 40-60% NaCl and 250-5000 ppm Cu. Evidence supporting the transportation of magma-sourced metals and fluids from the porphyry to the high-sulfidation epithermal environment is better supported due to the proximity of high-

sulfidation systems to intrusive porphyries. One goal of this study is to test the hypothesis that epithermal and porphyry deposits can be genetically connected. Understanding the evolution of a magmatic fluid and its origin is central to understanding the transition between porphyry and epithermal environments. A fluid can be a single magmatic volatile phase that separates from a magma chamber at depth and is then transported to the epithermal environment, or it may separate into two phases at the source chamber or during ascent (Fig. 10). After separation from dense brine in the porphyry environment, the less dense, more buoyant vapor phase may continue to rise until it reaches the epithermal environment (Henley and McNabb, 1978; Sillitoe, 1983; Hedenquist et al., 1998; Heinrich et al., 1999; Muntean and Einaudi, 2001; Heinrich et al., 2004).

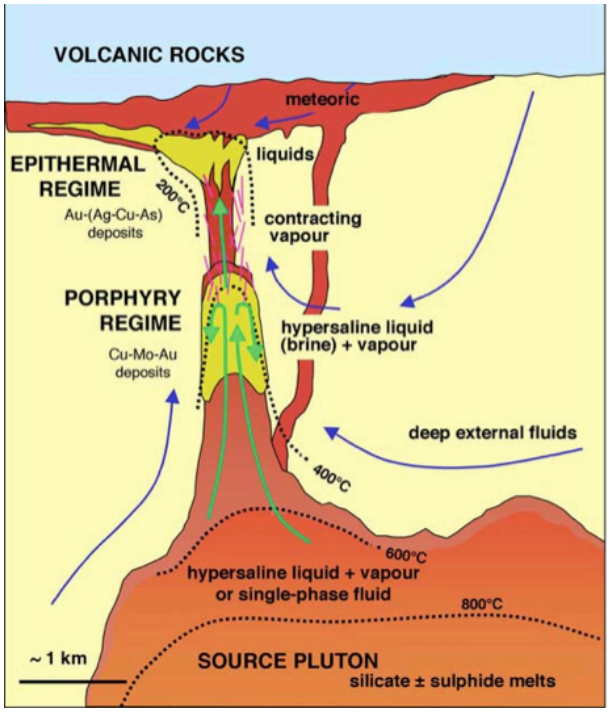

Fig. 10. Schematic cross section of a magmatic-hydrothermal system showing source magma reservoir, and the two possible ore-fluid evolutions in the transition between porphyry and epithermal environments (Heinrich, 2005).

Both carbon and sulfur isotopes in epithermal environments can certainly show a magmatic signature, however some input from sedimentary sulfur and organic carbon also exists (Hedenquist and Lowenstern, 1994). Porphyry deposits typically show the same distribution, with most yielding evidence of magmatic sources for metals and others with indications of country rock sources. The influence of country rock leaching of metals does not exclude the existence of an original and overarching magmatic source. This model provides implications for metal sources in porphyry and epithermal environments.

Later work has shown that magmatic fluids can transport Au from the porphyry environment into shallower epithermal systems (Heinrich et al., 2004; Heinrich, 2005). Henrich et al. (2004) used fluid inclusion studies, thermodynamic modeling, and gold solubility experiments to show that epithermal and porphyry mineralization can both be linked to the cooling of hydrous magma chambers. Phase stability modeling of the NaCl-H_2O system has shown stability fields where vapor, a single-phase fluid, hypersaline liquid brine, and an acqueous in pressure, temperature, and salinity space (Heinrich, 2005).

The isotopic composition of lead locked in gold ores can be used to interpret the origin of the precious metal. Pb isotope compositions of mid-Miocene epithermal deposits in the Northern Great Basin suggest a mafic magma Pb source (Kamenov et al. 2007). Trace lead in gold, electrum, and naumanite from the ores as well as Pb from local mafic rocks in close proximity to these deposits show similar compositions to the middle Miocene bimodal volcanics and to the Columbia River Basalts. The 15.5-16.5 Ma age range for both the ores and for the magmatism associated with the track of the Yellowstone hotspot/plume coupled with the overlap in lead compositions, indicates a

magmatic lead source for local mafic rocks and for the Au±Ag metal in the considered ore deposits (Kamenov et al., 2007). The Ladolam epithermal deposit of Lihir Island, Papua New Guinea similarly showed lead isotopic compositions suggestive of a magmatic Pb source (Kamenov et al., 2005).

Precious metals in sulfide mineralization at the Taupo Volcanic Zone, New Zealand show isotopic Pb signatures consistent with a magmatic origin as well (Hedenquist and Gulson, 1992). Exsoluton of magmatic volatiles from magmas at depth produces a low-density brine carrying Pb, Zn, Sn into the "deep porphyry" environment while a vapor phase likely transports Au, Cu, As, and Hg into shallower epithermal systems (Heinrich, et al., 1994, 2004; Kamenov et al., 2007). Therefore the comparison between Pb isotope compositions of metals in epithermal deposits and spatially associated porphyry deposits may suggest the presence of a related Pb source.

3. METHODOLOGY

Field Methods

Fieldwork was completed during the summer of 2013 in the La Plata Mountains, north of Mancos and west of Durango, Colorado. Samples for this study (Fig. 11) were collected from both porphyry and epithermal deposits in the district, but sampling focused on the mineralization associated with the Allard stock. Samples collected from historic mine dumps and from outcrops were described in the field and their locations were recorded using a Garmin GPS receiver unit. Sampling focused on finding the least altered samples of syenite and diorite-monzonite porphyry, on obtaining both massively mineralized samples and stockwork samples, and on gathering samples to represent the overall character of the ores as a whole. Fieldwork was conducted by a team of three from Auburn University: the author, Dr. James Saunders, and fellow graduate student Michael Mason. Mines visited during fieldwork included the Allard Tunnel, the Copper Hill Glory Hole, the May Day/Idaho mine, and the mine dumps of Cumberland, Columbus, Tomahawk, and Bessie G. mines. Samples totaling 250 pounds were shipped back to Auburn University for further study.

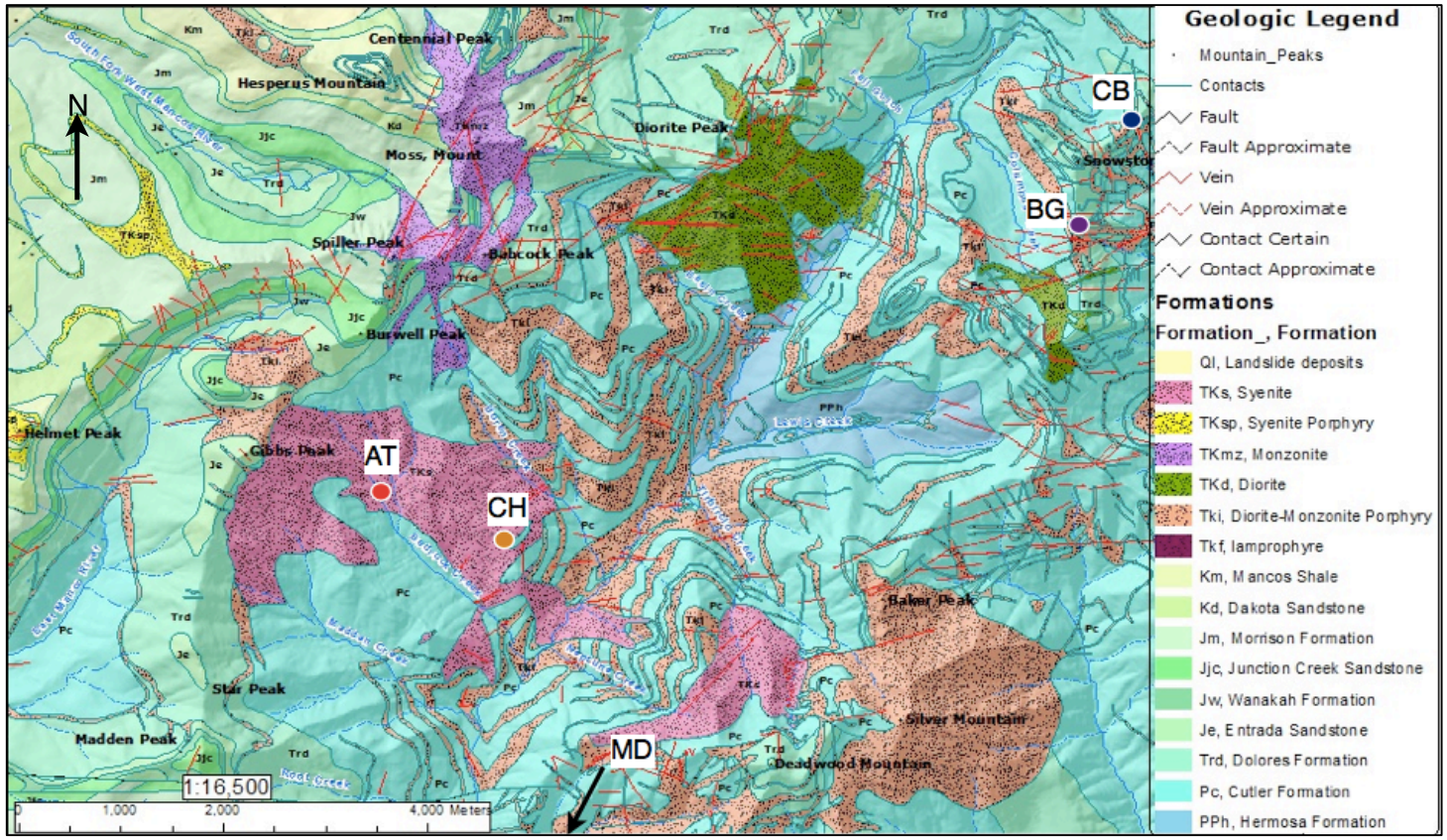

Fig 11. A geologic map showing a portion of the La Plata district and the field area for this study. Mine locations are indicated by a colored circle and the appropriate abbreviation. Modified from Schiowitz (2008) who digitized this version, and from Eckel (1949) who published the original map.

Ore Petrography

Samples were sorted and thin section blanks were selected and cut with the goal of characterizing the most representative or interesting features of each deposit Quality Thin Sections in Tuscon, Arizona prepared the standard and polished thin sections used in this study. Polished ore mounts were prepared by the author in the thin section lab at Auburn University. Petrography was preformed using a transmitted and reflected light microscope. Mineral identification, mineral relationships, and textural relationships were aided by the accompanying geochemical data and with the electron microprobe at the University of Georgia.

Using the JEOL 8600 electron microprobe at the University of Georgia Geology Department, minerals from six samples were analyzed using an accelerating voltage of 15 kV and a beam current of 15 nA. Pure element, alloy, or metal standards were used to calibrate the microprobe before analysis. Mineral grains were quantitatively identified using UGA's Beuker 5010 Silicon Drift Detector (SDD) energy dispersive X-ray (EDS) detector controlled by a Bruker Quantax energy dispersive spectrometers (WDS) automated with Advanced Microbeam, Inc. electronics and Probe for EPMA software, using 10 second counting times and natural and synthetic mineral standards. Counting times increased to 30 or 60 seconds to verify measurements as needed. Analyses were calculated using Armstrong's (1988) Phi-Rho-Z matrix correction model. Backscattered electron (BEI) and X-ray maps were acquired using imaging software of the Quantax analysis system.

Geochemistry

A majority of the samples used for geochemical analysis in the present study were collected in the field. Several samples were collected and provided by David A. Gonzales from Fort Lewis College, in Durango, Colorado. Samples from Bessie G. were supplemented from the collection of Dr. James Saunders, which he collected during his PhD research on the Bessie G mine. Sample splits were made and all samples were analyzed by ACME Analytical Labs LTD in Vancouver, British Columbia. Each sample was sawed in half, and the remaining split was used to make a thin section, ore mount, or was used for isotope analyses. Geochemical samples were selected to contain a high ratio of ore to gangue and host rock. Therefore, precious metal concentrations were maximized and do not necessarily indicate prospective mining grades for each deposit. At ACME, 6 of the 23 samples (250 g) were crushed, split, and pulverized to 200 mesh; 17 samples were pulverized to 85% passing 200 mesh. After samples were appropriately prepared, 21 samples (15 g each) underwent 1:1:1 (1 part sample: 1 part HCl: 1 part HNO_3) Aqua Regia digestion Ultratrace ICP-MS analysis. Two samples (30 g each) then underwent fire assay fusion for Au-Pt-Pd by ICP-ES. 4 samples (0.2 g each) underwent whole rock analyses (oxide weight %) via $LiBO_2$/Li2B_4O_7 fusion ICP-ES.

Isotopic Analyses

Sulfur, copper, and lead isotope analyses were completed on selected samples from this study. Samples selected generally consisted of remaining portions of samples used for ore mounts, thin sections, or for geochemical analyses.

Sulfur isotope analyses were performed by the author and fellow graduate student Michael Mason at the University of Georgia's Stable Isotope laboratory. Chalcopyrite and pyrite were drilled out of samples from Allard Tunnel and Copper Hill under a binocular microscope using a dental drill. Drilling out of the minerals continued until sufficient mass to perform analyses was gathered in powder form (chalcopyrite 6 to 8 mg, pyrite 4-6 mg). The mass was multiplied by the theoretical yield of SO_2 for respective minerals (chalcopyrite 10.9, pyrite 16.67). The result was then divided by two, which gave the mass needed of each of the three reagents, vanadium pentoxide (V_2O_5), copper metal powder, and quartz powder. V_2O_5 provides the necessary oxygen to react with sulfur to make SO_2 gas and the copper metal powder buffers the oxygen fugacity to suppress the formation of SO and SO_3. Silica powder acts as an abrasive during grinding.

The mineral sample and the reagents were combined with an agate mortar and pestle under a fume hood, until combined enough so that the mineral sample began to bond with the reagents (approximately 5-10 minutes). The sample was then scraped out of the mortar and pestle and was then loaded into a 6 mm quartz tube, which was packed with silica fibers on either end. Samples were labeled and loaded into the dessicator to await analysis. The sample was then loaded into a 1050° C furnace and combusted for 10 minutes. The resultant SO_2 gas was then cryogenically isolated from the other gasses

produced (non-condensable gases, CO_2, and H_2O) on the cryogenic purification line. The resultant amount of isolated SO_2 gas was measured using a calibrated mercury manometer and reported as the actual SO_2 yield. Actual yield was compared to theoretical yield and recorded as percent yield. The gas was collected in a Pyrex breakseal tube and was analyzed using a Finnigan MAT 252 mass spectrometer. An error of ± 0.03 σ was calculated on replicate analysis of standards. Results are presented relative to the standard, the Vienna Canyon Diablo Troilite (VCDT).

Copper Isotopes

Dr. Ryan Mathur of Juniata College, using the laboratory facilities at the University of Arizona, conducted copper isotope analyses on samples of chalcopyrite for this study. Chalcopyrite rich samples were dissolved at Auburn University using HF and the residuals were separated under a binocular microscope. The chalcopyrite samples were sequentially passed through two sets of column chemistry to separate the Cu from the possible Fe. Resulting samples were injected into a Multicollector Inductively-Coupled-Plasma mass spectrometer (MC-ICP-MS), the Micromass Isoprobe at the University of Arizona in low-resolution mode using a microconcentric nebulizer to increase sensitivity. The nebulizer flow was adjusted so that the intensity of the 63 Cu beam remained constant at 2 V. Both on and off peak blank corrections were applied to the data and yielded the same result. The standard used was the NIST 976 Cu standard. Two blocks of 25 ratios are reported as an average for each run. Within each run the

measurement error was less than $\delta^{65}Cu = 0.01‰$ for all analyses. This protocol was adapted from Mathur et al. (2009).

Lead Isotopes

Dr. George Kamenov analyzed six mineralized porphyry samples for this study at the Department of Geological Sciences at the University of Florida. Samples were dissolved in HF and the residual sulfide or silicate mineral was picked for Pb isotopic analysis. Analyses were conducted using a Nu Plasma multi-collector ICP-MS (Nu Instruments, UK). Fresh Pb-Tl mixtures were prepared following the Tl normalization technique developed by Kamenov et al. (2004). Both sample and standard solution were aspirated into the plasma source using a Micromist nebulizer with a GE spray chamber. Preamplifier gain calibrations were determined before each analysis. Analyses were conducted in static mode simultaneously acquiring ^{202}Hg on low-1, ^{203}Tl on low-2, ^{204}Pb on Axial, ^{205}Tl on high-1, ^{206}Pb on high-2, ^{207}Pb on high-3 and ^{208}Pb on high-4 Faraday detectors. All standard and sample results were normalized with $^{205}Tl/^{203}Tl = 2.38750$ and age corrected using an approximate age for the Allard stock (67 Ma). Results are reported as ratios of $^{206}Pb/^{204}Pb$, $^{207}Pb/^{204}Pb$, and $^{208}Pb/^{204}Pb$.

4. RESULTS

Geochemistry

The Allard stock contains considerable Cu relative to Ag>Au, and is therefore classified as a Cu-Ag-Au porphyry. The USGS Porphyry Copper Model database estimates that the Allard stock has a 200 million metric ton resource at 0.4% Cu and 5 g/t Ag (John et al., 2010). The most intriguing feature of the stock, however, is the occurrence of PGEs at the Copper Hill mine, first noticed by Eckel (1949). For this study, whole rock analyses and trace element concentrations were conducted on samples from the La Plata District (Table 4). Both representative and "high-graded" samples were sent for geochemical analysis. In addition to samples from the porphyry mines, Allard Tunnel and Copper Hill, samples were also analyzed from the epithermal Cumberland and Bessie G deposits along with apparent the skarn-type deposits May Day and Idaho. The goal was to evaluate data that might show a link between porphyry and epithermal environments in the La Plata district.

All of the Copper Hill samples analyzed and some of the Allard Tunnel samples contain ≥ 1% Cu, 2.5-10 g/t Ag, and 0.01-1.39 g/t Au. Pd values range from 0.026-0.96 ppm, however most analyses from Allard Tunnel were below the 10 ppb detection limit for Pd. Pt values range from 0.005-1.67 ppm. Both Pt and Pd values are noticeably higher in samples from Copper Hill than in samples from Allard Tunnel. Fire assay analyses for

Allard Tunnel yielded 0.096 ppm Au, ≤0.003 ppm Pt, and 0.003 ppm Pd, while Copper Hill assays yielded 1.34 ppm Au, 1.09 ppm Pt, and 0.855 ppm Pd.

Table 4. La Plata District Geochemical Data

Sample	Mo	Cu	Pb	Zn	Ag	Ni	Co	Mn	As	U	Au	Th	Sr
AT-1B	2.08	>10000.00	22.95	166.50	5.86	7.80	15.80	1441.00	40.50	2.60	0.01	21.60	109.50
AT-2	6.43	>10000.00	35.59	208.10	18.99	20.20	12.60	5104.00	<0.1	3.90	0.03	1.40	127.10
AT-4	10.26	2318.56	11.58	119.00	2.52	5.40	19.50	1531.00	<0.1	1.30	0.01	11.20	85.90
AT-6	7.20	>10000.00	65.64	473.40	10.79	7.00	16.20	3193.00	6.10	6.70	0.02	19.80	120.10
AT-7	25.95	1866.84	23.27	80.80	4.01	4.30	27.30	753.00	5.10	1.80	0.12	7.90	153.10
AT-8	1.68	6359.51	9.37	292.90	5.75	15.50	19.70	2395.00	3.10	2.40	0.17	10.20	102.00
AT-9	5.81	>10000.00	101.08	704.90	46.50	14.90	19.60	1071.00	122.30	1.90	0.12	8.20	67.70
AT-10	7.72	>10000.00	69.62	351.00	17.08	56.80	53.60	3202.00	<0.1	8.80	0.02	0.90	104.70
CH-1	1.51	>10000.00	28.61	285.40	61.83	3.30	40.10	995.00	91.70	3.20	0.43	15.30	160.80
CH-2	2.05	>10000.00	105.85	486.30	100.00	2.60	17.30	254.00	89.70	4.20	1.07	9.30	140.10
CH-3	1.57	>10000.00	23.44	279.40	65.80	2.90	45.10	875.00	<0.1	2.30	0.99	15.00	181.00
CH-6B	6.39	>10000.00	260.36	503.20	100.00	5.60	51.70	1351.00	<0.1	1.70	1.39	7.40	151.10
CH-7	1.37	>10000.00	22.38	249.00	27.12	3.30	27.50	1506.00	51.10	2.90	0.36	17.80	120.40
CB-2	2.67	4934.57	56.26	966.80	100.00	5.70	3.80	96.00	517.40	<0.1	12.44	<0.1	110.50
CB-8	2.00	2046.63	71.64	701.40	100.00	2.10	2.80	156.00	352.90	0.20	12.13	0.20	296.40
CB-4	2.94	1299.04	1268.28	5991.60	100.00	6.90	2.80	118.00	193.50	<0.1	5.68	<0.1	61.20
BG-1	1.83	134.64	19.04	42.20	100.00	7.10	4.60	107.00	50.80	1.70	100.00	0.70	53.50
MD-3	2.99	82.71	683.35	2676.00	100.00	4.10	2.30	58.00	101.70	0.20	100.00	0.20	44.20
MD-4	3.00	24.35	43.34	319.50	9.04	3.50	3.10	126.00	183.10	0.10	4.46	0.20	20.30
FSY	1.53	68.34	13.25	75.60	25.24	3.80	14.00	1006.00	4.50	1.20	1.40	8.70	174.80
FBRDMP	1.36	48.46	6.83	48.30	1.67	2.20	3.40	346.00	3.30	0.90	0.27	3.60	67.80

Table 4;: Geochemical data for Allard tunnel (AT), Copper Hill (CH), Cumberland (CB), Bessie G (BG), Mayday (MD), and country rocks, (FSY, FRDMP) analyses are in parts per million (ppm).

Table 4 Contd.

Sample	Cd	Sb	Bi	V	La	Cr	Ba	Hg	Se	Te	Ga	Pd	Pt
AT-1B	0.84	0.22	4.62	247	69.4	9.7	40.9	137	12.5	0.10	7.0	<0.01	0.01
AT-2	1.48	0.96	3.36	626	32.4	70.1	34.1	<5	16.4	0.21	3.0	<0.01	0.06
AT-4	0.33	0.10	0.60	178	27.4	3.3	29.6	<5	9.7	0.07	2.1	<0.01	<0.002
AT-6	1.58	0.21	3.33	1119	87.6	92.0	10.1	<5	6.1	0.04	8.5	<0.01	0.01
AT-7	0.29	0.32	1.77	163	38.6	5.3	115.7	<5	9.4	0.73	3.7	<0.01	<0.002
AT-8	1.67	0.23	1.57	644	39.1	170.1	151.9	9	2.3	0.17	13.8	<0.01	0.01
AT-9	5.07	1.42	11.62	70	32.5	6.0	21.7	20	33.4	0.23	2.0	<0.01	<0.002
AT-10	1.92	2.37	6.28	651	11.9	74.7	10.7	<5	37.1	0.18	3.1	0.03	0.04
CH-1	2.20	0.19	8.75	82	36.9	3.5	104.8	<5	46.3	2.23	3.4	0.17	0.07
CH-2	1.68	0.33	69.59	292	62.3	87.2	23.8	<5	82.8	4.46	4.6	0.76	1.15
CH-3	2.63	0.10	25.27	120	134.6	3.0	69.7	<5	>100.0	9.30	4.9	0.97	1.67
CH-6B	4.79	0.16	151.12	109	84.1	104.5	19.0	<5	>100.0	5.33	2.8	0.34	0.37
CH-7	1.61	0.13	7.21	130	49.0	2.5	43.9	75	18.6	1.06	3.6	0.10	0.06
CB-2	7.85	1499.48	5.96	17	1.5	234.9	419.4	>50000	>100.0	242.56	2.1	<0.01	<0.002
CB-8	6.51	567.91	1.58	426	1.4	5.0	524.2	>50000	>100.0	>1000.00	0.9	<0.01	<0.002
CB-4	32.50	213.63	0.75	60	0.5	301.8	161.2	>50000	9.0	28.57	0.9	<0.01	<0.002
BG-1	0.55	40.75	0.81	148	3.4	5.3	80.7	>50000	3.0	819.71	1.2	0.01	0.00
MD-3	15.84	24.73	0.06	50	<0.5	225.4	473.4	2561	1.6	>1000.00	1.1	<0.01	<0.002
MD-4	2.77	6.46	0.05	7	0.6	6.0	60.6	2999	0.6	8.56	0.6	<0.01	<0.002
FSY	0.15	0.88	0.07	120	45.6	94.0	196.2	260	0.3	6.58	6.2	<0.01	<0.002
FBRDMP	0.07	0.42	0.07	67	20.8	4.5	142.9	386	<0.1	1.05	4.4	<0.01	0.00

Table 4 Contd; Geochemical data for Allard tunnel (AT), Copper Hill (CH), Cumberland (CB), Bessie G (BG), Mayday (MD), and country rocks, (FSY). All analyses are in parts per million (ppm).

Statistical Analysis

A Pearson correlation matrix was calculated in Excel, using the geochemical data on the La Plata district gathered for this study. Linear correlations were determined for every pair of elements calculated from Mo, Cu, Pb, Zn, Ag, Ni, Co, Mn, Fe, U, Au, Cd, Sb, Bi, V, Cr, Hg, Se, Te, Pd and Pt. Although there are far too few data points to accurately characterize the district overall, results indicate several moderate to strong correlations between different elements. Plots were produced using both log normalized (Table 5) and "raw" (Table 6) concentration data.

There is a strong correlation between Pb and Ag, presumably within galena. Co, Mn, Fe, Bi, V, Se, and Pt are strongly correlated with Cu, while Au and Ag show a negative correlation to Cu. Ag is positively correlated to Au, Cd, Sb, Se, and Te. Sb, Hg, and Te are all positively correlated with Au, which likely occur as gold-bearing tellurides. Bi and Sb show a strong positive correlation, and the Allard Stock contains anomalous bismuth (Werle et al., 1984). Pt and Pd strongly correlate with Cu, Co, Fe, U, Bi and Se. Pt and Pd show are not correlated with Te.

Table 5. Log Normal Correlation Matrix

	Cu	Pb	Zn	Ag	Co	Mn	Fe	Au	Cd	Sb	Bi	V	Cr	Hg	Se	Pd	Pt
Mo	0.222682	0.178916	0.012894	-0.2889	0.277419	0.319431	0.271456	-0.42179	-0.02594	-0.13251	0.130395	0.203933	0.080462	-0.43227	0.210572	-0.24467	-0.17682
Cu		0.073896	0.21561	0.153893	**0.678549**	**0.596137**	**0.526534**	-0.52966	0.268656	-0.31709	**0.87783**	**0.526797**	0.05474	-0.57031	**0.795976**	0.412196	**0.555709**
Pb			**0.877794**	**0.639489**	-0.25891	-0.39533	-0.26626	0.394835	**0.831731**	0.456119	0.159597	-0.18346	**0.543546**	0.23566	0.34714	0.060069	-0.00306
Zn				**0.569352**	-0.27115	-0.33568	-0.30266	0.309717	**0.935136**	0.479321	0.159391	-0.18533	**0.550896**	0.255378	0.405383	-0.02087	-0.03961
Ag					-0.12888	-0.44815	-0.22186	**0.675806**	**0.698374**	**0.50706**	0.382708	-0.17522	0.297672	0.324056	**0.564643**	0.438071	0.292228
Co						**0.789521**	**0.867364**	-0.62394	-0.22255	-0.76111	**0.669563**	0.439226	-0.1707	-0.86287	0.439335	**0.585879**	**0.638782**
Mn							**0.765569**	-0.87052	-0.3511	-0.73363	0.382675	**0.654993**	-0.07135	-0.79477	0.147747	0.125761	0.372262
Fe								-0.63008	-0.27257	-0.75087	**0.550254**	0.448138	-0.06251	-0.87443	0.247291	**0.515698**	**0.667752**
As								**0.500756**	0.296067	**0.533543**	-0.25148	-0.41779	0.003027	**0.667355**	-0.09651	-0.26904	-0.45663
Au									0.411863	**0.686862**	-0.2618	-0.53568	0.161938	**0.728151**	-0.04899	0.070832	-0.16171
Cd										**0.527714**	0.271569	-0.21426	0.421479	0.295193	**0.551912**	0.093791	0.057509
Sb											-0.28372	-0.35603	0.316068	**0.847213**	0.081765	-0.38252	-0.50287
Bi												0.333631	0.01917	-0.50905	**0.827546**	**0.686744**	**0.735931**
V													0.11712	-0.49711	0.214975	0.074609	0.308924
Cr														0.098059	0.041439	-0.16406	-0.01942
Hg															-0.25456	-0.42964	-0.59649
Se																0.491088	0.476743
Te																0.052872	-0.16787
Pt																	**0.898924**

Table 5: Bold numbers signify strong positive correlations.

Table 6. Raw Correlation Matrix

	Cu	Pb	Zn	Ag	Co	Mn	Fe	Au	Cd	Sb	Bi	V	Cr	Hg	Se	Pd	Pt
Mo	-0.06475	-0.08854	-0.12497	-0.33694	0.234188	0.184053	0.143474	-0.16456	-0.14907	-0.134	-0.0014	0.12103	-0.16277	-0.21617	-0.15375	-0.18003	-0.16446
Cu		-0.26442	-0.26431	-0.06582	**0.653445**	**0.557894**	**0.604814**	-0.45331	-0.2689	-0.14575	0.393675	0.395807	-0.1652	-0.41699	0.398773	0.427791	0.38332
Pb			**0.979713**	0.475823	-0.24298	-0.26912	-0.21975	0.260122	**0.967112**	0.040921	0.041618	-0.2158	**0.728679**	0.367122	-0.10695	-0.08403	-0.08385
Zn				0.466048	-0.31135	-0.28215	-0.26806	0.198868	**0.990284**	0.165201	-0.07617	-0.19655	**0.748951**	0.460196	-0.081	-0.11399	-0.10292
Ag					-0.11041	-0.51395	-0.1508	0.482952	**0.531885**	0.427189	0.400692	-0.33563	0.426782	**0.626335**	**0.601522**	0.338548	0.296006
Co						0.348162	**0.764589**	-0.37385	-0.30897	-0.32858	**0.501699**	0.126066	-0.26398	-0.49444	0.363657	0.460057	0.397692
Mn							**0.535001**	-0.34567	-0.32098	-0.29093	-0.03816	**0.74693**	-0.07402	-0.43582	-0.19281	-0.14403	-0.11725
Fe								-0.33428	-0.28728	-0.31907	0.389093	0.364375	-0.09493	-0.4549	0.263232	0.397169	0.384254
As								0.091152	0.402165	**0.896739**	-0.14476	-0.27283	0.358015	**0.726973**	0.454772	-0.16471	-0.1612
Au									0.220581	0.030626	-0.14474	-0.20471	0.202488	0.372252	-0.1995	-0.15228	-0.14003
Cd										0.24626	-0.04448	-0.24353	**0.750051**	**0.512247**	0.006134	-0.11264	-0.10343
Sb											-0.10082	-0.15785	0.412082	**0.67807**	0.495445	-0.14647	-0.1307
Bi												-0.10836	0.050259	-0.18206	**0.57419**	**0.521182**	0.434604
V													0.023937	-0.1719	-0.11195	-0.11993	-0.08505
Cr														**1**	0.362885	0.0151	-0.13201	-0.12004
Hg															0.247922	-0.2158	-0.19573
Se																**1**	**0.616724**	**0.581186**
Te																-0.18583	-0.16834
																	0.987106

Isotope Geochemistry

Isotopic analyses conducted as part of this study on the Allard stock include isotopes ratios for sulfur, copper, and lead isotopes. Mineralized samples of chalcopyrite and pyrite from both Allard Tunnel and Copper Hill were analyzed for sulfur isotopes (Table 7). Relative to standards, results had an error of ± 0.03 σ. A histogram of $\delta^{34}S_{(VCDT)}$ values is shown in Figure 12. Sulfur values fall within the normal expected range for porphyry Cu deposits. The range $\delta^{34}S_{(VCDT)}$ for the Allard Stock is perhaps indicative of a slight sedimentary sulfur input from wall rocks (as evidenced by a depleted $\delta^{34}S$), coupled with a mostly magmatic sulfur signature, at 0‰.

Table 7. Sulfur isotope values for AT and CH.

Sample	Sulfide Phase	Theoretical Yield	Yield	% Yield	$\delta^{34}S_{(VCDT)}$
AT-1B	CPY	76.3	52.1	68.3	-6
AT-2	CPY	87.2	60.8	69.7	-5.5
AT-4	Pyrite	100.0	52.6	52.6	-3.6
AT-3	CPY	76.3	66.4	87.0	-6.8
AT-7	Pyrite	100	70.1	70.1	-5.1
AT-8	CPY	76.3	18.4	24.1	0.3
AT-9	Pyrite	100.0	74.7	74.7	-4.3
AT-10	Pyrite	100.0	82.0	82.0	-3.8
CH-1	CPY	65.4	53.0	81.0	-6.2
CH-2	CPY	87.2	90.4	103.7	-7.8
CH-3	CPY	87.2	67.3	77.2	-5.1
CH-5	CPY	65.4	50.7	77.5	-4.0
CH-6B	CPY	76.3	35.0	45.9	-6.2
CH-7	CPY	65.4	60.8	93.0	-7.7

Table 7. Table of sulfur isotope analyses conducted at the UGA Stable Isotope Laboratory, n=15 samples.

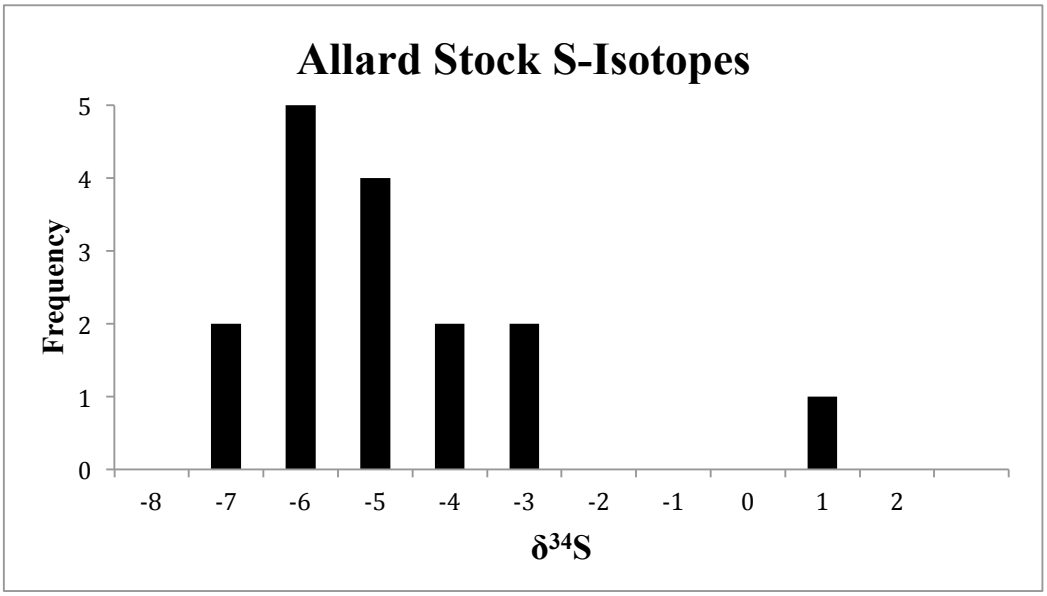

Fig. 12. Distribution of sulfur isotope values for La Plata analyses, n=17 samples. Values reported as $\delta^{34}S_{(VCDT)}$. Includes two data points from commercial analyses CH-1 ($\delta^{34}S$ = -5.8) and AT-1 ($\delta^{34}S$ = -6.0).

Copper Isotopes

Analyses carried out by Dr. Ryan Mathur are shown in Figure 13. Separates from chalcopyrite mineralization at Allard Tunnel and Copper Hill were analyzed for this study, and fall within the typical range for porphyry Cu-deposits (± 3 ‰ δ^{65}Cu) that show a magmatic Cu source. Two samples were collected by Dr. Gonzales from Ft. Lewis College and therefore have no concrete spatial data to accompany them. The other two samples were collected by the author during field work and are splits of samples used for other geochemical analyses and for petrography. Copper isotope ratios are reported in the familiar delta notation:

$$\delta^{65}\mathrm{Cu}(‰) = \left[\left(\frac{^{65}\mathrm{Cu}/^{63}\mathrm{Cu}_{\mathrm{sample}}}{^{65}\mathrm{Cu}/^{63}\mathrm{Cu}_{\mathrm{NIST976}}}\right) - 1\right] \times 1000$$

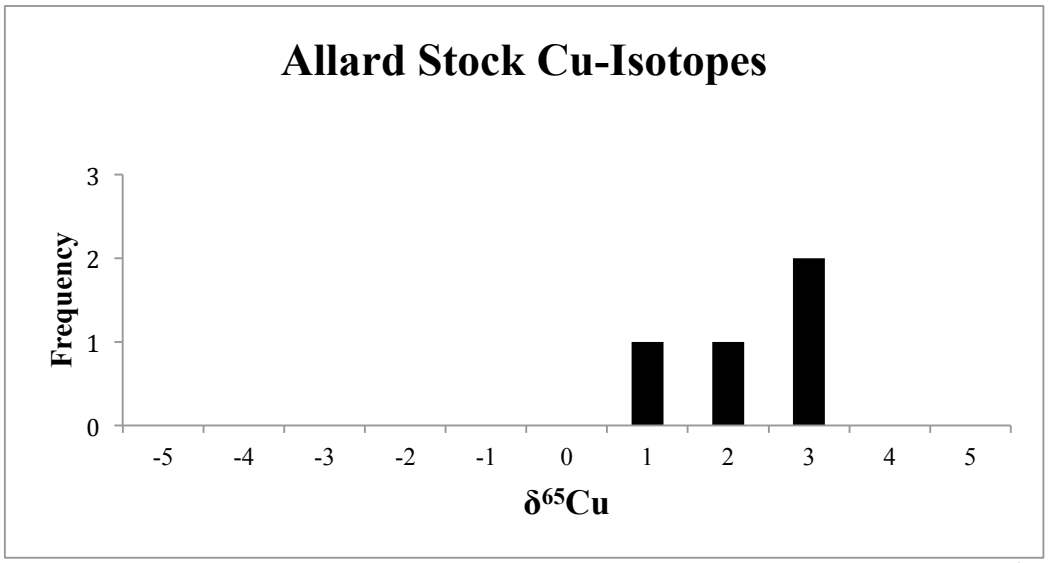

Fig. 13. Distribution of copper isotope values for La Plata analyses, n=4 samples. Values reported as $\delta^{65}Cu$. Samples collected from the Allard Stock by Dr. Gonzales at Ft. Lewis College yielded $\delta^{65}Cu$ of 0.965 ‰ and 1.380 ‰. Samples collected by the author were AT-9 (2.700 ‰) and CH-6 (2.570 ‰).

Lead Isotopes

Lead isotope analyses were conducted on ten La Plata district samples to determine the source of lead within the sulfide mineralization, with 3 from Allard tunnel, 3 from Copper Hill, 2 from Bessie G, and 2 from Cumberland (Table 8 and Fig. 14). Samples include AT-1, AT-9, CH-1, CH-3, and CH-6. $^{206/204}Pb$ values range from 17.91 to 19.5, $^{207/204}Pb$ values range from 15.59 to 15.67, and $^{208/204}Pb$ values range from 37.8 to 38.51.

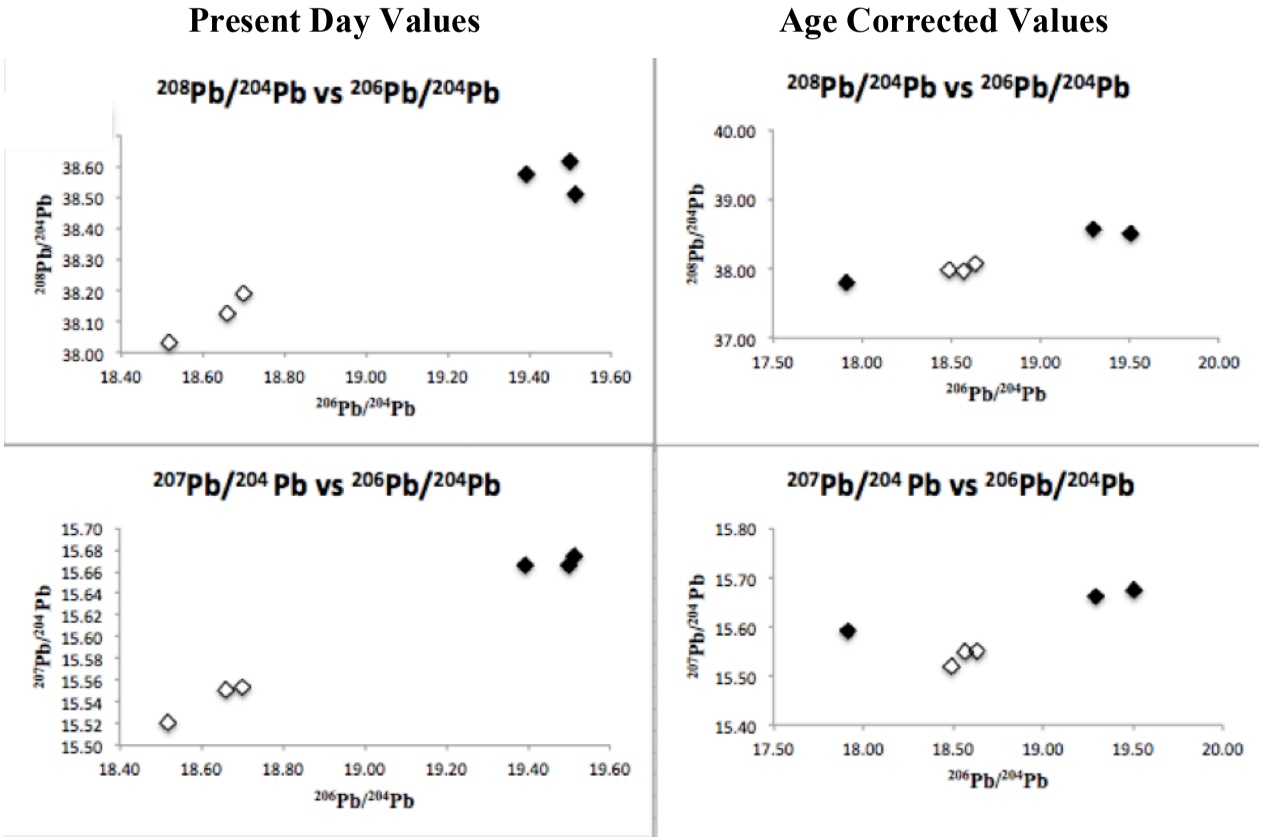

Fig 14. Plots of lead isotope results showing Allard Tunnel (closed diamonds) and Copper Hill (open diamonds). Present day values are presented on the left and age corrected values are on the right.

Table 8. Lead Isotope Analysis Results

Pb Isotopes and U, Th, Pb Concentrations

Present Day

Sample	$^{206}Pb/^{204}Pb$	$^{207}Pb/^{204}Pb$	$^{208}Pb/^{204}Pb$
AT-1 HF fraction (silicate)	19.500	15.666	38.618
AT-1 sulfide	19.393	15.666	38.575
AT-9 sulfide	19.513	15.674	38.513
CH-1 sulfide	18.701	15.554	38.191
CH-3 sulfide	18.519	15.521	38.032
CH-6 sulfide	18.661	15.551	38.127
CB-1 silicate	21.533	15.860	38.996
CB1-naumanite	21.832	15.896	39.108
BG-1 silicate	22.197	15.926	39.233
BG-1 naumanite	20.622	15.770	38.558

Sample	Pb (ppm)	U (ppm)	Th (ppm)
AT-1 HF fraction (silicate)	0.238	0.487	0.781
AT-1 sulfide	21.119	2.678	0.165
AT-9 sulfide	165.572	1.355	1.908
CH-1 sulfide	11.767	2.067	10.852
CH-3 sulfide	5.482	0.211	1.091
CH-6 sulfide	46.555	1.603	9.837
CB-1 silicate	306.496	0.200	0.041
CB1-naumanite	30.076	0.256	0.051
BG-1 silicate	6.605	0.448	2.718
BG-1 naumanite	3.795	0.032	0.285

Sample	^{204}Pb	$^{238}U/^{204}Pb$	$^{235}U/^{204}Pb$	$^{232}Th/^{204}Pb$
AT-1 HF fraction (silicate)	1.337	151.974	1.102	245.826
AT-1 sulfide	1.340	9.396	0.068	0.582
AT-9 sulfide	1.339	0.607	0.004	0.861
CH-1 sulfide	1.362	12.811	0.093	67.733
CH-3 sulfide	1.369	2.794	0.020	14.541
CH-6 sulfide	1.364	2.506	0.018	15.496
CB-1 silicate	1.292	0.050	0.000	0.010
CB1-naumanite	1.285	0.657	0.005	0.133
BG-1 silicate	1.276	5.279	0.038	32.242
BG-1 naumanite	1.317	0.643	0.005	5.698

Age Corrected (67 Ma)

Sample	$^{206}Pb/^{204}Pb$	$^{207}Pb/^{204}Pb$	$^{208}Pb/^{204}Pb$
AT-1 HF fraction (silicate)	17.913	15.591	37.802
AT-1 sulfide	19.295	15.662	38.573
AT-9 sulfide	19.506	15.673	38.510
CH-1 sulfide	18.568	15.547	37.966
CH-3 sulfide	18.489	15.519	37.984
CH-6 sulfide	18.635	15.550	38.075
CB-1 silicate	21.532	15.860	38.996
CB1-naumanite	21.825	15.895	39.108
BG-1 silicate	22.142	15.923	39.126
BG-1 naumanite	20.615	15.770	38.539

Petrology and Petrography of Ores and Associated Rocks

Eckel (1949) provided a generalized but thorough petrographic analysis of ore samples and country rocks in the La Plata district, however only a cursory description of the Allard stock and associated mineralization was completed. This study further investigates the host rock and ore petrography at the Allard tunnel and Copper Hill deposits within the Allard stock. A brief analysis of the Cumberland, Bessie G. and May Day deposits' ore petrography is also included. Throughout the district, gold, tellurium, copper and silver are the most abundant elements in mineralization with gold (both native and in Au-Ag tellurides) being the largest commodity mined historically. Lead, silver, and copper were also productively mined but to a lesser extent.

What Eckel (1949) refers to as diorite monzonite porphyry, is actually a range of monzonitic to dioritic to syenitic intrusive porphyries. Eckel (1949) chose the naming scheme of diorite monzonite porphyry and syenite porphyry as simplistic field names to differentiate between two general types of porphyries in the district. Samples collected in this study plot in the monzonite, monzodiorite, and syenite fields on a total alkali vs silica (TAS) diagram, further evidencing their overlap. The diorite monzonite porphyry (DMP) has a porphyritic texture with feldspar ± hornblende ± augite in a gray to brown groundmass. It is much darker in color than the syenite porphyry and has smaller phenocrysts of feldspar. The DMP is not as extensively mineralized as the syenite (Eckel, 1949). The syenite porphyry contains larger feldspar phenocrysts, is more feldspathic, and contains augite rather than hornblende. The syenite porphyry is also more heavily altered than the diorite monzonite porphyry and feldspars are converted to sericite ±

kaolinite ± zoistite ± carbonate (ankerite?) and pyroxenes have altered to hornblende ± limonite ± chlorite. “Fresh” syenite contains plagioclase ± orthoclase ± augite ± apatite ± sphene ± chlorite. Even the most unaltered syenite found during field work for this study showed moderate seritizitation and pyritization, evidence of the pervasive potassic alteration, local propylitic (Fig. 15) alteration, the slight and quartz-sericite-pyrite alteration of the Allard stock.

Ore minerals in the Allard stock consist of chalcopyrite ± pyrite ± magnetite ± hematite (specular) ± galena ± sphalerite (Fig. 16). Mineralization at Allard tunnel typically occurs within breccias, stockwork veins (Fig. 15) and is also moderately disseminated throughout most of the Allard stock. At Copper Hill, the glory hole contains massive chalcopyrite (Fig. 17) with azurite ± malachite with minor covellite ± bornite (Fig. 16). A major northeast trending vein appears to be the conduit for mineralizing fluids at Copper Hill (Fig. 18), as is the trend throughout the district. Allard tunnel samples contain roughly 30% more pyrite relative to chalcopyrite than those from Copper Hill.

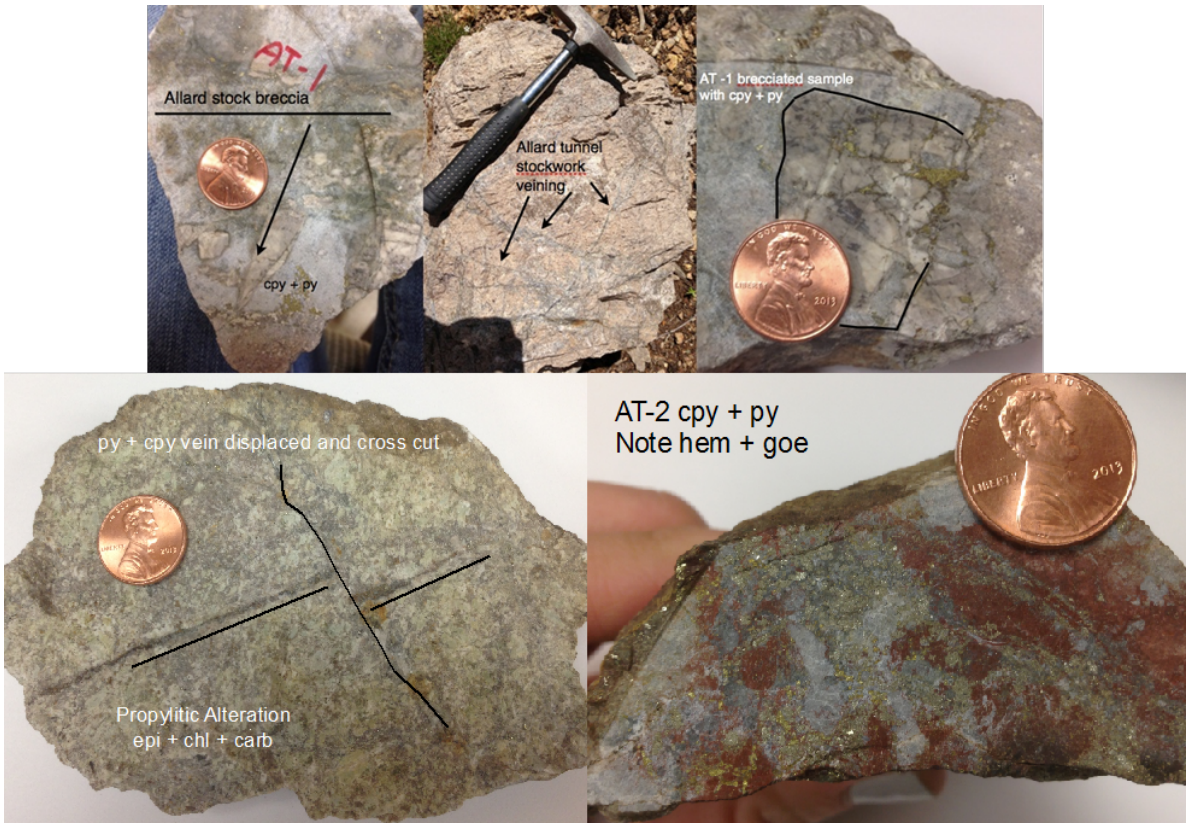

Fig. 15. Photomicrographs of mineralization from Allard Tunnel. From top left to bottom right: An example of hydrothermal brecciation, stockwork pyrite and chalcopyrite veins within pink syenite, brecciation cemented by chalcopyrite and chalcopyrite, propylitic alteration and offset veining, and pyrite, chalcopyrite, hematite, and goethite as evidence of oxidation.

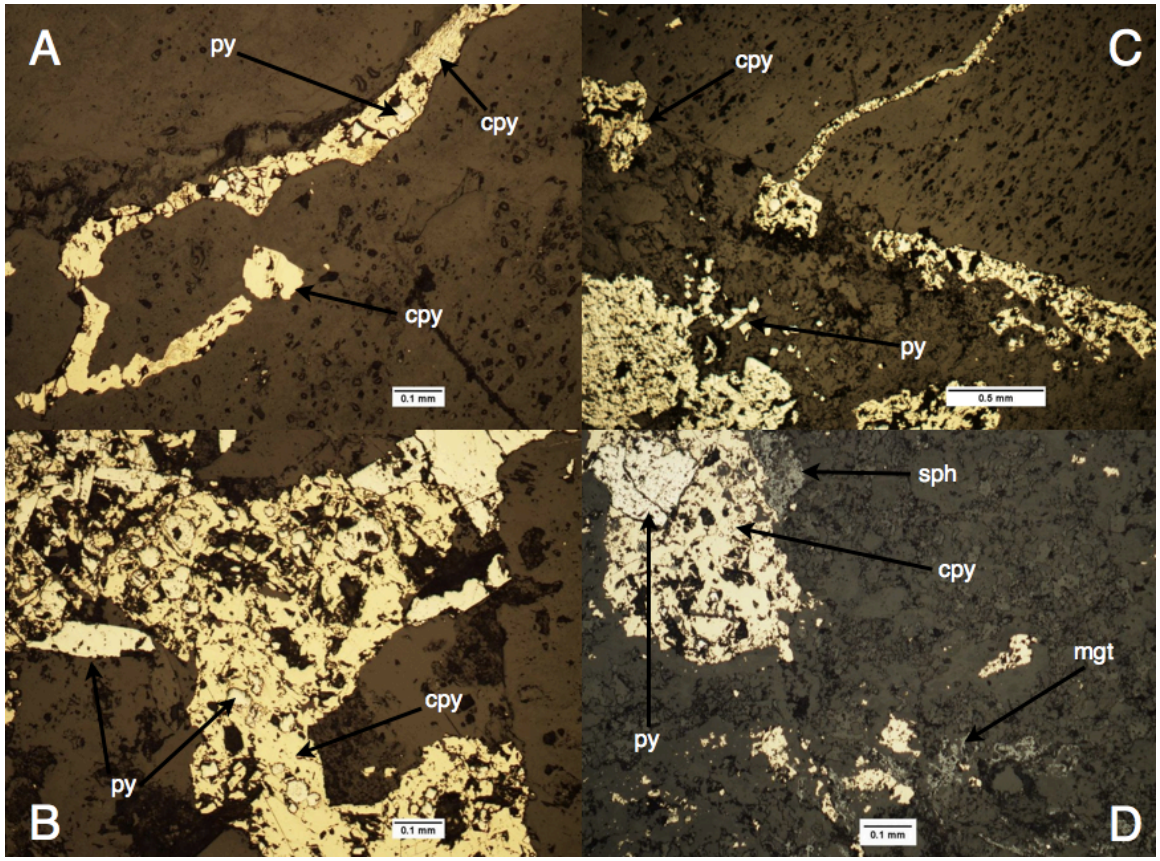

Fig. 16. Photomicrographs of Allard tunnel samples in reflected light. A) pyrite surrounded by chalcopyrite in veinlets. B) massive chalcopyrite with pyrite, C) veinlets and blebs of chalcopyrite and pyrite, note finer grain size than previous photomicrograph, D) pyrite grain surrounded by chalcopyrite and sphalerite with minor magnetite.

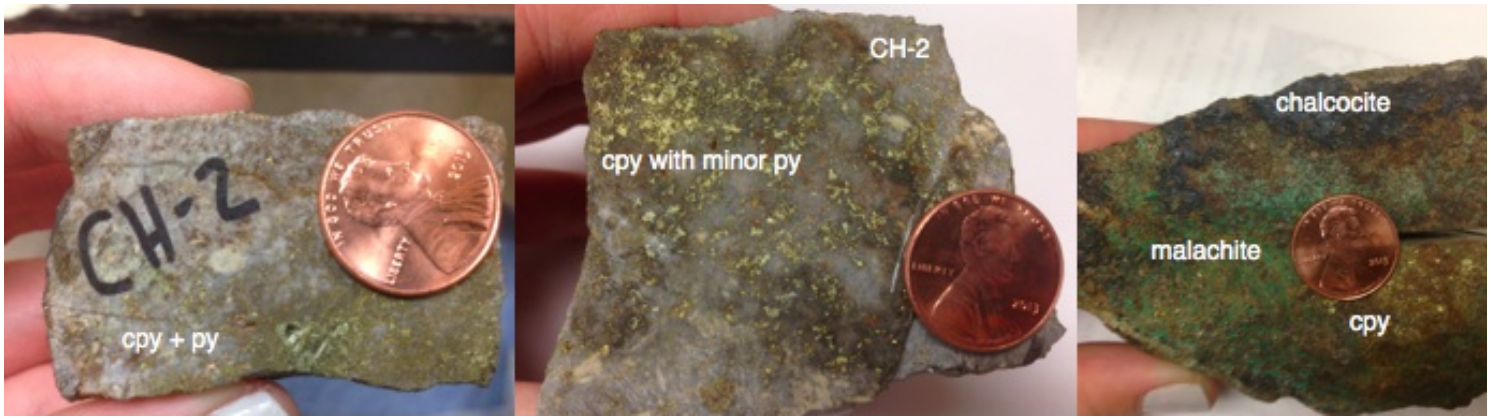

Fig. 17.Photographs of hand samples from the Copper Hill glory hole show extensive chalcopyrite mineralization within a contact-metamoprhic setting between the Allard stock syenite and the surrounding sedimentary rocks (likely the Pony Express limestone). Mineralization at copper hill contains much less pyrite than mineralization at the Allard tunnel and far more chalcopyrite. Copper oxidation minerals at Copper Hill consist of malachite and azurite, however some chalcocite and chrysocolla are also present in outcrop at the glory hole.

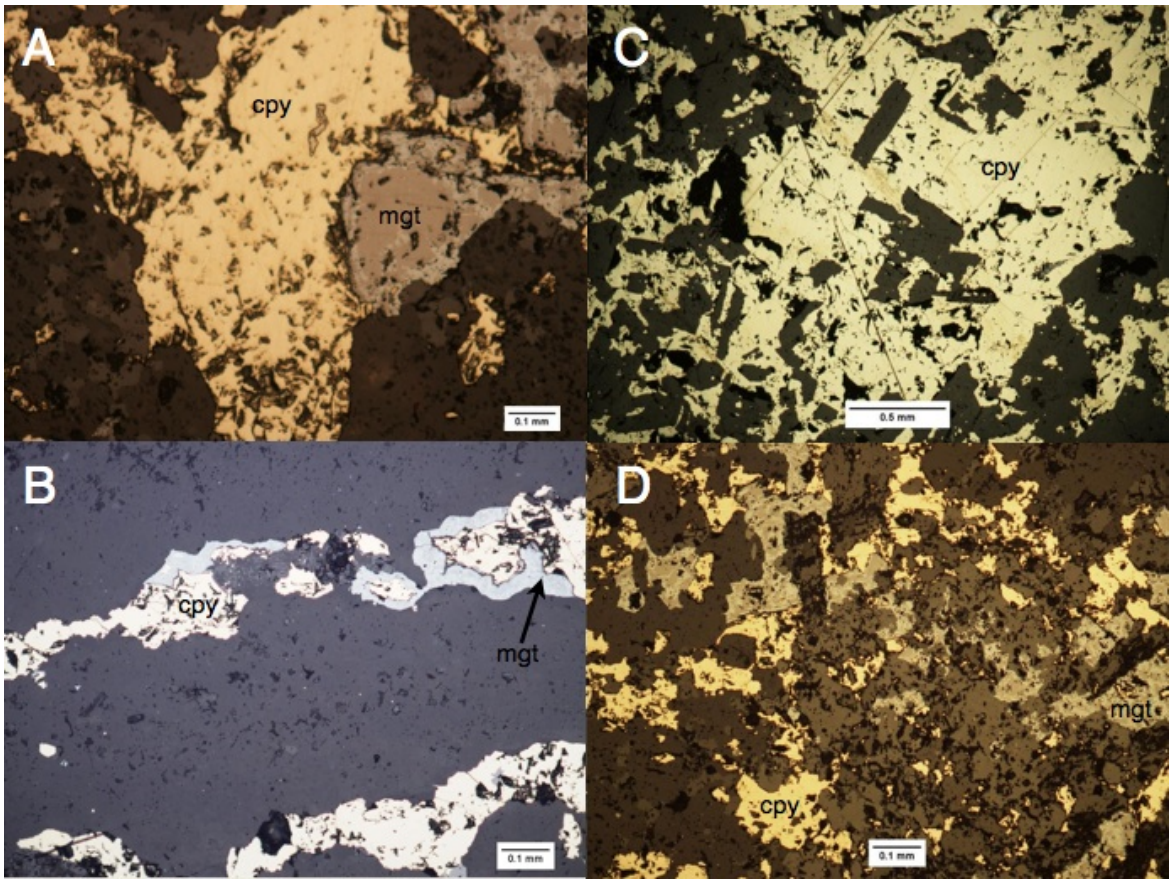

Fig 18. Photomicrographs in reflected light from Copper Hill. A) Common relationship between chalcopyrite and magnetite, B) magnetite wrapping around chalcopyrite within a veinlet, C) massive chalcopyrite around of apatite and minor quartz, D) Example of disseminated magnetite and chalcopyrite.

.

Fig. 19. Outcrop photographs from the Copper Hill glory hole and the NE-trending vein mined there. The first photo looks down on the vein from the entrance to the glory hole, and the second photo looks up the vein from the bottom of the glory hole. This main vein, however, is not the only source of chalcopyrite in the vicinity of the glory hole. Chalcopyrite is massive in and around the glory hole

Ore mineral paragenesis in the Allard stock is typically uniform; however some differences in mineralogy do exist between the samples from Allard tunnel and Copper Hill (Table 9). The generalized paragenetic sequence determined by this study is as follows. (1) Pyrite and bornite appear to be the earliest ore phases, followed by (2) covellite, magnetite/iron oxides, and sphalerite, then ruby silvers and acanthite, and chalcopyrite, galena, and Pt-Pd-Bi-tellurides seem to be the latest ore phases. Gangue minerals within hypogene veins include (1) sanidine, (2) quartz, and (3) calcite±fluorite. Vein calcite is abundant and vein quartz is also present. Werle et al. (1984) detailed the vein occurrences within the Allard stock: (1) iron oxide – pyrite – copper sulfarsenite – copper sulfide – calcite – quartz veins; (2) calcite – quartz – sphalerite – galena – chalcopyrite – pyrite veins; (3) fluorite – quartz – pyrite – chalcopyrite – marcasite veins. Small base metal sulfide veins and mantos and quartz – pyrite – fluorite – telluride veins that occur peripheral to the stock may have formed at the same time as vein types (2) and (3) within the stock.

Sample AT-4 shows the best evidence for the paragenetic sequence in the Allard tunnel samples (Fig. 20). Bornite with possible chalcopyrite exsolution textures is surrounded by covellite, both are rimmed by chalcopyrite, and sphalerite occurs after chalcopyrite. Covellite, bornite, and chalcopyrite are all hydrothermal hypogene minerals. Another example from AT-4 shows an interesting exsolution texture within bornite, which seems to be indicative of chalcopyrite exsolving bornite (Fig. 21). Chalcopyrite occurs much less abundantly within the Allard tunnel samples than within the Copper Hill samples.

Table 9: Allard Stock Ore Minerals in order of Abundance for AT and CH

Allard Tunnel	**Copper Hill**
Pyrite	Chalcopyrite
Chalcopyrite	Bornite
Sphalerite	Pyrite
Magnetite (minor)	Covellite
Galena (minor)	Magnetite/ Iron Oxides
-	Sphalerite
--	Galena
-	Ruby silvers (Pyrargyrite)
-	Acanthite
-	Pt+Pd+Bi+Tellurides

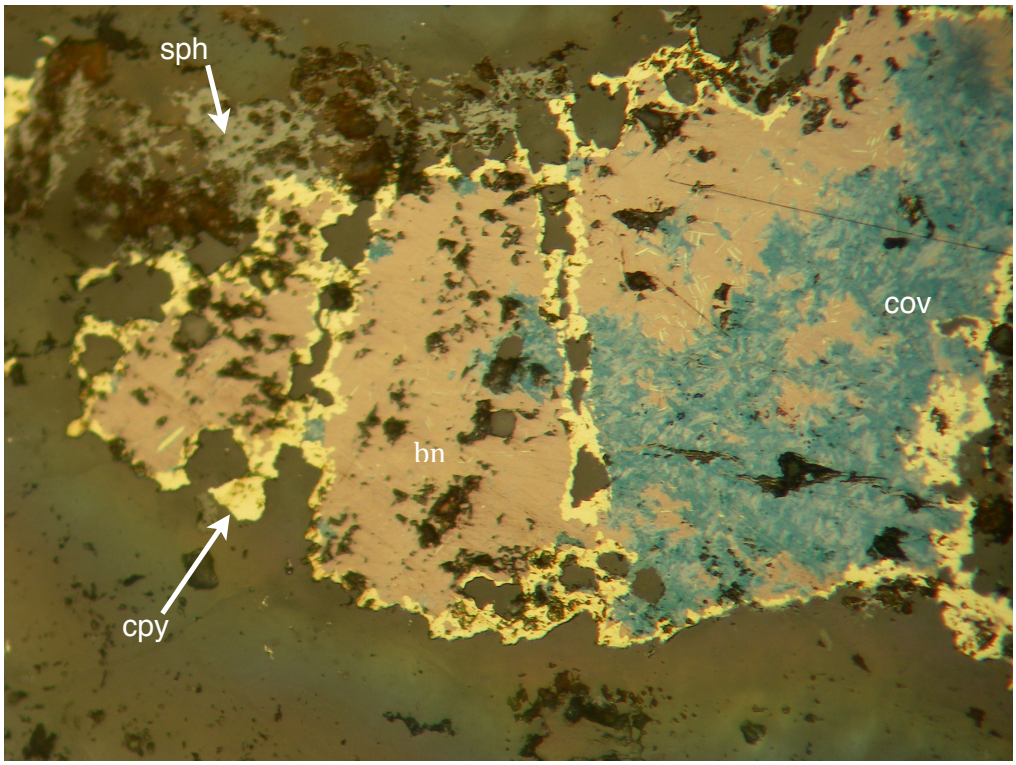

Fig. 20. Reflected light photomicrograph of the paragenetic sequence at the Allard stock (minus pyrite). Minerals include chalcopyrite (cpy), bornite (bn), covellite (cov), and sphalerite (sph). Field of view is 1 mm.

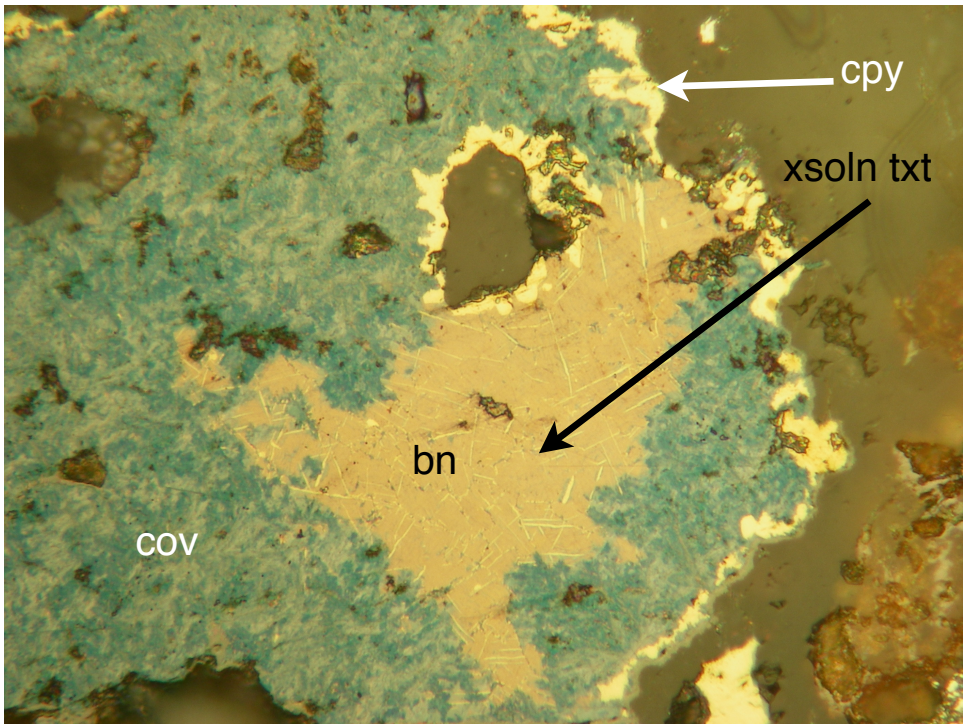

Fig. 21. Reflected light photomicrograph of AT-4 showing the relationship between chalcopyrite (cpy), bornite (bn), and covellite (cov) with a possible bornite exsloution texture (bn to cpy). Field of view is 1 mm.

Hydrothermal calcite veining is abundant in the Allard stock, as is the associated propylitic alteration of the porphyry system (Fig. 15). Clearly a CO_2 rich source existed at depth to provide such volatile rich fluid when this deposit formed. Ore minerals chalcopyrite and pyrite are abundant in calcite veins in the Allard stock (Fig. 22), and most commonly occurs within the Allard tunnel samples. Framboidal pyrite also appears in mineralization at the Allard stock (Fig. 23.) Ruby silvers (pyrargyrite±proustite) were found using reflected light microscopy (Fig. 24) as was acanthite (Fig. 25). Using the electron microprobe, Ag-tellurides were also identified.

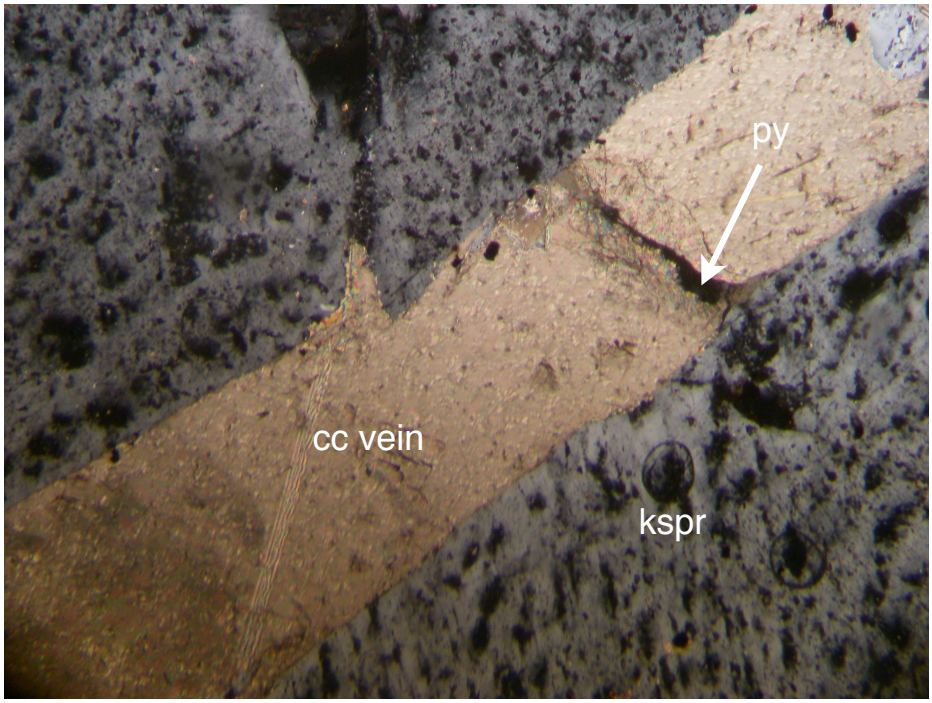

Fig. 22. Transmitted light Photomicrograph of a calcite vein crosscutting potassium feldspar in sample AT-1. Note the association of opaque minerals (pyrite) within the hydrothermal calcite vein. Ore minerals chalcopyrite and pyrite are abundant in calcite veins in the Allard stock. Field of view is 2 mm.

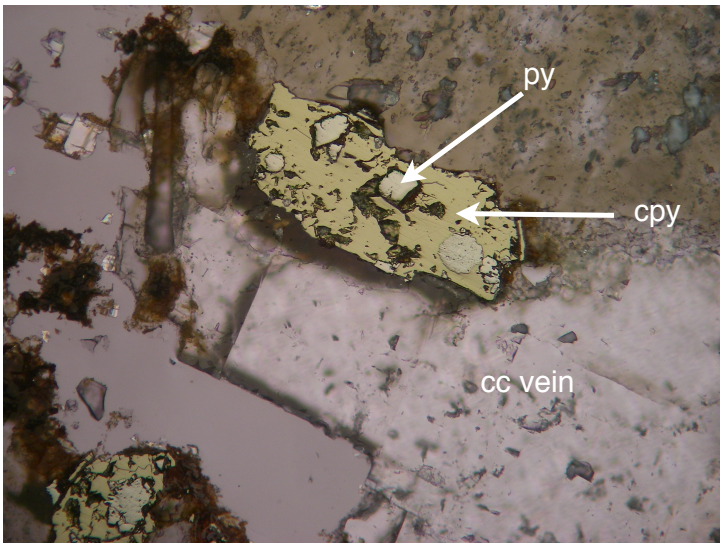

Fig. 23. Photomicrograph using both transmitted and reflected light to show the ore minerals (pyrite and chalcopyrite) as well as the calcite vein. Framboidal pyrite also exists in the Allard stock (grain directly under the chalcopyrite arrow).

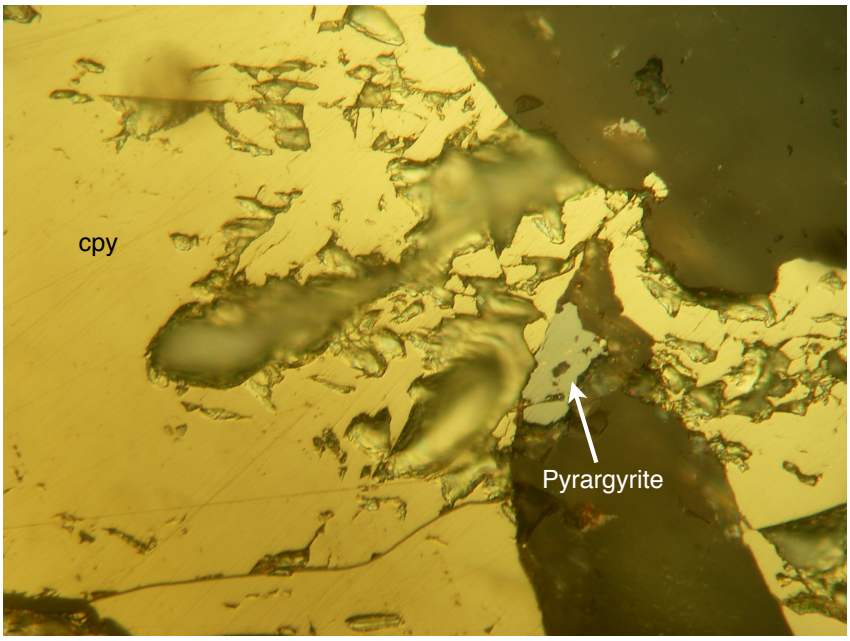

Fig. 24. Photomicrograph of pyrargryite associated with massive chalcopyrite at Copper Hill. Field of view is 1 mm.

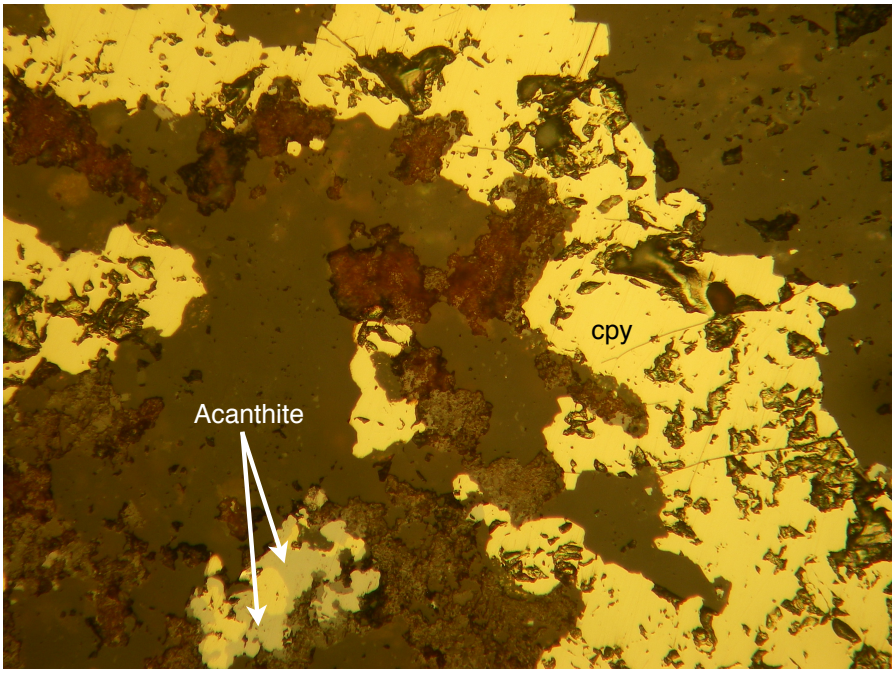

Fig. 25. Photomicrograph of acanthite associated with massive chalcopyrite at Copper Hill. Field of view is 1 mm.

Two other epithermal deposits and one limestone replacement/skarn deposit were included in this study (Fig. 26). At Cumberland and Bessie G, Au-Ag tellurides are common as is native gold. Cumberland samples contain conspicuous azurite and malachite, possibly as remnant evidence of Cu-tellurides. Mayday ore occurs as veins within a limestone replacement/skarn type deposit with galena±sphalerite±tellurides

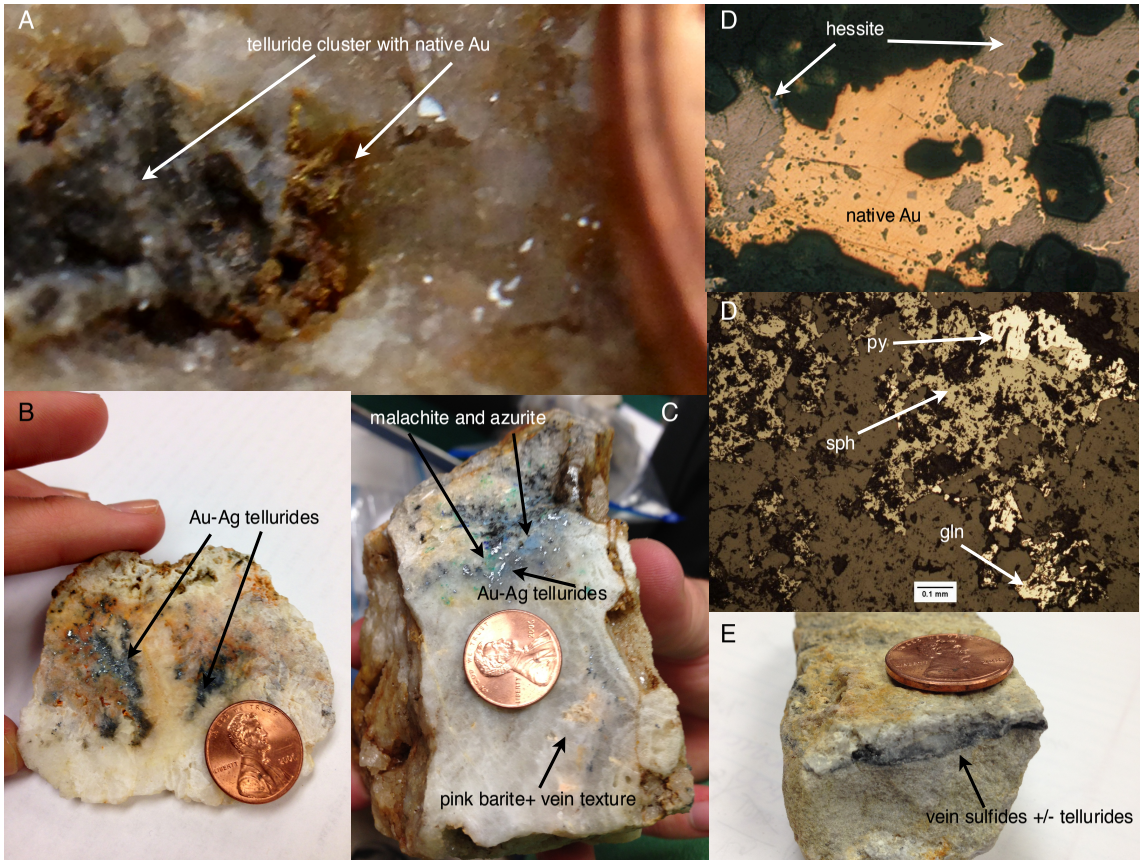

Fig. 26. Photos and photomicrographs of La Plata district epithermal and limestone replacement-type deposits. A) Native gold on Au-Ag tellurides, Cumberland. B) Au-Ag tellurides in hand sample with quartz and barite. C) Cumberland hand sample showing azurite and malachite (supergene?) in association with tellurides (coloradoite, hessite, etc) and pink barite with a typical epithermal open-space-filling vein texture with banding. D) Photomicrograph of a Bessie G sample in reflected light showng native Au associated with hessite. E) Reflected light photomicrograph of a Matyday sample showing sphalerite, galena, and pyrite. E) Handsample from Mayday showing vein sulfites likely in association with tellurides.

Electron microprobe analysis of 6 samples from the Copper Hill glory hole resulted in the recognition of PGE-bearing mineral grains with several different compositions and mineral associations. Samples for microprobe analysis were chosen based on Pt and Pt compositions from geochemical analyses, with concentrations >1 ppm selected as the most favorable for analysis. Element peaks, element maps, and compositional analyses were gathered for grains if they were sufficiently large enough (>3 μm) to permit accurate compositional analysis. Atomic proportions and elemental weight percent of compositional analyses (Table 10) are reported for PGE-mineral grains, and several Ag-Se-Bi minerals. Microprobe-EDS images and spectra are presented below in figures 27-44 and will be discussed in the following section of this thesis.

Table 10. Microprobe Analyses for Copper Hill

Atmoic Proportions

	Fe	S	As	Cu	Se	Ag	Bi	Te	Au	Pt	Pd
CH-2-1	0.37	17.74	2.24	3.96	1.79	72.51	1.17	0.07	0.03	0.09	0.03
CH-3-1	11.34	40.02	-0.02	26.40	2.43	0.45	0.04	19.36	-0.04	0.01	0.01
CH-3-2	10.21	39.36	-0.10	26.63	2.82	0.40	-0.02	20.76	0.00	-0.07	0.02
CH-3-3	14.49	0.26	0.14	1.57	-0.03	0.38	2.76	52.77	1.10	19.31	7.25
CH-3-4	1.05	0.35	-0.05	1.61	0.07	0.78	4.61	59.74	0.48	14.67	16.69
CH-4-1	3.12	10.63	-0.06	5.06	0.46	29.95	0.01	29.06	0.07	-0.10	21.81
CH-2-2	0.21	0.04	0.00	0.11	0.01	1.12	0.83	64.30	0.40	3.59	29.39
CH -Z-1	2.12	31.36	0.03	10.68	0.06	2.43	11.26	21.26	0.42	9.63	10.77

Weight Percent

	Fe	S	As	Cu	Se	Ag	Bi	Te	Au	Pt	Pd
CH-2-1	0.22	5.93	1.75	2.62	1.47	81.57	2.55	0.09	0.06	0.18	0.03
CH-3-1	9.71	19.68	-0.02	25.73	2.94	0.74	0.14	37.89	-0.11	0.03	0.01
CH-3-2	8.40	18.59	-0.11	24.92	3.28	0.63	-0.05	39.02	-0.01	-0.20	0.03
CH-3-3	6.31	0.06	0.08	0.78	-0.02	0.32	4.49	52.45	1.69	29.35	6.01
CH-3-4	0.46	0.09	-0.03	0.80	0.05	0.66	7.51	59.44	0.74	22.31	13.85
CH-4-1	1.56	3.06	-0.04	2.88	0.32	28.98	0.02	33.26	0.12	-0.17	20.82
CH-2-2	0.10	0.01	0.00	0.06	0.01	1.01	1.45	68.67	0.66	5.86	26.18
CH -Z-1	1.20	10.25	0.02	6.92	0.05	2.67	23.97	27.64	0.83	19.15	11.68

Weight Percent Oxide

	FeO	SO_3	As_2O_3	Cu_2O	SeO_2	Ag_2O	Bi_2O_3	TeO_2	Au_2O_3	PtO	PdO
CH-2-1	0.28	14.81	2.31	2.95	2.07	87.62	2.84	0.11	0.07	0.20	0.04
CH-3-1	12.50	49.14	-0.03	28.97	4.14	0.79	0.16	47.39	-0.12	0.03	0.02
CH-3-2	10.81	46.41	-0.15	28.06	4.61	0.68	-0.05	48.81	-0.02	-0.22	0.03
CH-3-3	8.11	0.16	0.11	0.88	-0.02	0.34	5.01	65.60	1.89	31.76	6.91
CH-3-4	0.59	0.22	-0.04	0.90	0.06	0.71	8.37	74.34	0.83	24.14	15.93
CH-4-1	2.01	7.63	-0.05	3.25	0.45	31.13	0.02	41.60	0.13	-0.18	23.95
CH-2-2	0.12	0.02	0.00	0.07	0.01	1.08	1.62	85.89	0.74	6.34	30.11
CH -Z-1	1.55	25.58	0.03	7.79	0.07	2.87	26.72	34.57	0.94	20.72	13.43

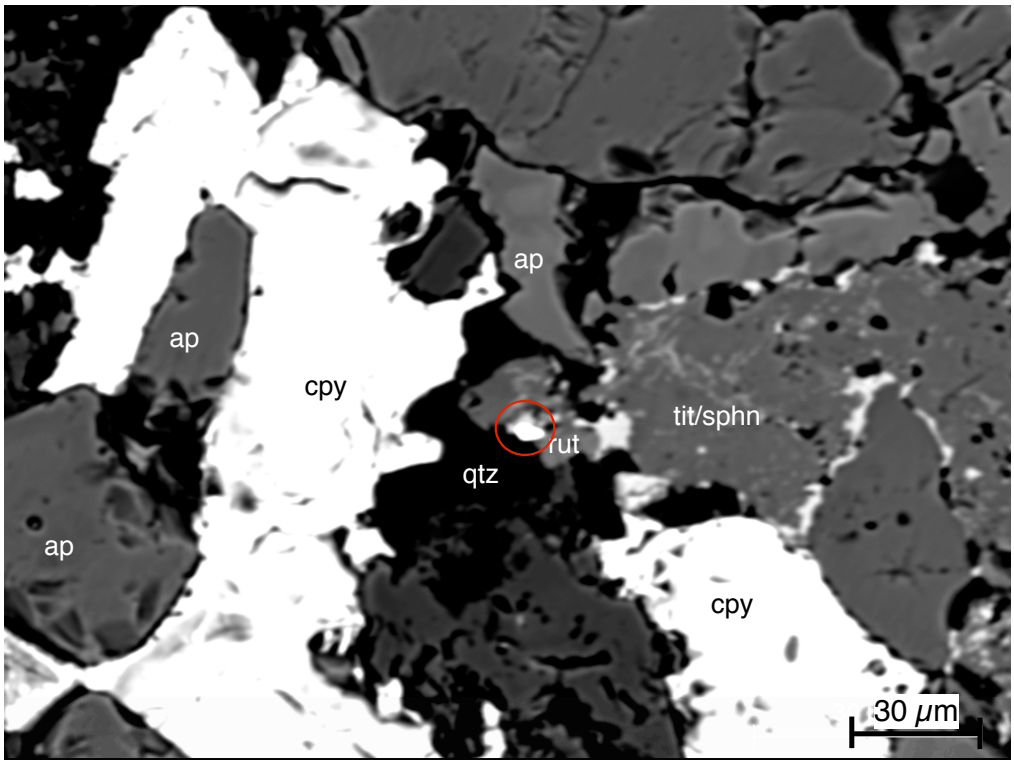

Fig. 27. A PGE-mineral grain (merenskyite) (red circle) in sample CH-3-3, shown in a backscatter electron (BSE) image. The PGE-mineral is surrounded by quartz (qtz) and rutile (rut), and in close association with apatite (ap), chalcopyrite (cpy), and titatinite,/sphene (tit/sphn).

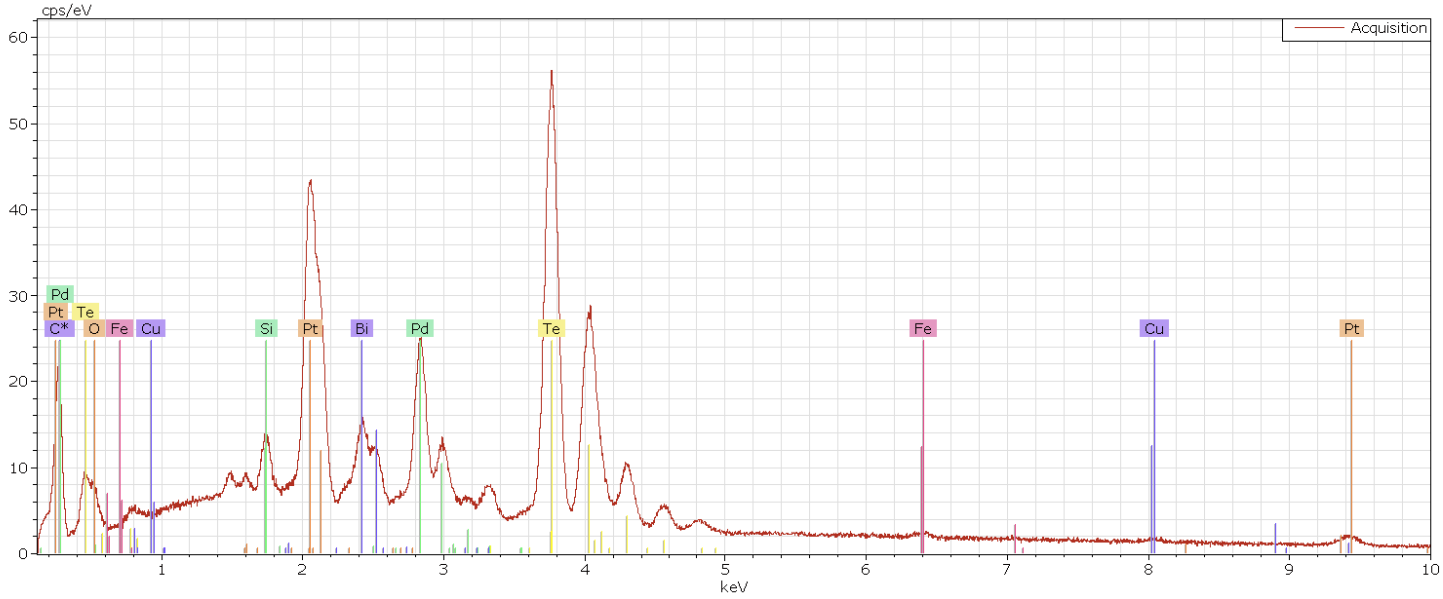

Fig. 28. The corresponding EDS spectrum for a PGE-mineral grain (merenskyite) found in CH-3-3 (Fig. 27). Note the peaks for Pt, Bi, Pd, and Te. Cu, and S peaks are background from the surrounding chalcopyrite, and the Si peak resulted from the background feldspar. .

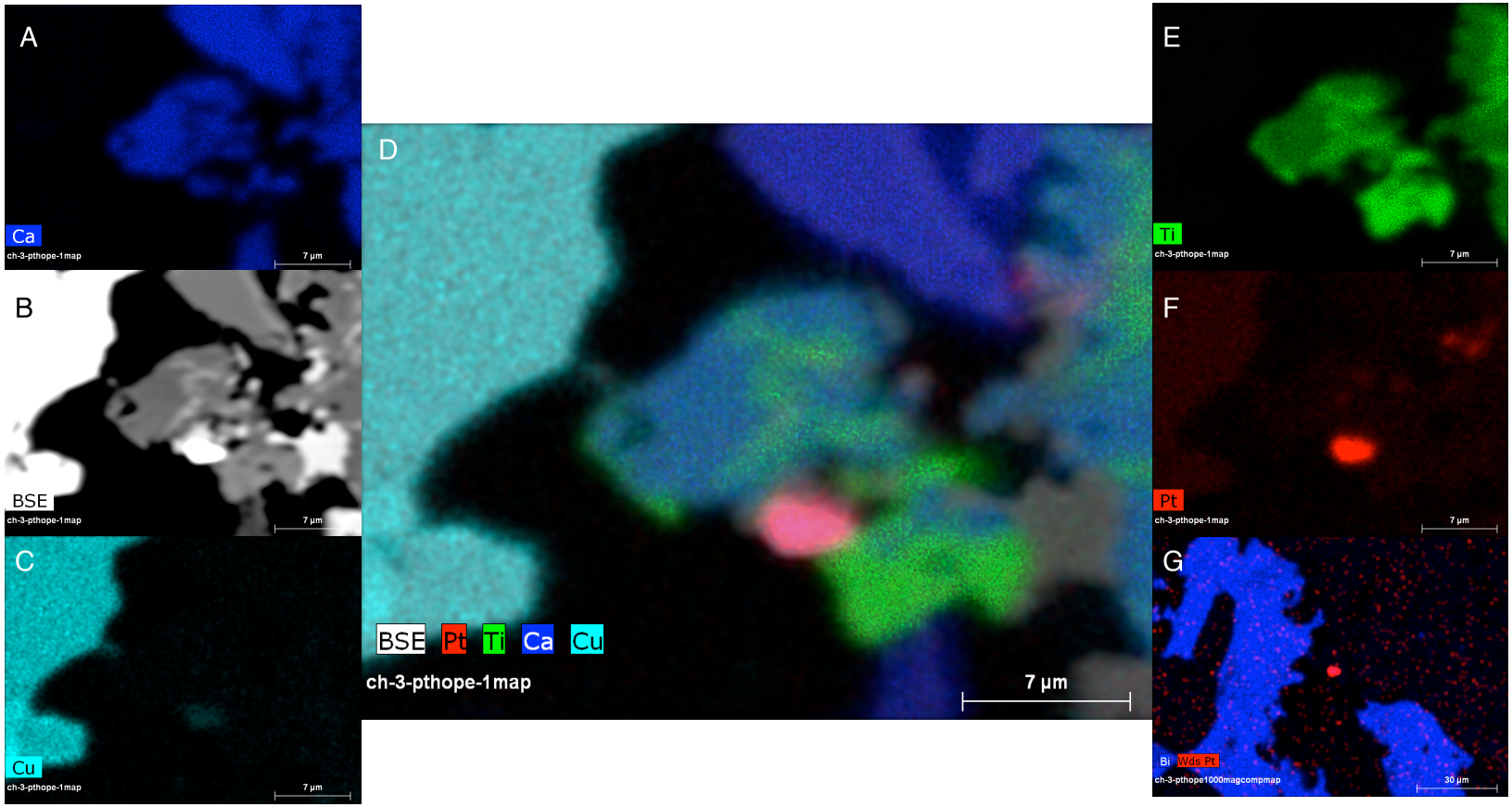

Fig. 29. EDS element maps of the PGE-mineral grain (merensykite) in sample CH-3-3 (Fig. 27, Fig. 28). From left to right, images are as follows: A) Calcium map showing sphene, B) Backscatter electron image, C) Copper map showing chalcopyrite, D) Composite element map, note platinum map of PGE-mineral grain in the center of the image, E) Titanium element map showing rutile and titanite/sphene, F) Platinum element map. Note concentration of Pt as bright red, however other areas of the image may show some indistinct noise, G) Bismuth and platinum element map at a larger scale, showing bismuth in chalcopyrite, but not within the PGE-mineral grain.

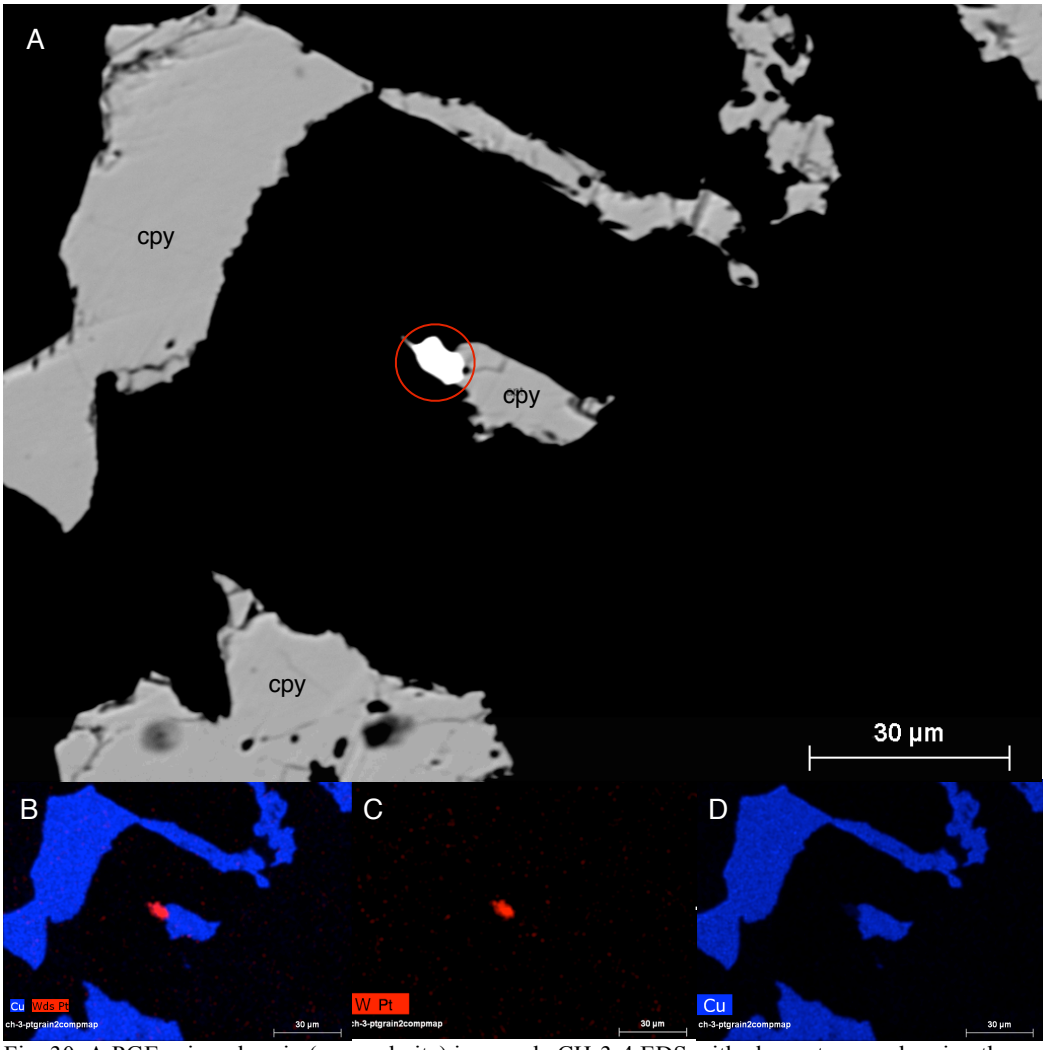

Fig. 30. A PGE-mineral grain (merenskyite) in sample CH-3-4 EDS with element maps showing the PGE-mineral in direct association with chalcopyrite. Other phases in the vicinity of the grain (not shown in image) include magnetite and apatite. A) is a backscatter electron image with the PGE-mineral circled in red. B) shows a composite element map showing copper in chalcopyrite and the PGE-mineral. C) a WDS element map showing platinum. D) an element map showing copper in chalcopyrite.

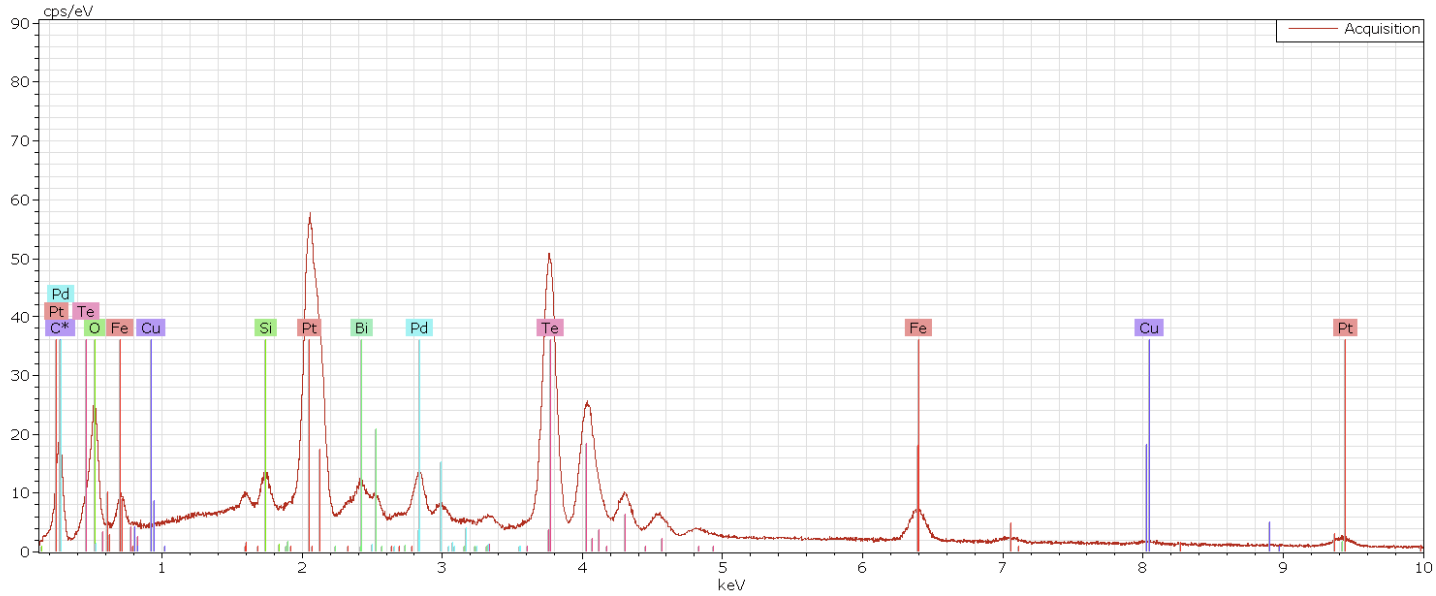

Fig. 31. Corresponding EDS spectrum for the PGE-mineral grain (merenskyite) in CH-3-4 (Fig. 31). Note the peaks for Pt, Pd, Bi, and Pd. Cu and Fe peaks are from background chalcopyrite and the Si peak is due to background silicate (feldspar)

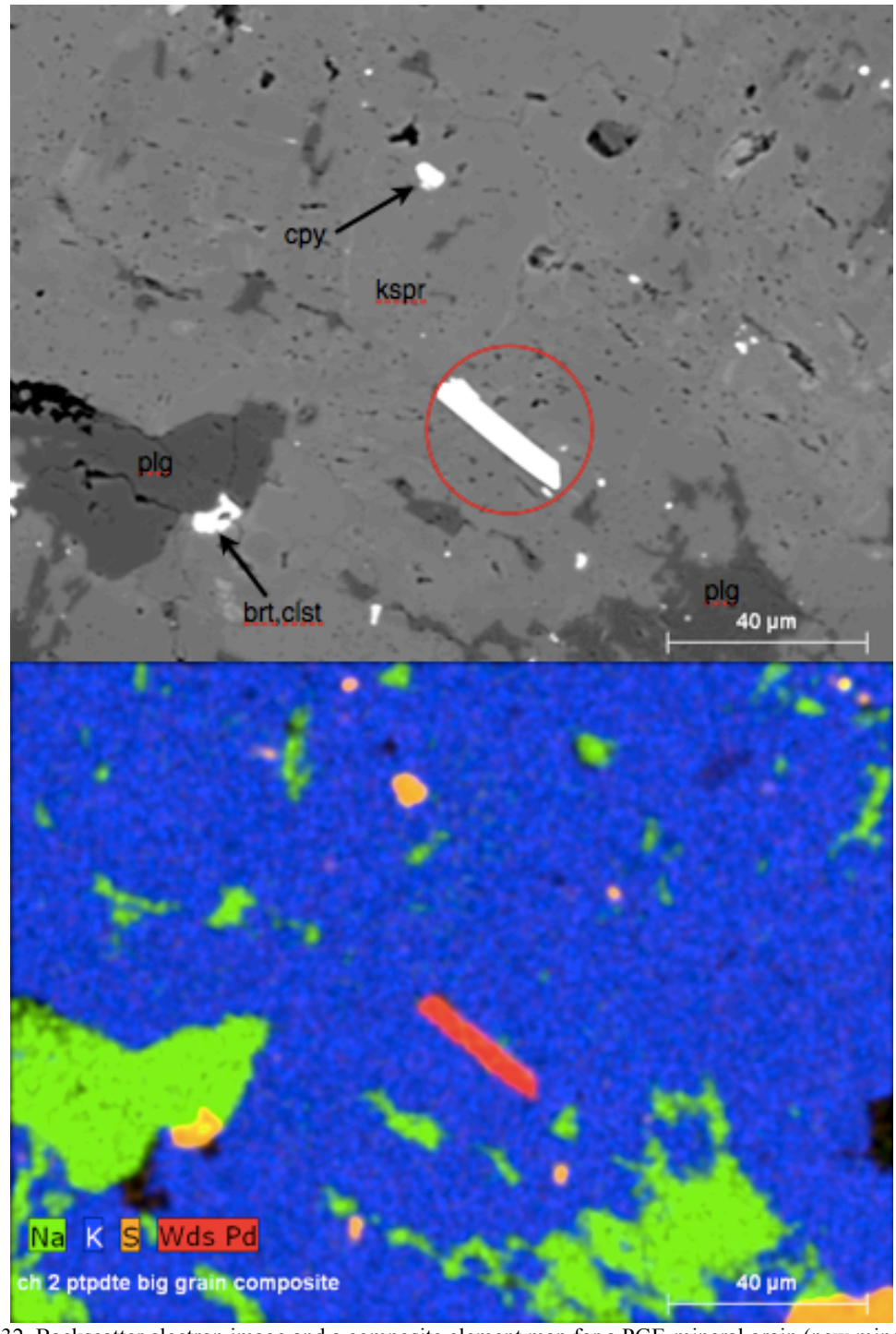

Fig. 32. Backscatter electron image and a composite element map for a PGE-mineral grain (new mineral?) (circled in red) found in sample CH-2-2 with phases labeled (top). The PGE-mineral is surrounded by potassium feldspar (kspr), plagioclase (plg), and a barium-strontium sulfate. The element map shows palladium in red, potassium in blue (to signify potassium feldspar), sodium in green (to signify plagioclase, specifically albite), and sulfur in yellow (to signify Ba-Sr-sulfate) (bottom).

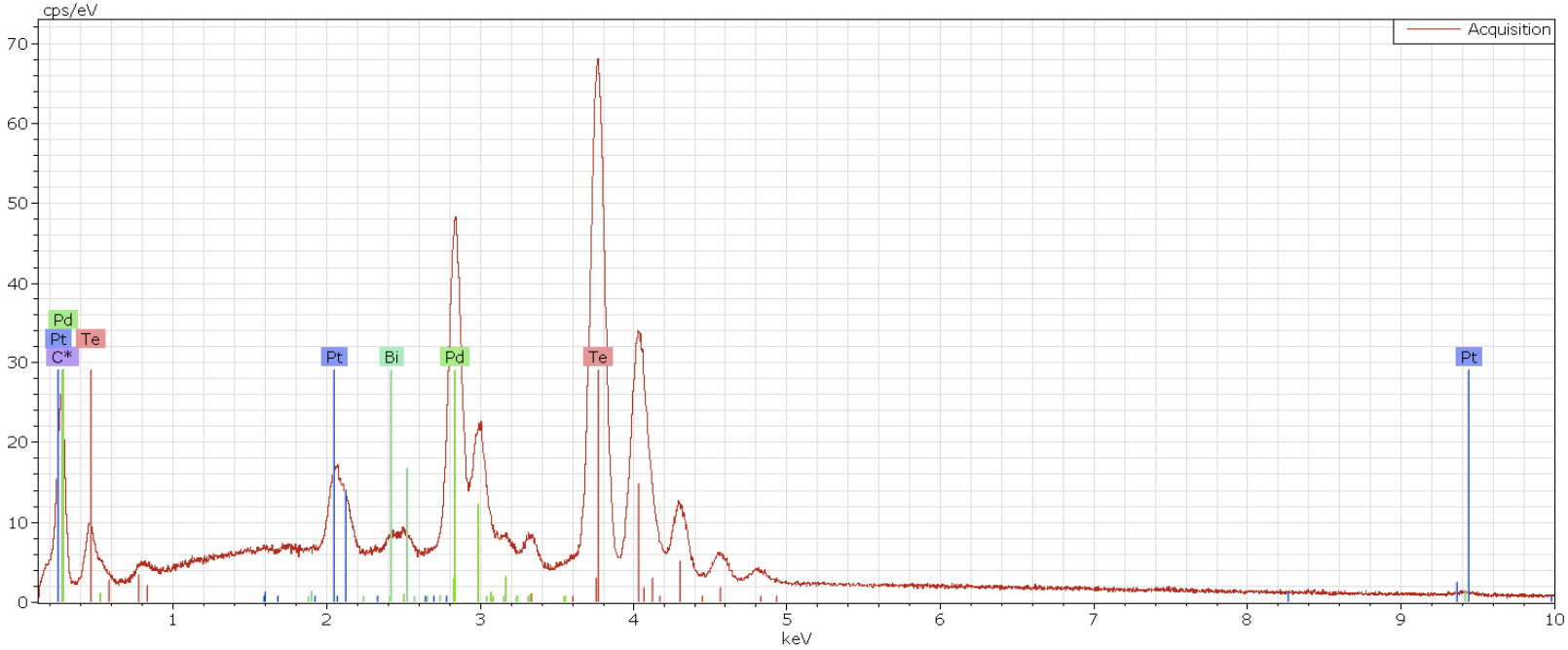

Fig. 33. Corresponding EDS spectra for the PGE-mineral grain (new mineral?) in CH-2-2 (Fig. 32). The Pd peak is larger relative to the Pt peak for this particular sample. Te appears to be a greater component in the mineral than Bi.

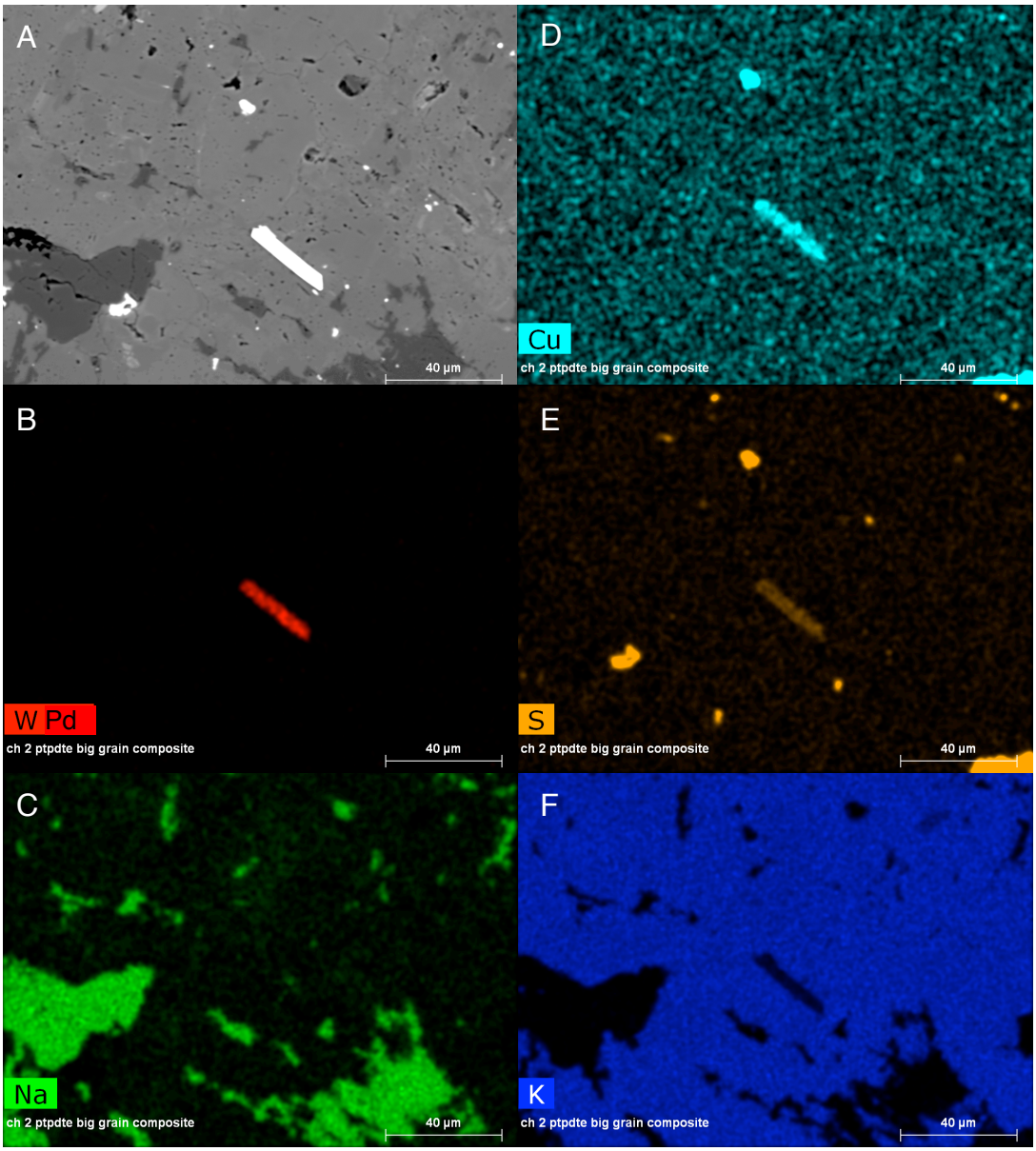

Fig. 34. Individual element maps of the unnamed/new PGE-mineral grain in sample CH-2-2 (Fig. 32, Fig. 33). From left to right, A) Backscatter electron image (same as Fig. 32, without phases labeled), B) Element map for palladium (Pd), C) element map for sodium (Na), signifying albite, D) element map of copper (Cu) signifying chalcopyrite, E) element map of sulfur (S) showing chalcopyrite and or pyrite, F) element map showing potassium (K) as evidence for potassium feldspar.

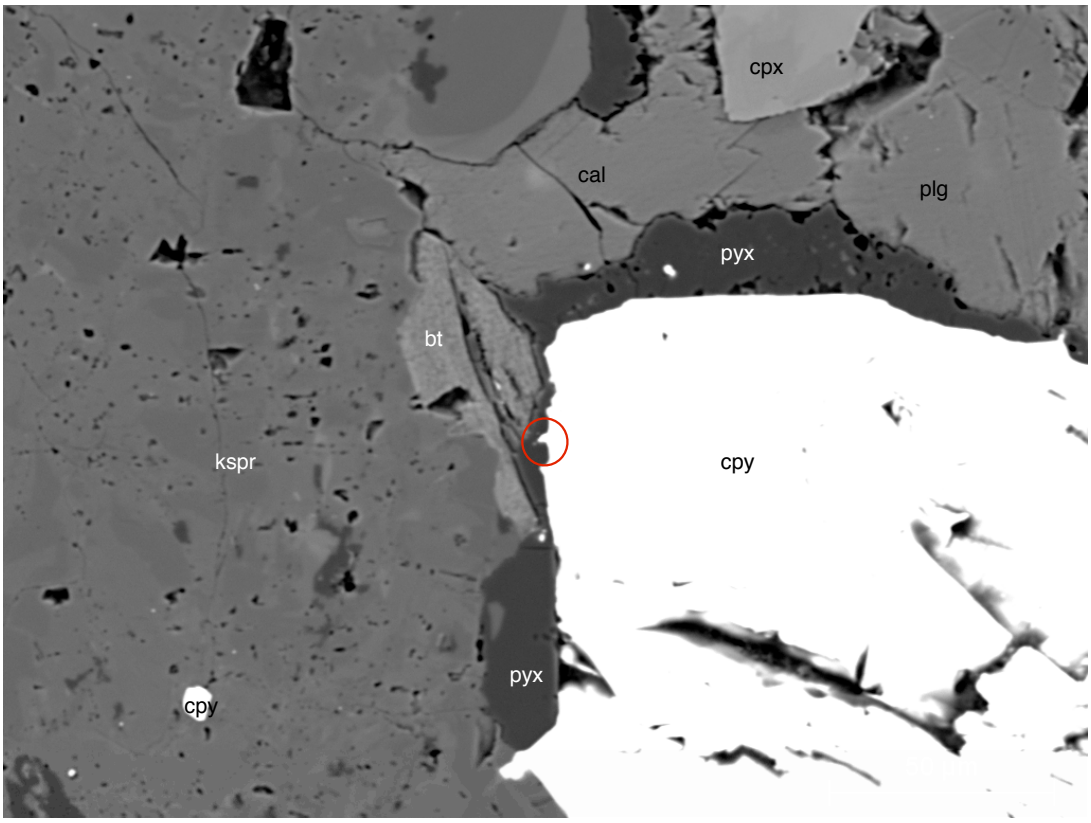

Fig. 35. Backscatter electron image of a PGE-mineral grain (sopcheite) found in sample CH-4-1. The PGE grain is circled in red with surrounding minerals biotite (bt), chalcopyrite (cpy) potassium feldspar (kspr), an alkali-rich pyroxene (pyx), calcite (cal), clinopyroxene (cpx), and plagioclase/albite (plg).

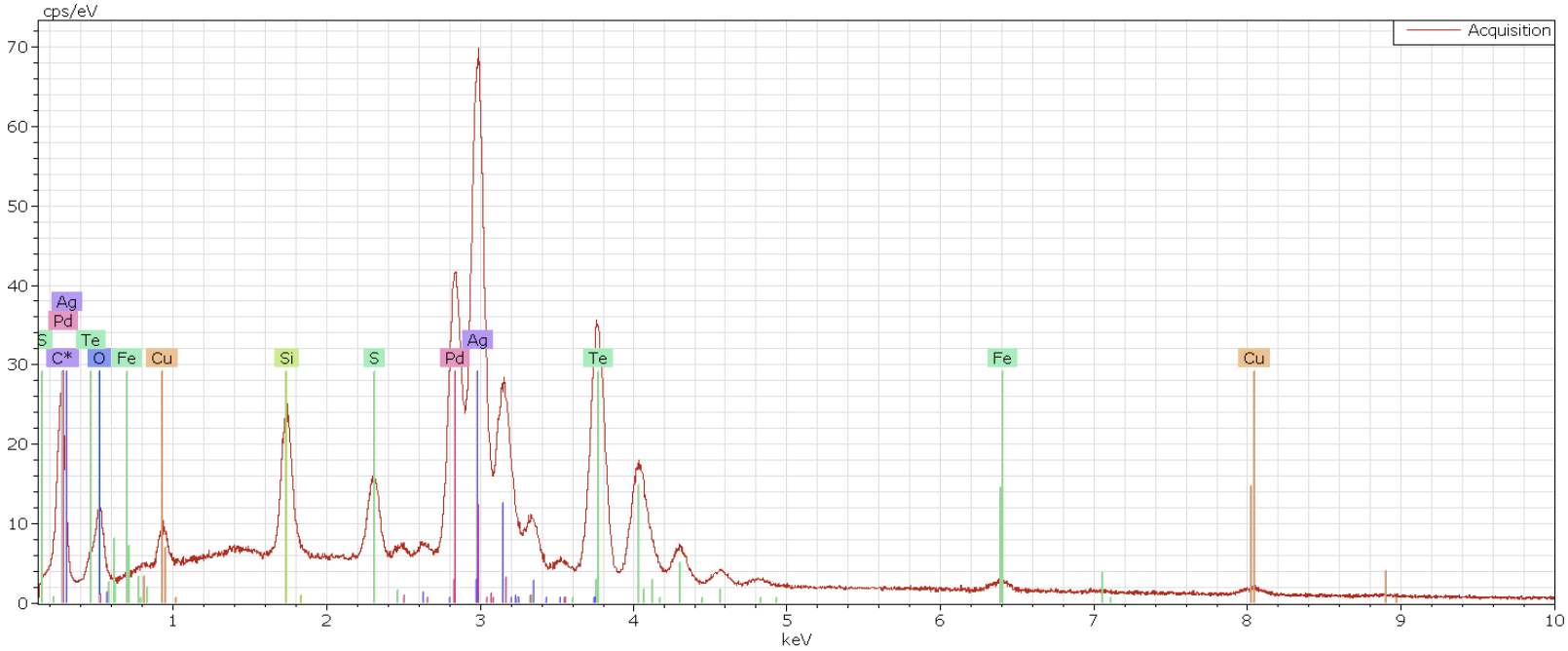

Fig. 36. Corresponding EDS spectra for the PGE-mineral (sopcheite) grain in sample CH-4-1 (Fig. 35). Note the absence of the Pt peak and the abundance of Ag, relative to Pd and Te. Cu, Fe, and S are background spectra from the nearby chalcopyrite.

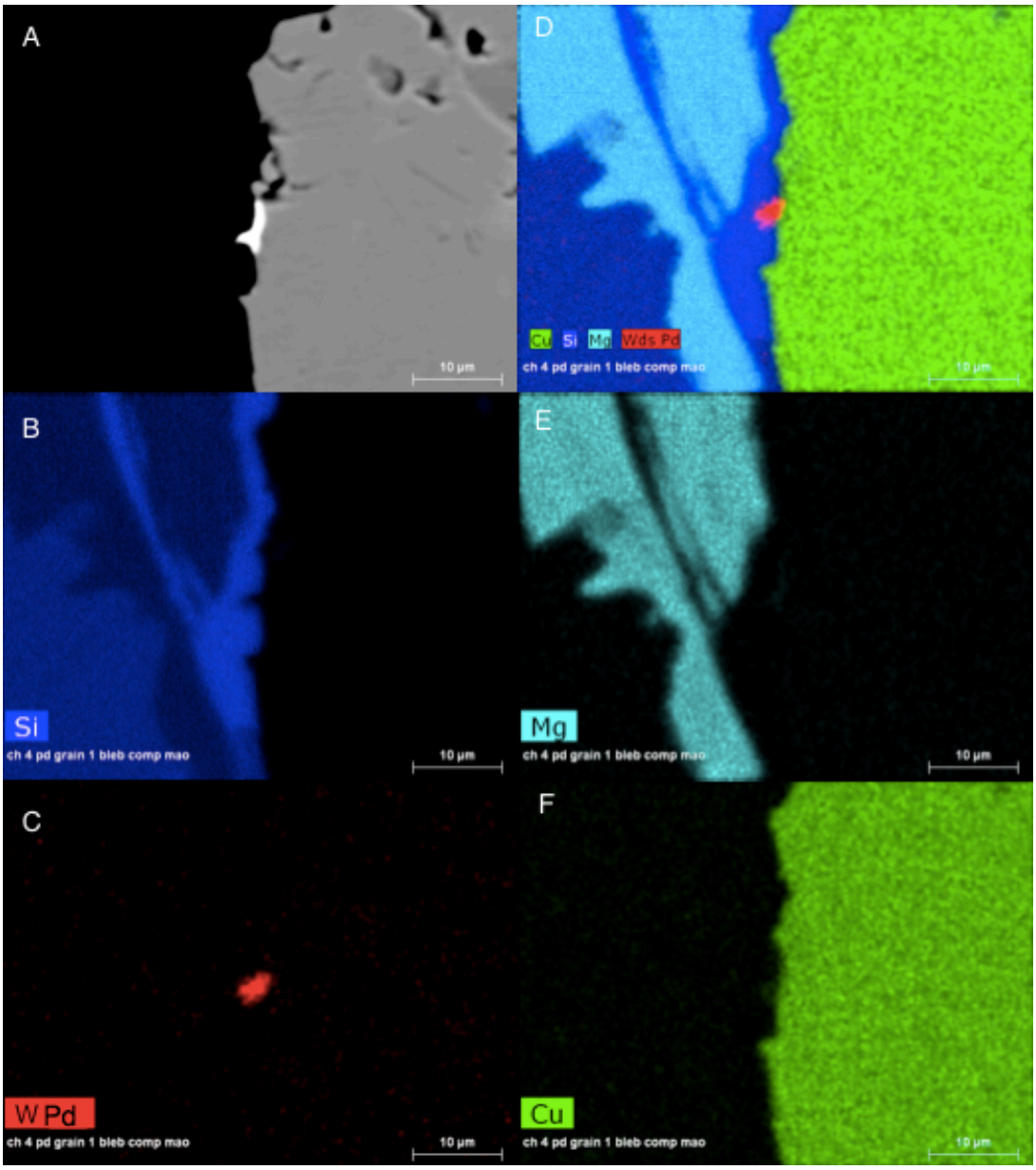

Fig. 37. Individual element maps for the PGE-mineral grain (sopcheite) in sample CH-4-1 (Fig. 35, Fig. 36). A) BSE image, B) silicon element map, signifying feldspar and biotite, C) Pd element map, D) composite element map showing phase relationships, E) magnesium element map signifying biotite, and F) copper element map signifying chalcopyrite.

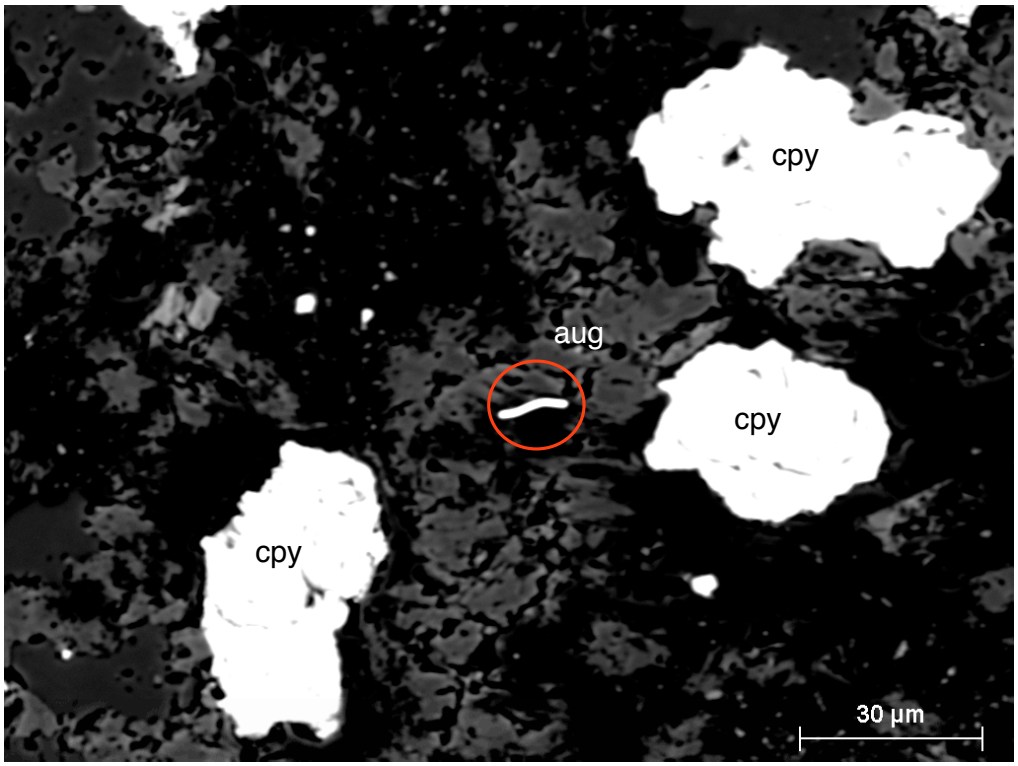

Fig. 38. Backscatter electron image of a PGE-mineral grain in sample CH-Z-2 showing a PGE-mineral grain (circled in red) hosted inside a Ca-Mg rich pyroxene phase (likely augite), that is near to but not hosted in chalcopyrite (cpy).

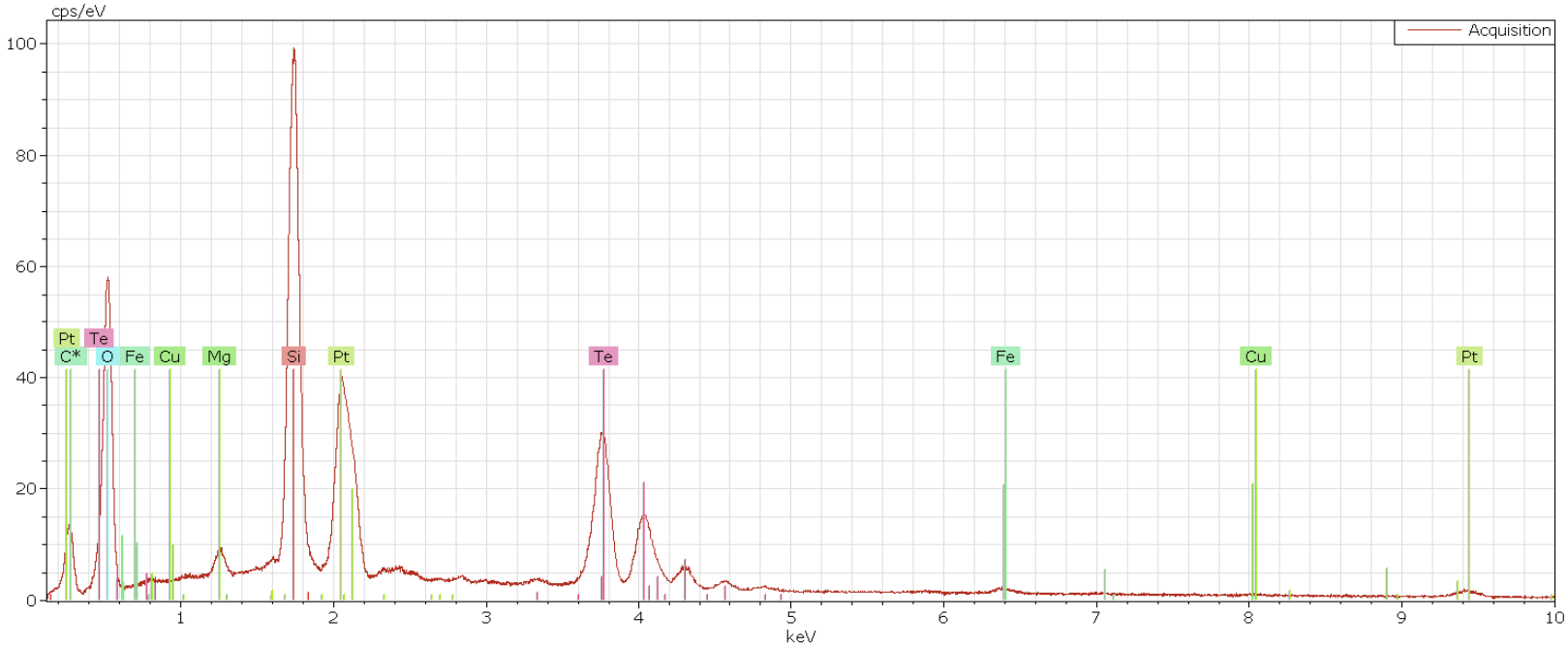

Fig. 39. Corresponding EDS spectra for the PGE-mineral grain in sample CH-Z-2 (Fig. 38). Pt and Te peaks are apparent, as it's the absence of Pd and Bi peaks. Cu, Mg, and Fe are background spectra from the surrounding mineral phases.

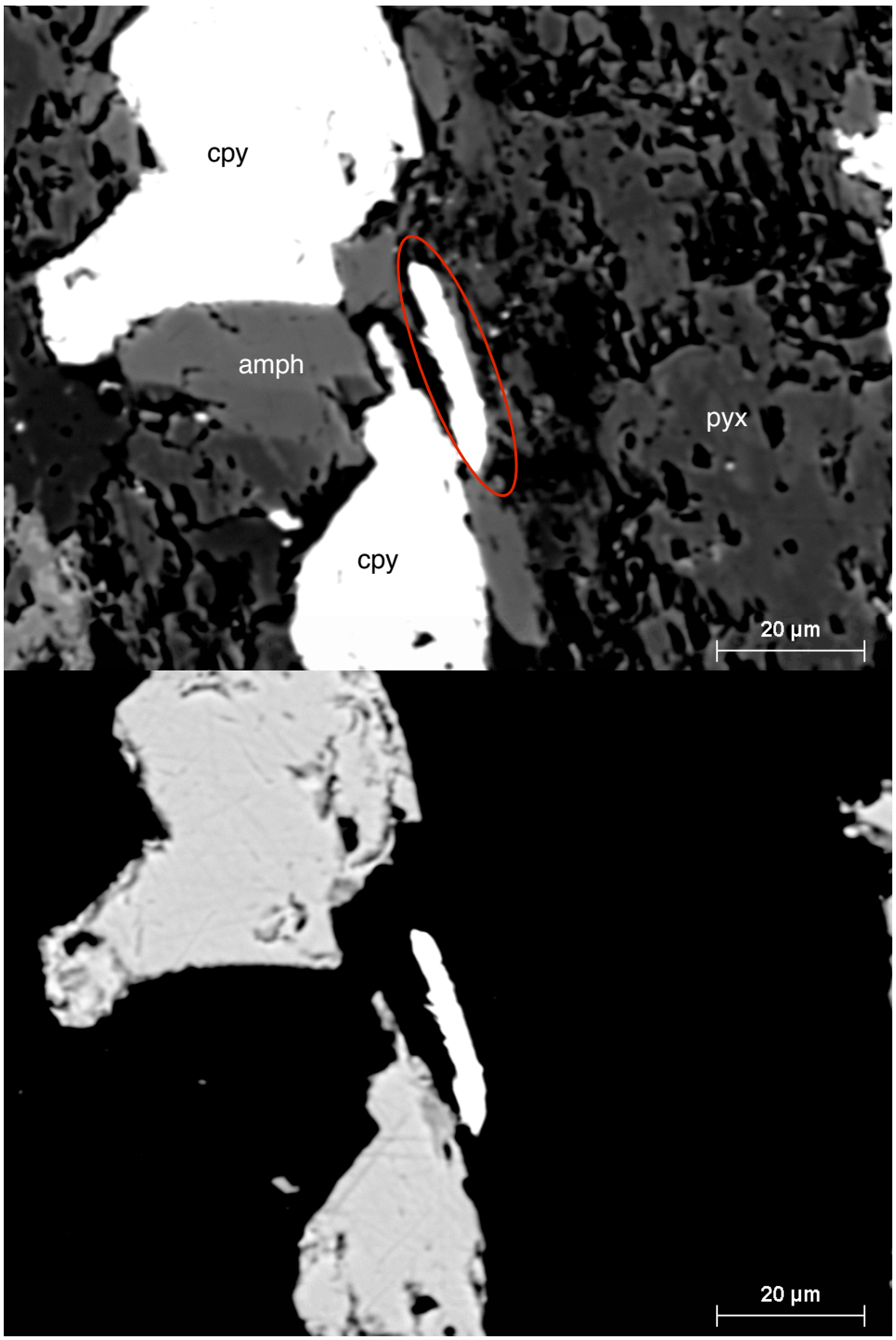

Fig. 40. Backscatter electron images for a PGE-mineral (mocheite) in sample CH-Z-1. The PGE-mineral grain (circled in red) is surrounded by chalcopyrite (cpy), an alkali-rich amphibole (aegerine?) (amph), and an alkali-rich pyroxene (augite?) (pyx).

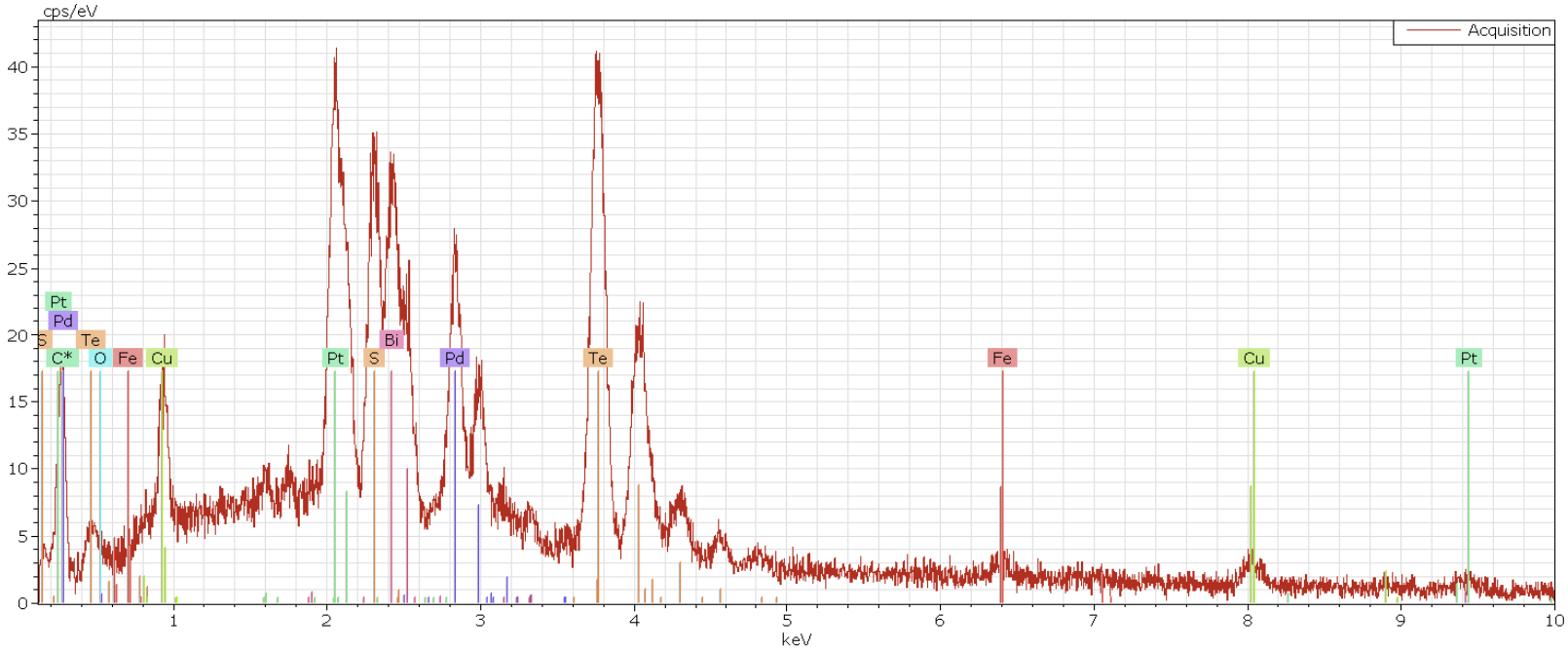

Fig. 41. Corresponding EDS spectra for the PGE-mineral grain (moncheite) in sample CH-Z-1 (Fig. 40). Pt, Pd, and Te all show prominent peaks. Cu, Fe, and S are background peaks from the nearby chalcopyrite.

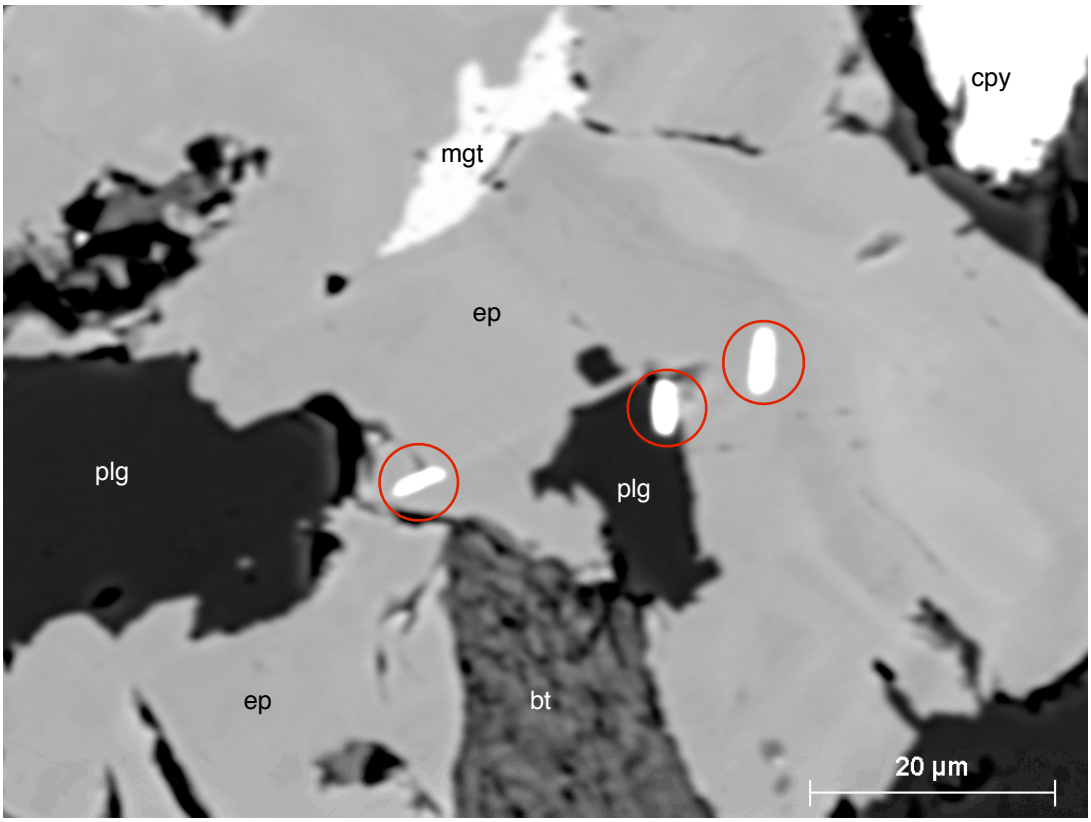

Fig. 42. Backscatter electron image of three PGE-mineral grains in sample CH-Z-3. The three PGE mineral grains (circled in red) are surrounded by epidote (ep) and plagioclase (plg). Biotite (bt), magnetite (mgt), and chalcopyrite (cpy) are also in the vicinity of the PGE-mineral grains.

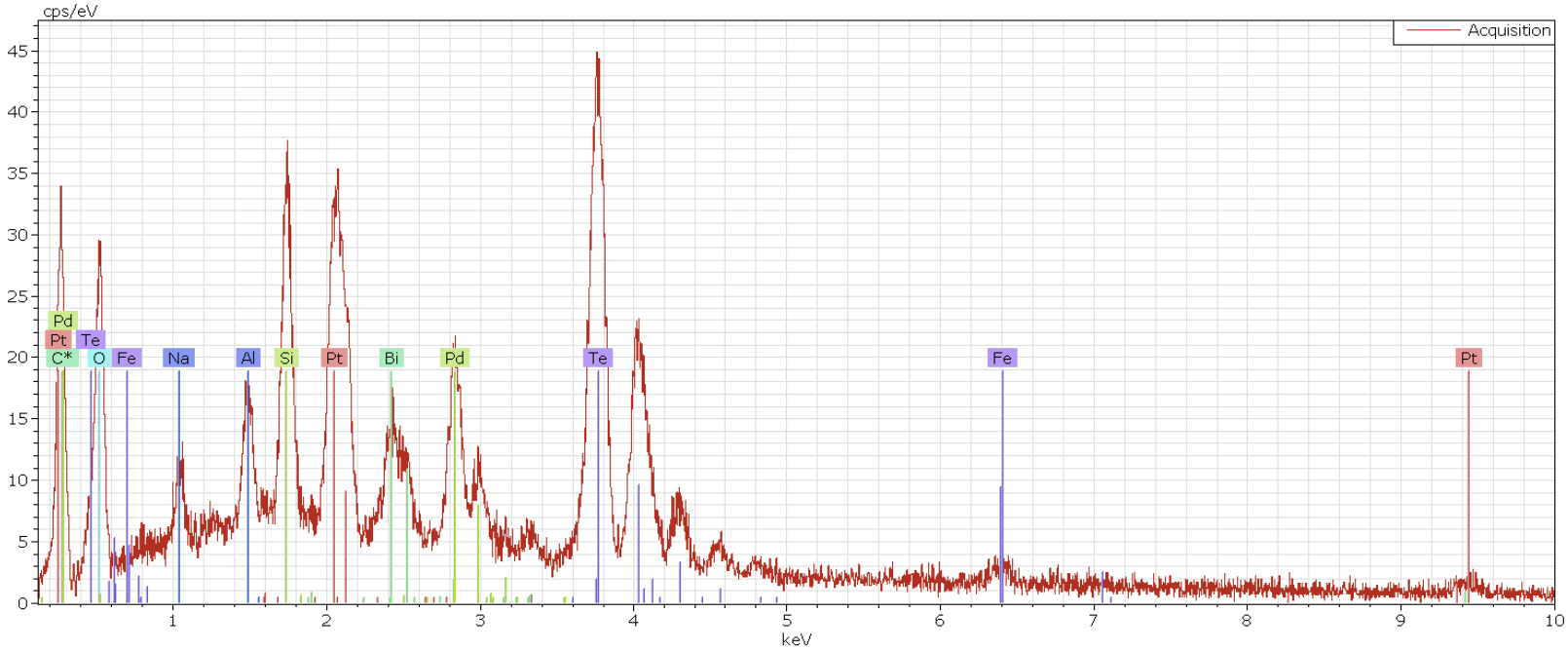

Fig. 43. Corresponding EDS spectra for one of the PGE-mineral grains (center grain in Fig. 42) in sample CH-Z-3. Peaks for a Pt-Pd-Bi-Te mineral are evident. Background Fe, Al, and Na are background spectra from the surrounding plagioclase.

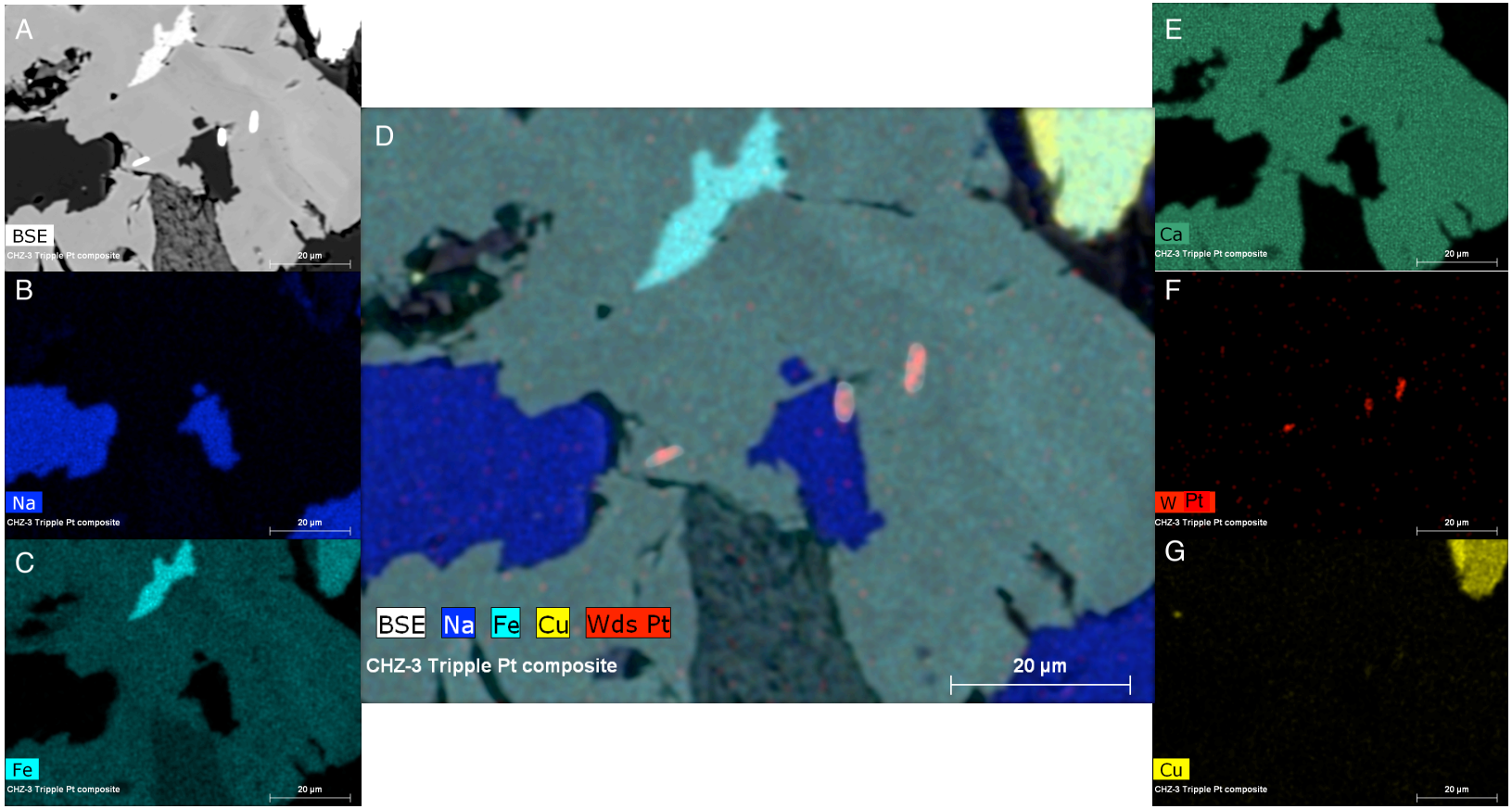

Fig. 44. Individual EDS element maps of the PGE-mineral grains in sample CH-Z-1. From left to right, A) BSE image, B) sodium element map, C) iron element map

5. DISCUSSION

Discussion of Geochemical and Whole Rock Data

Covariant plots for geochemical data in this study display element-element correlations in more detail. A covariant plot of Pt and Pd (Fig. 45) shows a strong positive correlation between the two elements, which supports the results from the above correlation matrix. This suggests that the Pt and Pd likely coexist together in a mineral phase. Also, phases with low Pd generally have two orders of magnitude more Pt. When concentrations of Pt or Pd approach the range of 10-100 ppb, a very strong positive correlation between Pt and Pd is evident (Fig. 45). Covariant plots for Pt and Pd versus Cu show no correlation until Cu concentrations reach 10,000 ppm, at which point Pt concentration increase from ~5 ppb to > 1 ppm, whereas Pd concentration increases from ~30 ppb to ~750 ppb. Generally, more Pt exists within the Allard stock, relative to Pd. Eckel (1949) reported that Pt and Pd likely occurred within or in association with chalcopyrite. From this geochemical data, this is only probably true in samples with at least 1% Cu, where Pt and Pd reach economically viable concentrations.

Diagrams plotting Pt and Pd versus Se and Te concentration within the porphyry and epithermal or skarn deposits (Fig. 46) show a generally positive correlation trend between Pt and Pd and Se and Te for the Allard stock porphyry deposits. The epithermal/skarn deposits do not fit this general trend, but have more Te relative to Se.

The presence of more Te is due to the occurrence of Au-Ag-telluride minerals at all three of the epithermal or skarn type deposits sampled for this study (Bessie G, Cumberland, May Day).

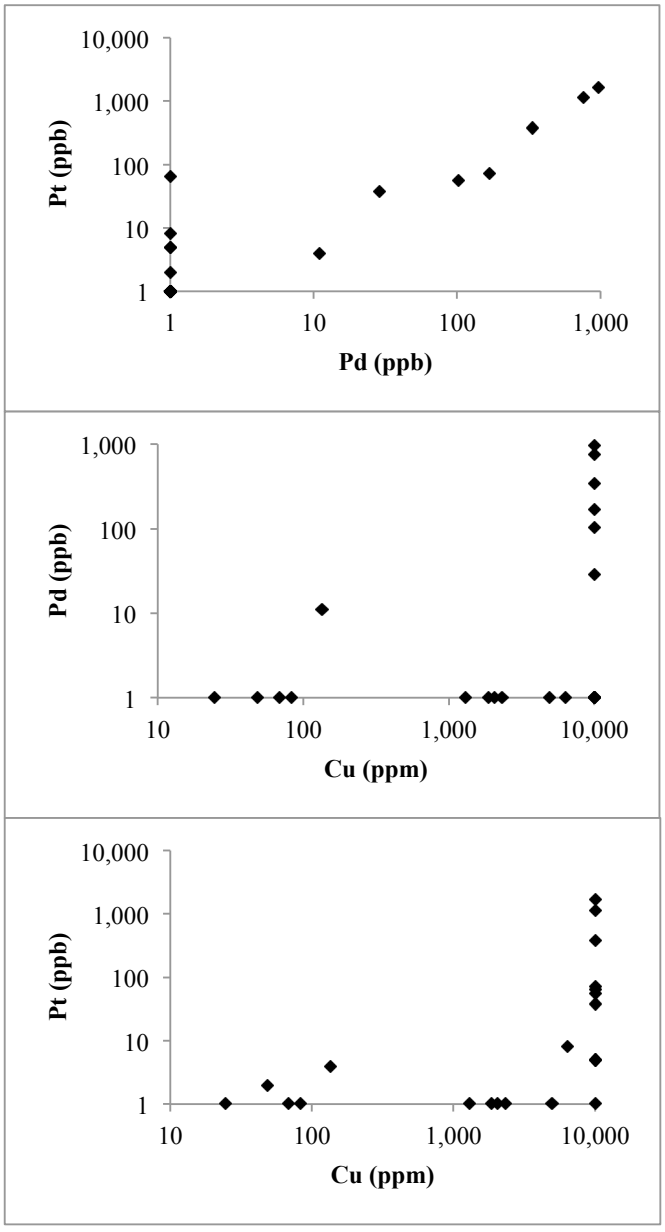

Fig. 45. Covariant plots of geochemical (Pt, Pd, and Cu) data in the La Plata district. Samples from the Allard tunnel, Copper Hill, Cumberland, Bessie G., and May Day deposits are included.

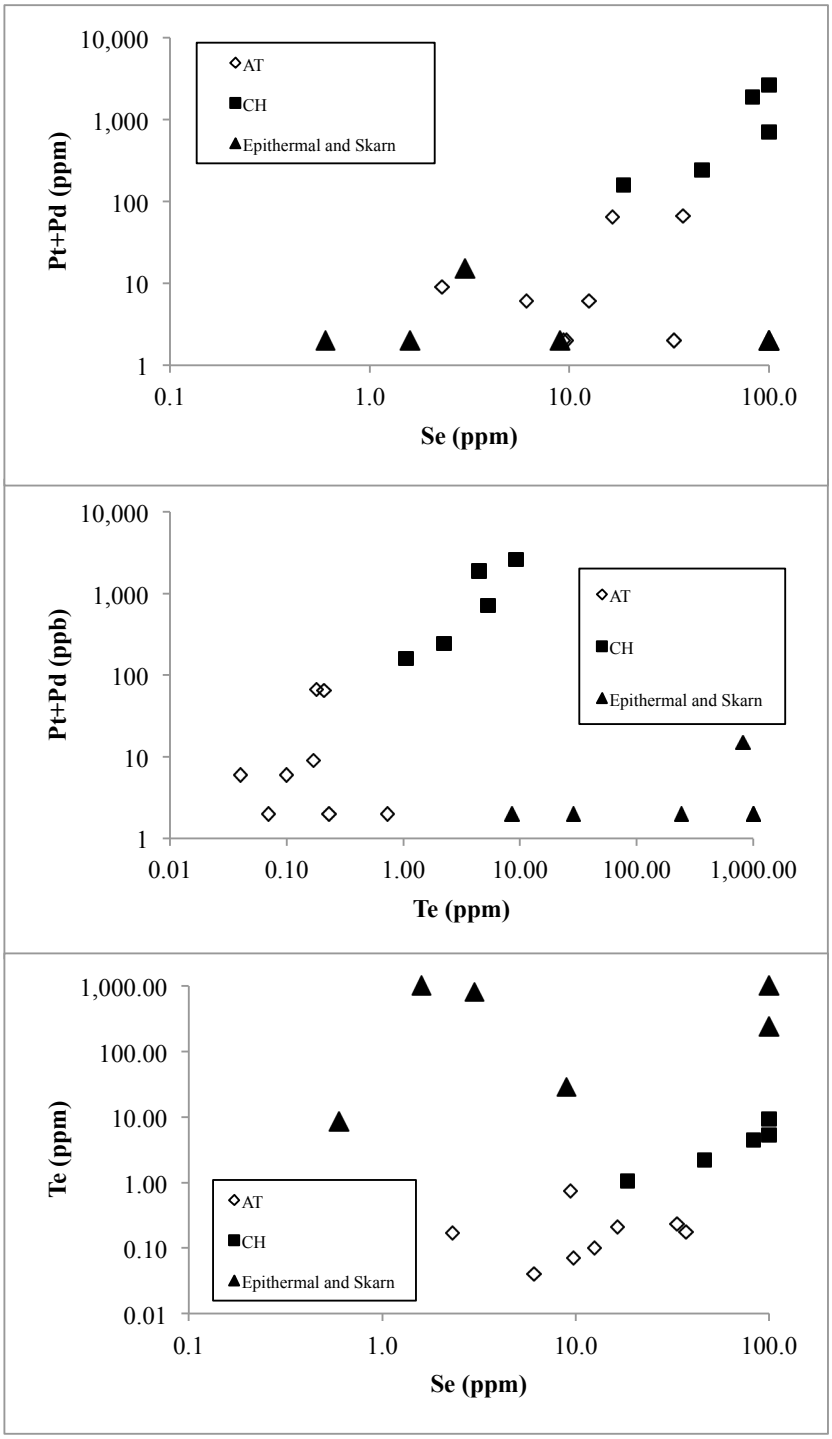

Fig. 46. Pd, Pd, Se, and Te covariant plots for La Plata district samples. Note the discrimination of locationand porphyry, epithermal and skarn deposit types.

Whole rock analyses of samples of syenite from the La Plata district for this study yielded similar values to those of Werle et al. (1984) and Wegert and Parker (2011). As compared to Werle et al. (1984), the whole rock analyses from this study do plot within the same field (Fig. 47), however Werle et al. (1984) recorded data with higher overall SiO_2 and Na_2O+K_2O values. Both studies show the alkaline nature of the Allard stock, as all analyses plot within the alkaline field. An average syenite composition, the USGS Syenite-STM1 standard, is also plotted for reference. Analyses for this study show an elevated K_2O/Na_2O (0.65-0.97) ratio, similar to shoshonites, as Werle et al. (1984) also found.

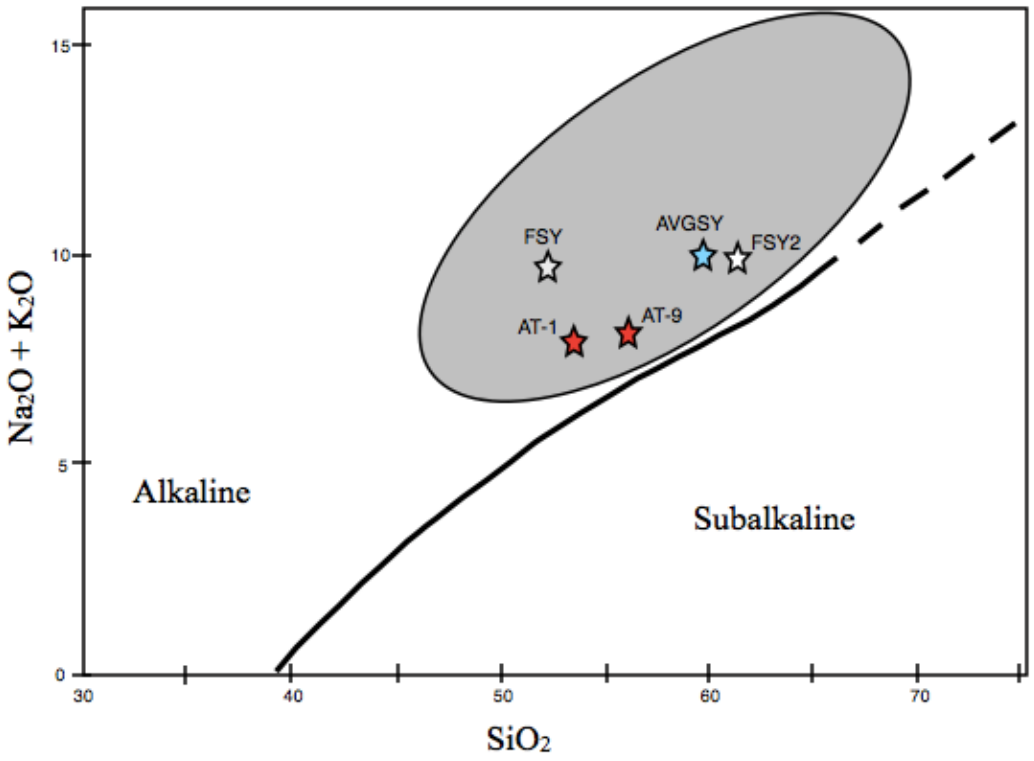

Fig. 47. TAS diagram for the La Plata district. Gray shaded region based on data range for the Allard stock from Werle et al. (1984). Abbreviations are as follows: AT = Allard tunnel, FSY = fresh syenite, AVGSY = USGS syenite STM-1 standard.

Data from Wegert and Parker (2011) comparing the McDermott formation, the Allad stock, other La Plata district rocks, and the Four Corners lower crustal xenolith average (Fig. 48) follows the same trend as data from Werle et al. (1984) and this study. Note that both Wegert and Parker (2011) and Werle et al. (1984) have analyses that plot farther into the trachyte field. Allard stock TAS values trend between basaltic trachyandesite, trachyandesite, to trachyte compositions. Samples from this study fall in the shoshonite field, as $Na_2O - 2.0 < K_2O$, however data from Werle et al. (1984) and Wegert and Parker (2011) plot as latite compositions. Allard stock samples AT-1, AT-9 and FSY and FSY2 follow the same trend of decrease (Fig. 49) in MgO content relative to increase in SiO_2 as Wegert and Parker (2011) showed. This trend begins at the Four Corners lower crustal xenolith average and SiO_2 content increases as fractional crystallization increases in the system, removing MgO.

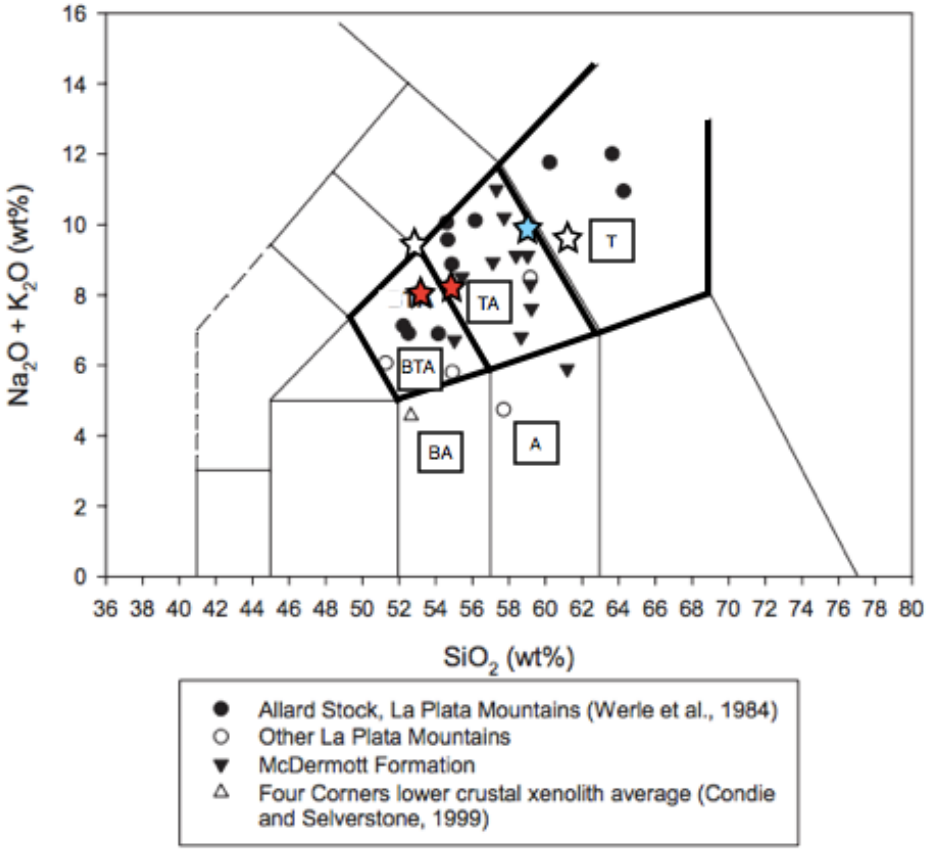

Fig. 48. TAS plot from Wegert and Parker (2001) superimposed with data from this study (stars). Red stars are Allard tunnel, white stars are fresh syenite, and the blue star is the USGS STM-1 syenite standard, following the same symbology as the previous TAS graph (Fig. 47).

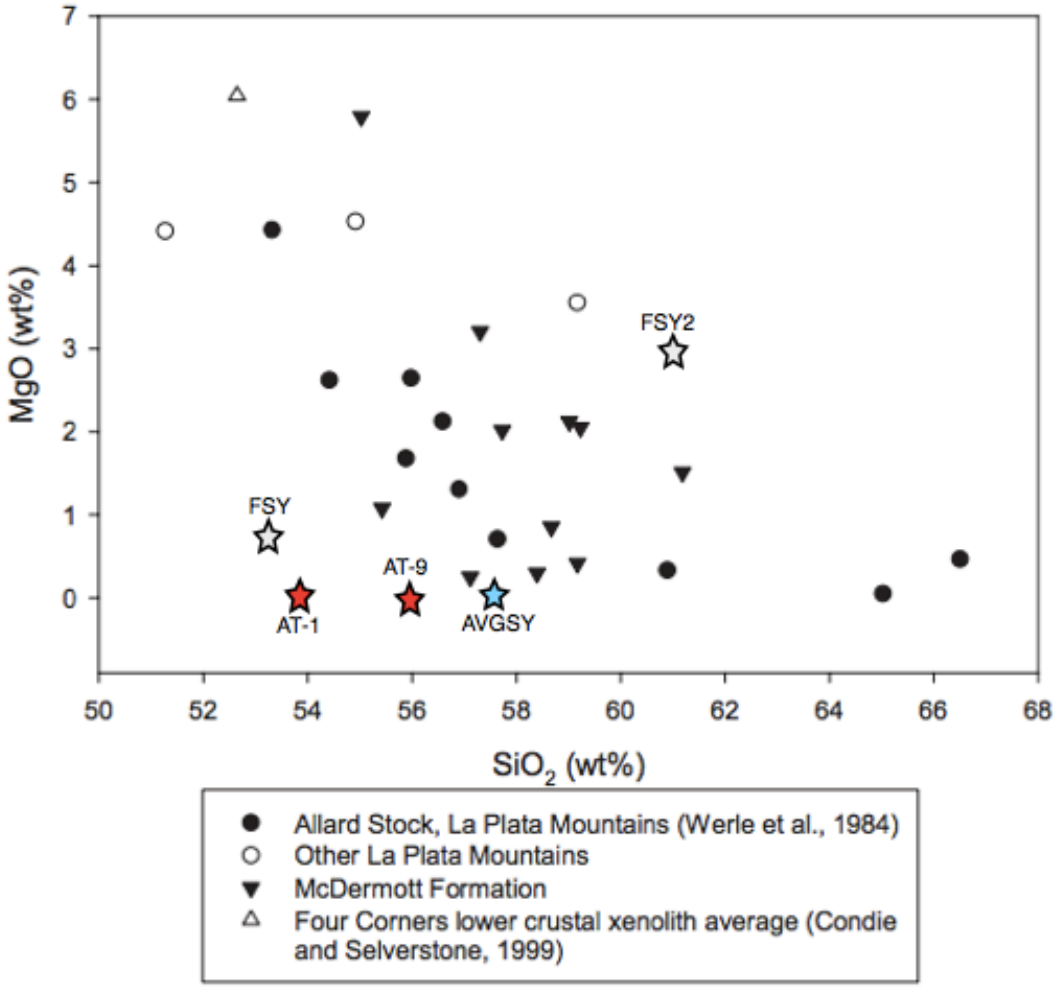

Fig. 49. Allard stock data plotted on an MgO versus SiO_2 graph {modified from Wegert and Parker (2011)] with data from previous studies on the Allard stock, the Mcdermott Formation, and the lower crustal xenolith average. The USGS STM-1 syenite standard is also included for reference.

Microprobe Analyses: Finding PGE-mineral Grains in Copper Hill Samples

In samples from Copper Hill that contained ~1 ppm Pt ±Pd, microprobe analyses indicated discrete grains of at least four PGE-minerals, which include merenskyite $(Pd,Pt)(Te,Bi)_2$, moncheite $(Pt,Pd)(Te,Bi)_2$, sopcheite $(Ag_4Pd_3Te_4)$, and an unnamed Pd-Te mineral ($PdTe_2$). EDS spectra and compositional results for these minerals can be found in Table 10 of the results section of this thesis. Merenskyite occurs most notably in the Merensky Reef of the Bushveld Complex, it also appears in the Great Dike in Zimbabwe, the Stillwater complex, Montana; the New Rambler Cu–Ni mine, Encampment district, Wyoming,the Key West Mine, Bunkerville district, Nevada, in Kambalda, Western Australia, in the Lac des Iles complex, Ontario, Canada, and in the Noril'sk region of Russia. Several of these deposits or districts were noted for PGE occurrence in the previous works section of this thesis. In the Allard stock, merenskyite was found in CH-3-3 (Fig. 27) occurring with rutile + quartz + apatite + sphene + chalcopyrite, and in CH-3-4 (Fig. 30) with chalcopyrite + magnetite + apatite. Moncheite, similar to merenskyite but usually more Pt rich, also occurs in the Bushveld complex, at Sudbury, Noril'sk, Stillwater, Kambalda, the Lac des Iles complex, and in the New Rambler and Key West mines. Typically moncheite occurs in small amounts in Pt–Pd-bearing massive Cu–Ni sulfide deposits, however at the Allard stock it occurs in association with epidote+plagioclase+biotite in sample CH-Z-1 (Fig. 40). It is obvious that these minerals are often associated with one another due to their similar chemical formulas and to the fact that Pt and Pd often allow and travel together in systems. Sopcheite typically occurs in veinlets cutting chalcopyrite (Monchegorsk deposits,

Russia), and has been found at the Lac des Iles complex, at Sudbury, and at the Santo Tomas II porphyry copper deposit, Benguet, Philippines. At Copper Hill, sopcheite was found in CH-4-1 (Fig. 35) surrounded by chalcopyrite+biotite+pyroxene. The unnamed, Pd-telluride is perhaps a new mineral, and occurs in CH-2-2 (Fig. 32) enclosed completely in epidote, although plagioclase and biotite are also in close association. PGE-grains range between 3-35µm in length. Disseminated Pt±Pd may also occur within chalcopyrite at the Allard stock, but other than the geochemical and assay analyses in this study, there are no data to support or negate the presence of disseminated PGEs within the Allard stock not in association with Te or within sulfides. ICM-MS analysis has shown that Pd can be homogenously distributed within chalcopyrite and tetrahedrite and could potentially be bound within the minerals' crystal lattices (Pasava et al, 2010; John and Taylor, 2014 in press).

Sulfur Isotope Geochemistry of the Allard Stock

Since the late 1940s, sulfur isotope geochemistry has been used to investigate many geologic processes including ore deposits, the origin and evolution of sulfur species in natural waters (including present-day and ancient marine), fractionation in bacterially influenced processes, and acid mine drainage (Marini et al., 2011). Sulfur isotope values are reported as per mil (‰) relative to Canyon Diablo Troilite (CDT) or to Vienna Canyon Diablo Troilite (VCDT), a fixed standard relative to CDT. Meteoritic sulfur (generally regarded as approximate bulk composition of Earth's primordial sulfur, relative to CDT or VCDT) and seawater are the most commonly used reference

reservoirs for sulfur isotopes in terrestrial systems. Geochemical conditions influence how sulfur partitions in a system. Relative to the parent material, oxidation produces resultants enriched in ^{34}S, while reduction produces species depleted in ^{34}S (Seal, 2006). Sakai (1968) first suggested that sulfur isotope fractionation in minerals could be controlled by the geochemistry of the ore-forming fluids. Marini et al. (2011), compiled extensive data that shows sulfur isotope ranges from a variety of sources (Fig. 50).

Mantle sulfur isotope composition, conventionally considered to be 0 ± 2‰ (Thode et al., 1961), could be heterogeneous as evidenced by the ranges for mantle xenoliths, mid ocean ridge basalt (MORB) sulfides, and ocean island basalt (OIB) sulfides (Fig. 51). Despite the evidence supporting sulfur isotope heterogeneity, values for magmatic sulfur do cluster around 0‰ (Seal, 2006). Rye and Ohmoto (1974) state, "Igneous sulfur is derived from the upper mantle or from the homogenization of large volumes of deeply buried or subducted materials."

Sulfur isotope studies on sulfur-bearing minerals in hydrothermal ore deposits yield a wide range of $\delta^{34}S$ values (Fig. 51), depending on the degree of fractionation and the isotopic signature of the original source of sulfur. Many porphyry deposits typically show a strong $\delta^{34}S$ signature of around 0‰ (Fig. 53), however porphyry deposits sulfur isotope values can range between –6 and +4‰ (Marini et al., 2001). Hydrothermal ore deposits range from ~ ±30‰ (Fig. 51) but show an overall signature clustering around 0‰ $\delta^{34}S$. Sulfur analyses on samples from Allard Tunnel and Copper Hill (Fig. 52) range from -7.7 to +0.3‰ $\delta^{34}S_{VCDT}$, with an average of -5.2‰ $\delta^{34}S_{VCDT}$ and a mode of -6.0 $\delta^{34}S_{VCDT}$. Therefore the Allard stock sulfur isotope range is comparable to that of most typical porphyry copper deposits (Fig. 52).

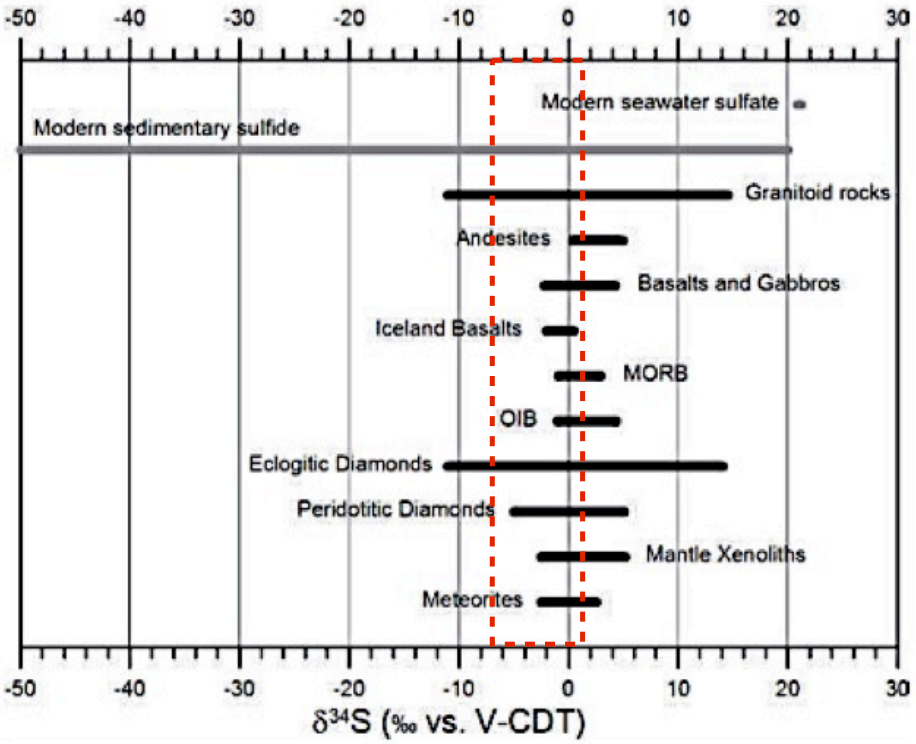

Fig. 50. Plot showing the range of sulfur isotope values for sulfides from meteorites, mantle xenoliths, diamonds, igneous rocks, and modern sediments with Allard stock data overlayed in red. Figure from Marini et al. (2001).

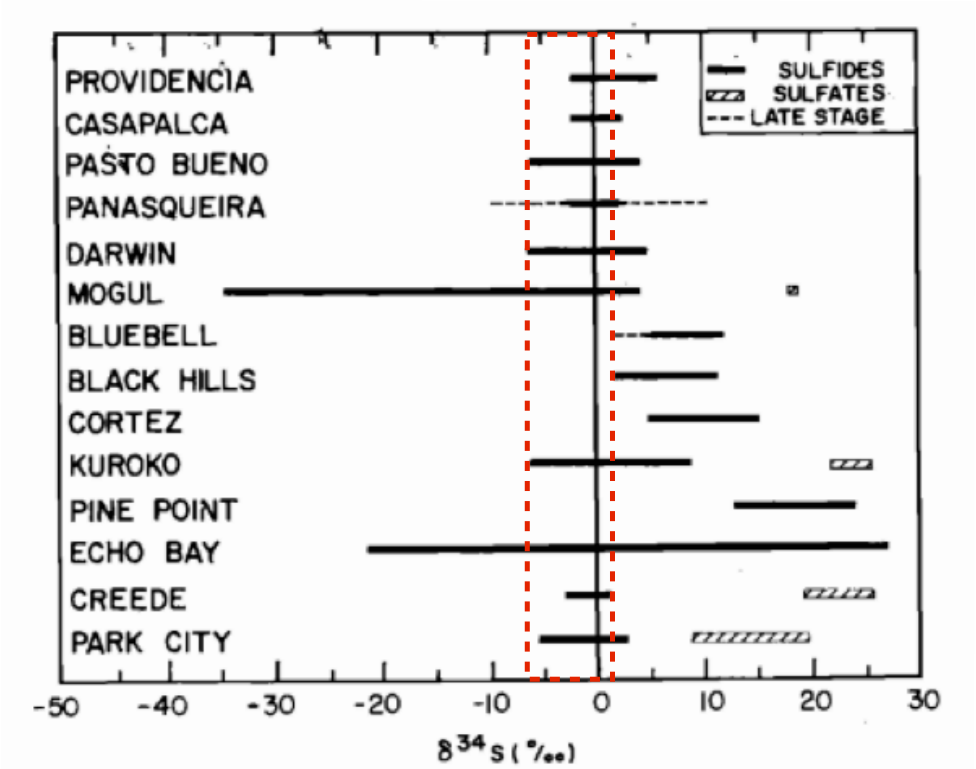

Fig. 51. Plot showing the sulfur isotope range for various hydrothermal ore deposits, showing $\delta^{34}S$ for sulfides and sulfates with Allard stock data overlayed in red. Figure from Rye and Ohmoto, 1974;

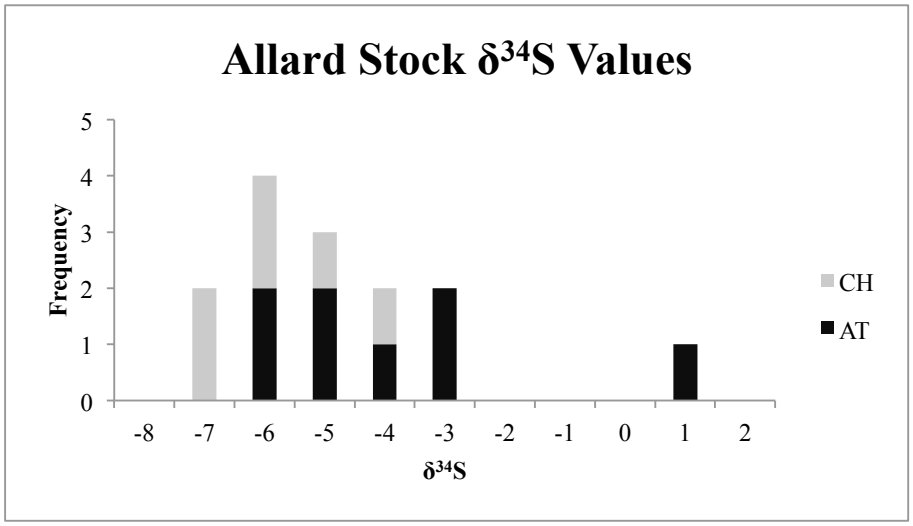

Fig. 52. Histogram showing data from Allard Tunnel samples and from Copper Hill samples with respect to their sulfur isotope values (relative to VCDT, per mil).

Figure 52 above shows the sulfur isotope data from both Allard Tunnel and Copper Hill. Sulfur analyses for the Allard Stock (n=14) appear to be enriched in the lighter isotope, ^{32}S relative to the heavier isotope, ^{34}S. As evidenced by the similarities to many porphyry copper deposits shown above, sulfur at the Allard Stock is apparently predominantly magmatic in origin, but apparently include some contribution of ^{32}S-enriched sedimentary sulfur from the strata intruded by the porphyry, potentially from the Cutler formation. No sulfate minerals are known to exist within the mineralization at the Allard Stock and were therefore not analyzed. A more robust study including sulfur analyses is needed to definitively determine the origin of sedimentary sulfur, and to better constrain the sulfur isotopic signature of this alkalic porphyry.

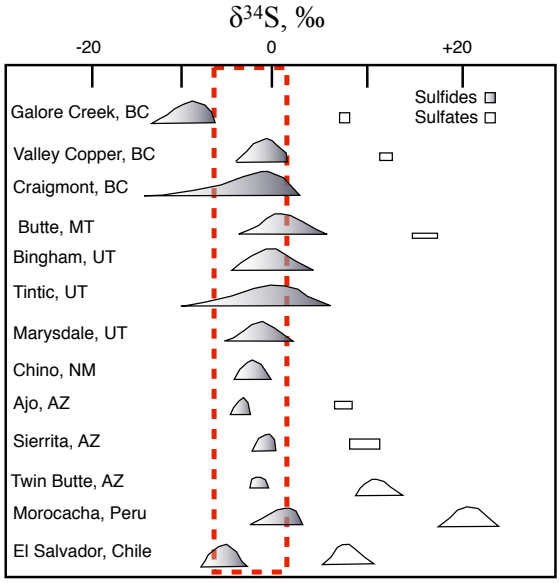

Fig. 53. Schematic plot of some typical copper porphyry sulfur isotope data with Allard stock data overlayed in red.. Modified from Barnes (1997).

Sulfur isotope fractionation arises from temperature differences, or most importantly, from oxidation and reduction reactions acting on the sulfur species. Other aqueous sulfur species may become important during ore deposition (HSO_4^-, KSO_4^-, $NaSO_4^-$, and HS^-) but the major factors controlling sulfur isotope composition for hydrothermal minerals are (1) temperature, determining interplay of the sulfur-bearing species' fractionations, (2) total $\delta^{34}S$ in the source and (3) amount of oxidized vs. reduced species in the ore forming solutions (Rye and Ohmoto, 1974). Oxygen fugacity and pH also induce variations $\delta^{34}S$ in hydrothermal minerals (Rye and Ohmoto, 1974). Under igneous system conditions, at high temperature, redox reactions tend to occur under equilibrium conditions, whereas disequilibrium conditions are present under low temperature conditions (Seal, 2006).

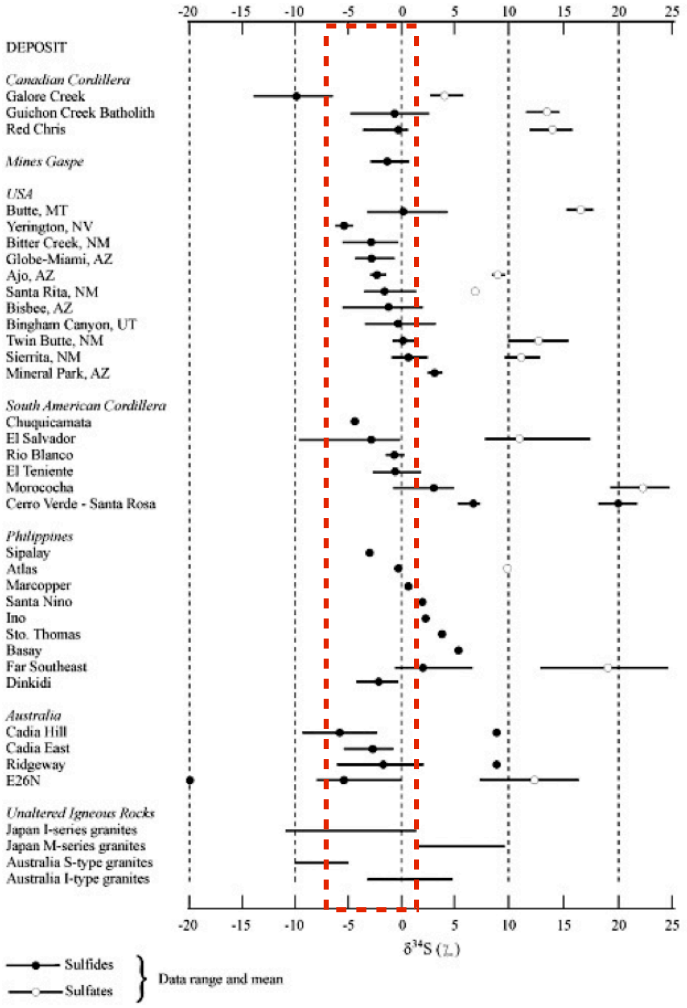

Fig. 54. Plot of porphyry copper (-gold) associated sulfide and sulfate ranges ($\delta^{34}S$ per mil). Some granitic rocks also included. Allard stock data is shown in red. Figure from Wilson et al. (2007).

Wilson et al. (2004) illustrates ranges of $\delta^{34}S_{sulfide}$ values determined for minerals associated with porphyry copper (-gold) deposits and with granitic rocks (Fig. 54). Based on this histogram, mean $\delta^{34}S_{sulfide}$ is -0.96‰, while the range for sulfides associated with porphyry copper deposits is –4.20 to +2.27‰, within one standard deviation of the mean. This generalized range does not take into account the individual ranges of sulfur values for each deposit or the sulfate analyses. Again, sulfide data cluster around 0‰ for the most of the porphyry deposits in the United States, Canadian

Cordillera, South American Cordillera, and the Philippines. Deposits in Australia show enrichment in ^{34}S, as does one Canadian deposit, Galore Creek, which shares similarities with the Allard Stock (Werle et al., 1984; Jensen and Barton, 2000; Wilson et al., 2004). Note that unaltered igneous rocks samples (granites) from Japan and Australia plot between ± 10‰, supporting the idea that ^{34}S for unmineralized rocks of mantle origin can range outside of exactly 0‰ if crustal contamination occurs.

The connection between porphyry and epithermal environments could perhaps be further strengthened by comparing the stable and radiogenic isotopes of both deposit types. In particular, it is especially useful where both environments overlap, such as in the La Plata district. Although not measured as part of this study, sulfur isotope studies on epithermal (Au-Ag-Te) deposits can yield somewhat similar $\delta^{34}S$ values. Takahashi et al. (2005) report the sulfur isotopic range for hydrothermal deposits in Kamchatka, Russia (Fig. 55). Averaged $\delta^{34}S_{CDT}$ values indicate a mostly positive signature of -0.7 to +3.8‰ (av. +1.7‰) for East Kamchatka and –1.8 to +2.0‰ (av. -0.1‰) for Central Kamchatka. Negative values for Central Koryak (av. -2.8‰) are attributed to slight contamination by isotopically light (^{32}S-enriched) sedimentary sulfur from surrounding country rocks. Takahashi et al. (2005) report isotopic data that is consistent with data from neighboring metallogenic belts. It has been suggested that perhaps the addition of an external sulfur source (sedimentary sulfur) is necessary to make economic PGE-Ni-Cu ores (Lesher and Keays, 2002).

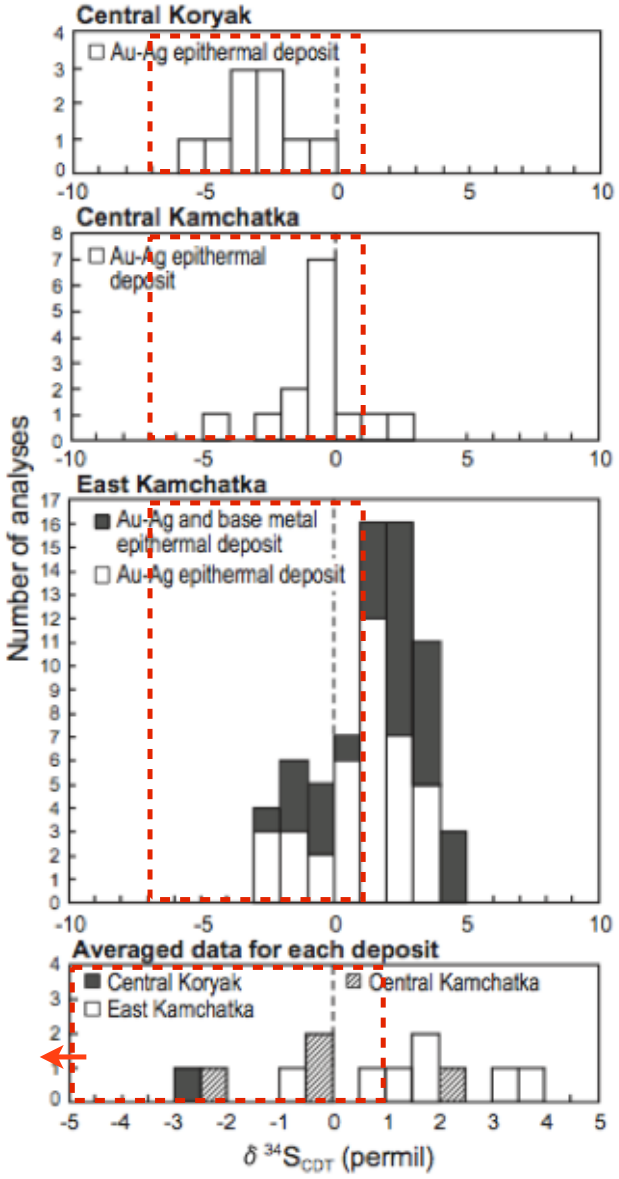

Fig. 55. Histogram of $\delta^{34}S_{CDT}$ values for the Cenozoic ore deposits in metallogenic belts in Kamchatka, Russia (Takahaski et al., 2005). Allard stock data is shown in red.

Data for low sulfidation epithermal systems are somewhat limited, however there are good constraints on high sulfidation epithermal systems (Seal, 2006). Seal (2006) notes that sulfur geochemistry of epithermal deposits can be identified using $\delta^{34}S$ values of

sulfide/sulfate mineral pairs of pyrite, pyrrhotite, chalcopyrite, anhydrite, alunite, barite, and sulfate-bearing apatite (Fig. 56). These epithermal deposits show a wider range of $\delta^{34}S$ compositions compared to typical porphyries, due to the lower temperature conditions needed to form epithermal ores. This is consistent with an inferred genetic relationship to intrusions (and porphyries) and equilibrium conditions are assumed (Seal, 2006).

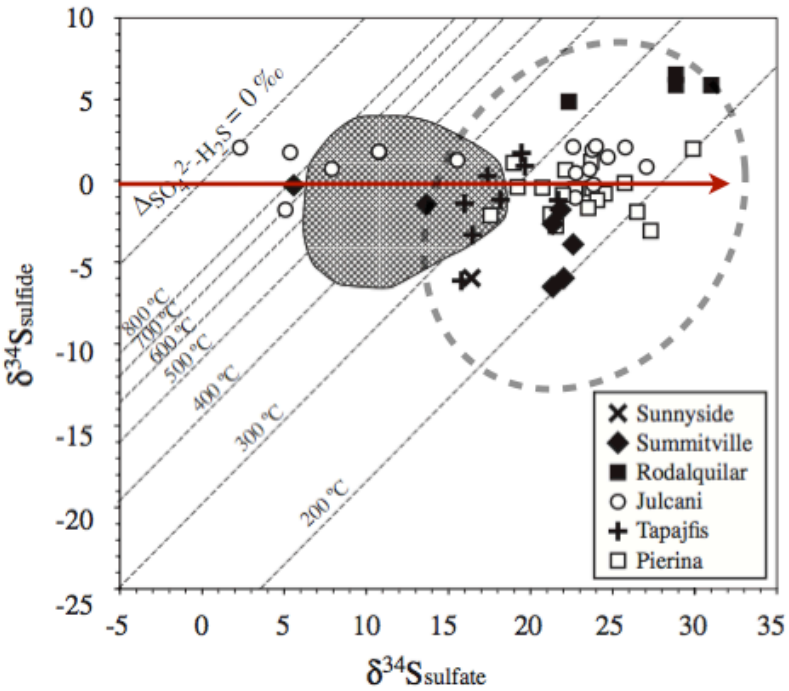

Fig. 56. Plot of $\delta^{34}S$ sulfide vs $\delta^{34}S$ sulfate values for epithermal hydrothermal systems from Seal, 2006. Included are the 0‰ line, indicated by the red arrow, the typical porphyry field, shown by the crosshatched area, and the dashed field for epithermal ores. Values in per mil (VCDT). Note the clustering around 0‰ and the overlap between porphyry and epithermal fields.

Shikazono (1995) plots the $\delta^{34}S$ values of Japanese Ag-Au vein-type epithermal deposits. Green tuff-type deposits occur in a submarine volcanic region, while non-green

tuff-type deposits occur in a subaerial volcanic region (Fig. 57). Both subsets show clustering around 0‰, however there is also evidence for the assimilation of both biogenic sulfate (^{32}S enriched) and seawater sulfate (^{34}S enriched) into the epithermal systems.

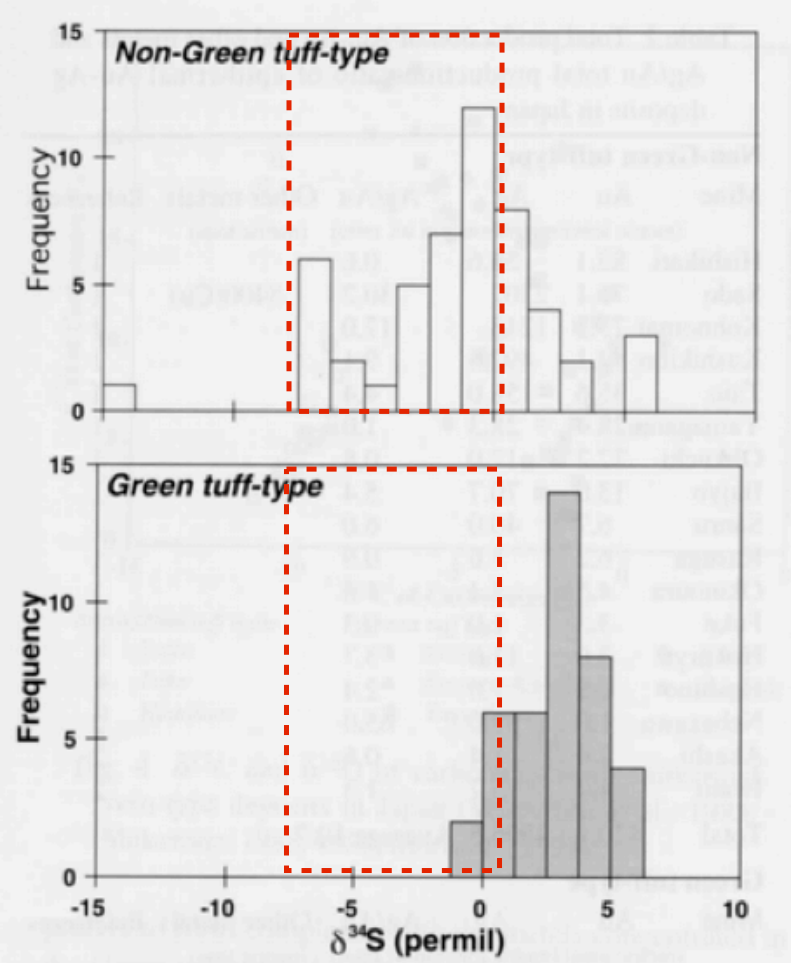

Fig. 57. Histograms of epithermal Ag-Au sulfur data originally obtained from Ishihara et al. (1986), Shikazono (1987), Hedenquist et al. (1994), Shikazono an Shimizu (1993), Ishihara and Sasaki (1994), Shimizu et al. (1995), and Nakata (unpublished). Figure is from Shikazono (1995). Allard stock data shown in red.

The best data available for sulfur isotopes on epithermal ores in the western US come from studies on the Mule Canyon deposit in Nevada. John et al. (2003) discuss the geochemistry, stable isotope, and fluid inclusion results for the Mule Canyon low sulfidation epithermal Au-Ag deposit. Sulfur isotope data for the Mule Canyon deposit (Fig. 58) show a range of $\delta^{34}S$ with a strong trend between 0 and +5‰.

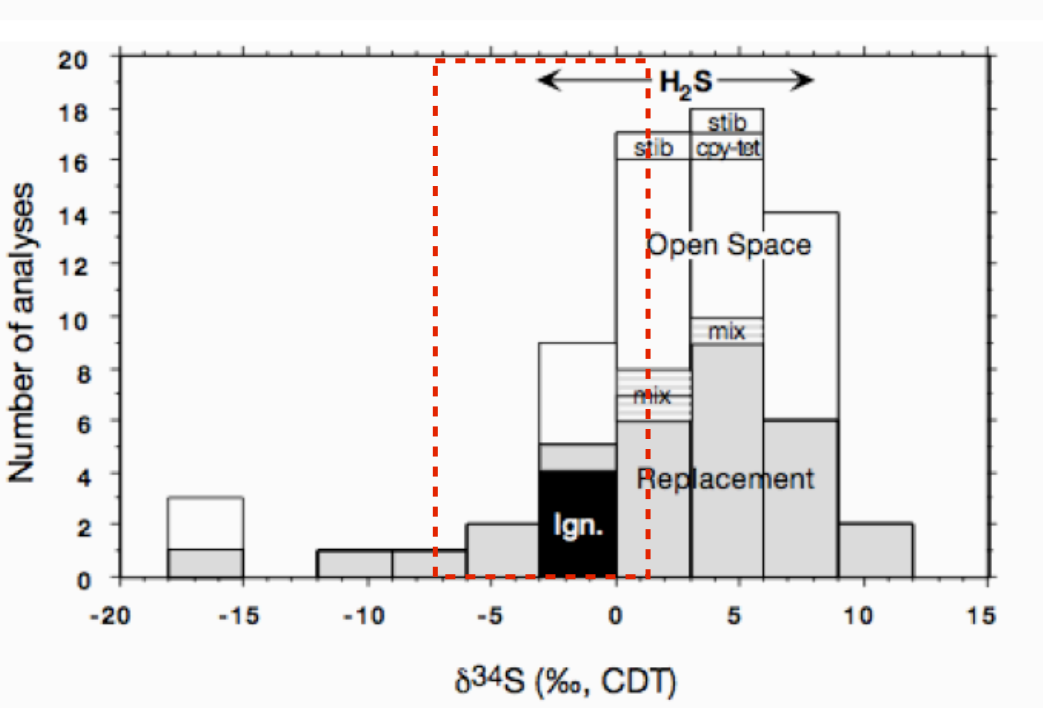

Fig. 58. Histograms showing Mule Canyon sulfur isotope data, primarily on pyrite, marcasite, and arsenopyrite. Allard stock sulfide data is shown in red. White = open-space-filling sulfides, gray = replacement sulfides, pattern – mixtures, and black = igneous pyrrhotite; cpy-tet = chalcopyrite/tetrahedrite mixture, Ign = igneous (melt inclusions), and stib = stibnite. Figure from John et al. (2003).

Sulfide $\delta^{34}S$ ranges for epithermal Au-Ag deposits of the Hauraki Goldfield, New Zealend, fall between -3.1 to +4.9‰ (n=399 analyses) and sulfur is suggested to be of magmatic origin. The $\delta^{34}S$ H_2S in solution was likely similar to the $\delta^{34}S$ of the sulfide

minerals present at Hauraki (Christie and Robinson, 1992; Christie et al., 2007). Averaged ranges for sulfide minerals include chalcopyrite (2.0 ± 0.8 per mil), sphalerite (2.0 ± 1.1 per mil), pyrite (2.1 ± 1.5 per mil) and galena (0.3 ± 1.0 per mil) (Christie et al., 2007).

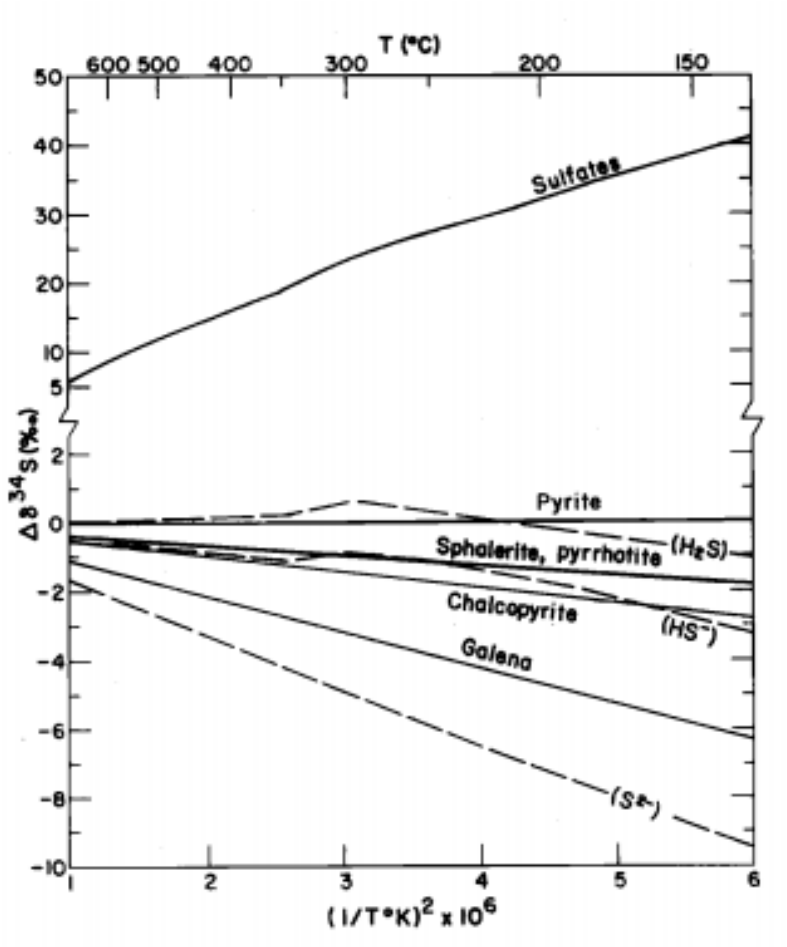

Fig. 59. Plot of ulfur isotope fractionations, considering sulfur species species and hydrothermal minerals, all plotted with respect to pyrite. Solid lines indicate minerals and dashed lines indicate species in solution (Rye and Ohmoto, 1974).

Ohmoto and Rye (1974) compiled sulfur isotope fractionation curves (Fig. 59) to model how sulfur species fractionate in minerals and waters with change in temperature. Fractionation in the high temperature porphyry environment (<700°C to <250°C) remains relatively negligible for pyrite, chalcopyrite, sphalerite and pyrrhotite. Due to this lack of considerable fractionation in $\delta^{34}S$ between the aqueous species and the mineral, pyrite and chalcopyrite are suitable mineral species for accurate $\delta^{34}S$ analyses and the result is more or less the same as the source sulfur reservoir. If temperature is known (via fluid inclusion studies) the curves (Fig. 52) can be used to determine the $\delta^{34}S$ fluid composition from the $\delta^{34}S$ mineral composition. Both porphyry and epithermal ore deposits may show sulfide signatures indicative of magmatic origins, as evidenced above.

Allard Stock Copper Isotopes in Relation to Other Porphyry Copper Deposits

Copper isotope geochemistry can be useful in constraining the source(s) of metals in hydrothermal ore deposits, however the interpretation of Cu isotope data in relation to metals in ore deposits is still being developed. Studies using copper isotopes to better understand high and low temperature aqueous processes have recently been published in the literature (Kimball et al. 2009; Mathur et al. 2005, 2009, 2010; Mathur and Schiltt 2010; Asael et al., 2007, 2009; Haest et al., 2009, Larson et al., 2003; Maher and Larson 2007; Rouxel et al., 2004; Li et al., 2010, Palacios et al., 2001). Li et al. (2010) compiled copper isotope data from several types rocks, sediments, and ore deposits including skarns, prophyries, and massive sulfides (Fig. 60).

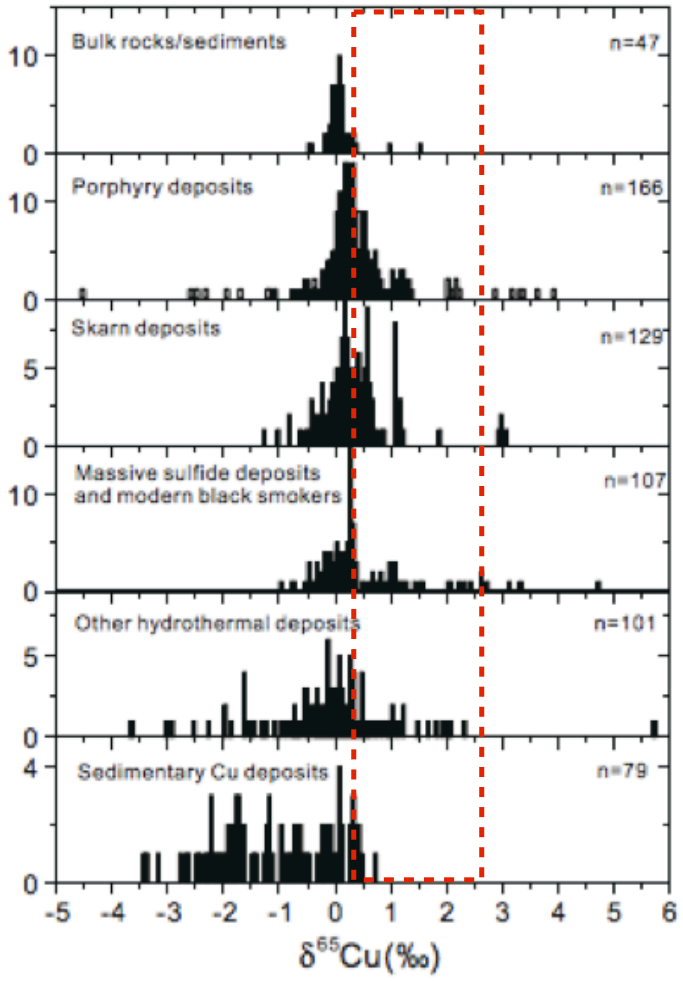

Fig. 60. Histograms showing a compilation of δ^{65}Cu isotope data from a variety of sources (Li et al. 2010). Original data sources listed in Li et al. (2010). Unfilled bars represent oxidized ores in porphyry deposits reported by Mathur et al. (2009), however some extreme values from this study are not plotted due to scale restrictions. Allard stock Cu data is shown in red.

Based on the above histogram, δ^{65}Cu data for porphyries, skarns, massive sulfides, and other hydrothermal deposits tends to cluster around 0‰, with a general range of ± 3 ‰ (Fig. 60). Oxidized copper in solution appears to be isotopically heavier than the mineral it is derived from via low temperature reactions inducing the dissolution of copper-bearing sulfides, namely chalcopyrite and chalcocite (Mathur et al., 2005; Seo et al.,

2007; Borrok et al., 2008; Pokrovsky et al., 2008; Kimball et al., 2009; Mathur et al., 2009). Oxidation of Cu-rich minerals should therefore produce isotopically lighter signatures. Supergene zones are isotopically heavier, and leached zones are isotopically lighter than the hypogene zone in a given porphyry system (Fig. 61). Copper minerals precipitated by high temperature fluids show much lower fractionation than copper minerals precipitated by low temperature fluids (Mathur et al., 2012). The δ^{65}Cu pattern observed by Mathur et al. (2012) is that the δ^{65}Cu values of the leach cap minerals > hypogene minerals > enrichment minerals.

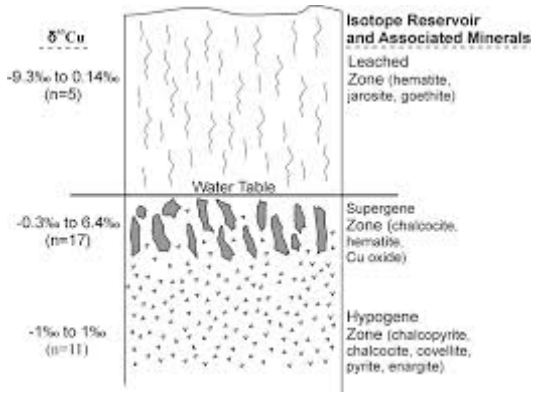

Fig. 61. Generalized profile of the typical porphyry copper stratigraphy, mineralogy, and δ^{65}Cu of leached, hypogene, and supergene reservoirs in a typical porphyry deposit. Figure from Mirnejad et al. (2010) with data from Mathur et al. (2009).

This pattern most likely reflects the continued weathering processes due to uplift processes where shallower portions are exposed to greater degrees of weathering whereas the deeper portions of the porphyry system are not exposed so such a great degree of oxidative weathering. The dissolution of Cu-rich minerals leaves depleted δ^{65}Cu residues (Fig. 62), and as the shallower part of the system weathers, the isotopic

composition of the residue will also become progressively depleted (Mathur et al., 2012).

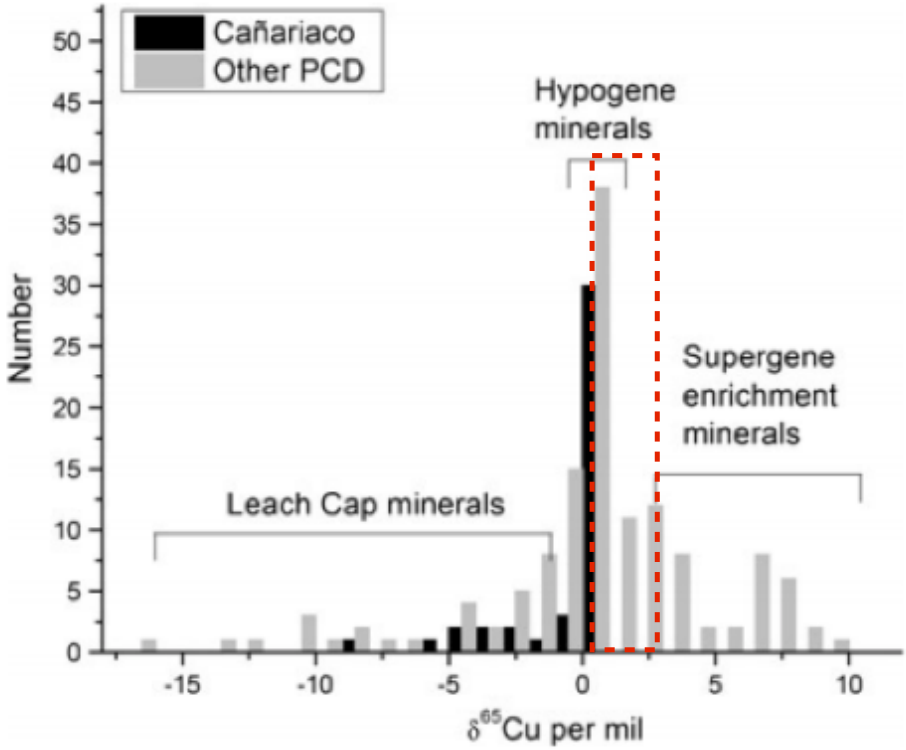

Fig. 62. Histogram of porphyry copper minerals δ^{65}Cu composition. Histogram from Mathur et al. (2012). Data taken from Mathur et al. (2005, 2010) and Zhu et al. (2000). Allard stock data is shown in red.

Mathur et al. (2012) state, "Copper migration and sequestration can be controlled by climate, pyrite/chalcopyrite ratio (ability to create sulfuric acid), fracture abundance (secondary permeability), metallic surfaces for copper to precipitate on, uplift, erosion, preservation, solubility/precipitation of minerals, and preservation of enrichment blankets."

Cu isotope fractionation in high temperature hydrothermal systems may be the result of variation in δ^{65}Cu compositions in source materials, or Cu fractionation during

the ore-forming process (mobilization, transport, and deposition), or both (Li et al., 2010). Copper preferentially partitions into the vapor phase rather than into brine (Heinrich et al., 1999; Williams-Jones and Heinrich, 2005). Simon et al. (2006) reported that this partitioning is promoted by low sulfur. Li et al. (2010) plot $\delta^{65}Cu$ against $\delta^{34}S$ for sample pairs from the Northparkes porphyry deposit (Australia), however no systematic correlation is evident (Fig. 73). They ascribe this to the differing chemical behavior of Cu and S in porphyry systems, where SO_2 and H_2S exhibit a strong equilibrium isotopic fractionation. Copper fractionates between two species only in oxidized, low-temperature hydrothermal settings, and only one main species occurs at high temperatures (Li et al. 2010). Rouxel et al. (2004) found similar results concerning the relationship between copper and sulfur isotopes in hydrothermal environments.

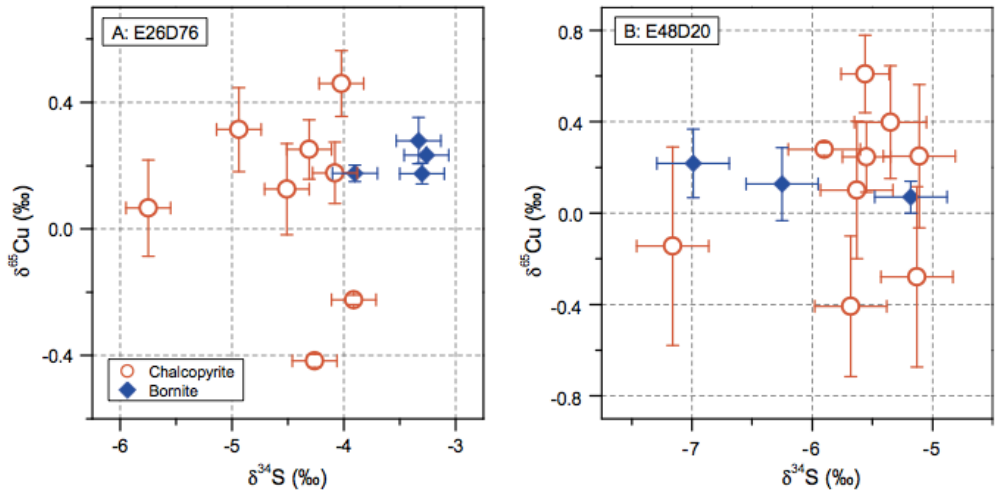

Fig. 63. Plots of $\delta^{65}Cu$ versus $\delta^{34}S$ plot from two ore bodies from Northparkes, Australia (Li et al. 2010). No systematic relationship between Cu and S was determined from their study.

In their study of two porphyry copper deposits, Mount Pinatubo (Phillipines) and Bingham Canyon (Utah, USA), Hattori and Keith (2001) compared major Cu porphyry

deposits' $\delta^{34}S$ values with their respective copper grades (million tonnes, Mt). The prospective range for the Allard Stock is denoted with a red box (Fig. 63). This placement is based on sulfur isotope values obtained by this study and the Allard Stock's estimated resource. The USGS porphyry copper model cites that the Allard Stock has 200 Mt at 0.4% copper and geochemical data from this study shows that the Allard Stock has <1% copper. Both tonnages are considered for the figure below in order to place the Allard Stock in perspective relative to other porphyry copper deposits.

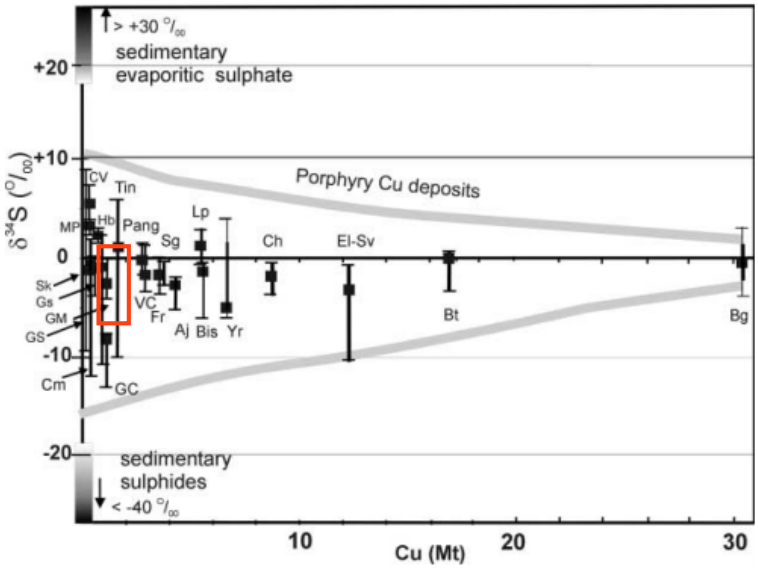

Fig. 64. Plot of $\delta^{34}S$ of sulfide minerals versus copper grade (million metric tonnes) of porphyry copper deposits (Hattori and Keith, 2001). Deposit abbreviations are as follows: Bg=Bingham, Utah, Bt=Butte, Montana, El-Sv = El Salvador, Chile, Ch=Chino, New Mexico, Yr=Yerrington, Nevada, Bis=Bisbee, Arizona, Lp=Le Panto Far Southeast, Phillipines, Aj=Ajo, Arizona, Sg=Sungun, Iran, Fr=Frieda River in Papua New Guinea, VC=Valley Copper, British Columbia, Pang=Pangua, Papua New Guinea, Tn=Tintic, Utah, GC=Galore Creek, Brittish Columbia, GM=Globe-Miami, Arizona, Cm=Craigmont, British Columbia, GSs, Gaspé Copper, Québec, CV= Cerro Verde-Santa Rosa, Peru, MP=Mineral Park, Arizona, Sk=Skouries, Greece, Hb=Hillsboro, New Mexico, GS=Golden Sunlight, Montana. Solid squares are averages and bars represent sample ranges. Individual deposit data sources listed in Hattori and Keith, (2001).

A $\delta^{34}S$ versus $\delta^{65}Cu$ graph, showing Allard stock samples and samples from Northern Great Basin epithermal ores (NGBs), is presented below. The graph (Fig. 65) shows no direct correlation between sulfur and copper isotope values, however both copper and sulfur values for porphyry and epithermal samples plot in or very near a "magmatic source" field. This further adds to supporting evidence that both copper and sulfur show a significant mantle signature, and that both metals and sulfur in hydrothermal fluids are derived from the mantle.

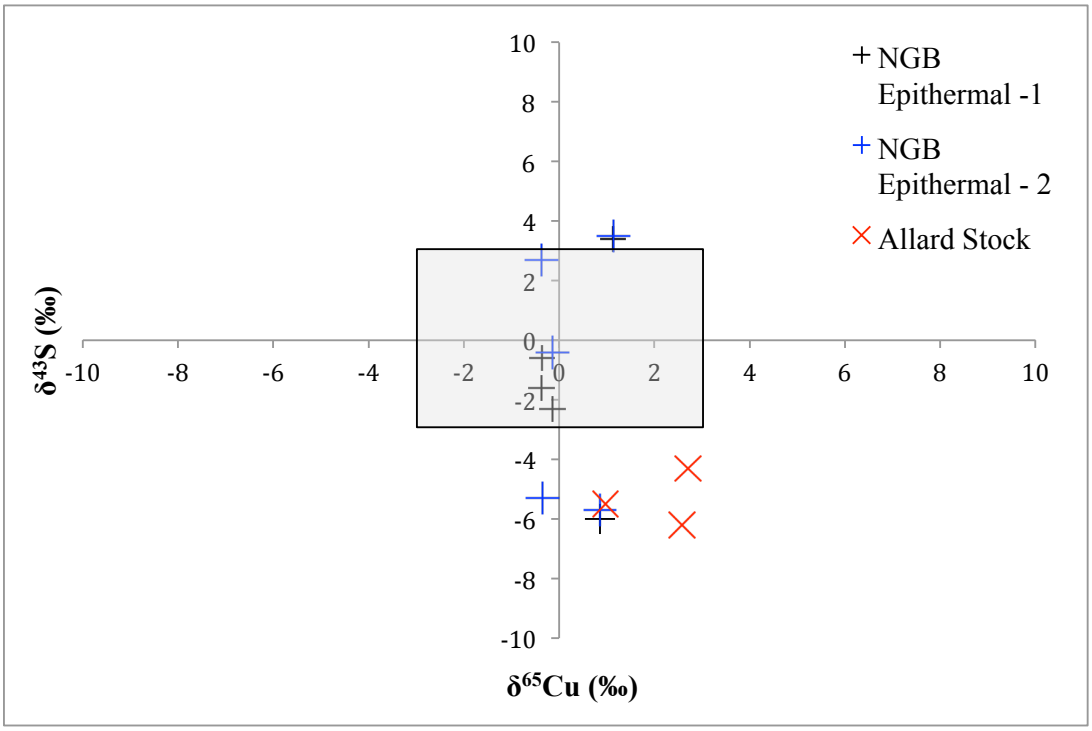

Fig. 65 Plot of $\delta^{34}S$ and $\delta^{65}Cu$ values for samples from the Allard stock porphyry along with epithermal samples from the Northern Great Basin (NGB). Samples were analyzed for sulfur isotopes at either a commercial lab (NGB-1) or at UGA's Stable Isotope Lab (NGB-2), and splits of the same samples were analyzed for copper isotopes. NGB ores include Buckskin National, NV; Midas, NV, Dewey, Trade Dollar, Idaho Tunnel, ID. Gray field indicates the range for a completely mantle sourced Cu and S magmatic signature. NGB epitheram samples are from MS thesis research by Michael Mason, Auburn University, unpublished.

Sources of Pb in the La Plata District Ores

Lead isotopes can be used as radiogenic tracers for sources of lead in both porphyry and epithermal deposits (and other Pb-bearing deposits). U, Th, and Pb strongly partition into the upper and lower portions of the crust (Zartman and Haines, 1988), and radiogenic lead isotopes ^{206}Pb, ^{207}Pb, ^{208}Pb arise from complex decay chains that begin at ^{238}U, ^{235}U, and ^{232}U, respectively. Half-lives vary but all are isotopes are reported relative to ^{204}Pb, the only non-radiogenic stable lead isotope. Doe and Zartman (1979) and Zartman and Doe (1981) originally provided the plumbotectonic model for variations in average lead isotopic compositions within different tectonic environments. This model, revised in Zartman and Haines (1988), hinges on the idea that U, Th, and Pb are extremely sensitive to bidirectional transport among reservoirs, due to the abundance of these elements in the crust relative to the mantle.

By analyzing the lead isotope values for ore deposits, the source of lead in the system, whether from the crust, mantle, or sediments, or perhaps mixtures, may be determined. Generally, lead isotope values for the Allard stock show a "primitive" mantle, less radiogenic signature. Data plot within the general area and trend for Kelly and Ludington (2002) show for the Colorado Plateau volcanics, the COMB, and the San Juan Volcanic Field (Fig. 66). Kelly and Ludington (2002) published data on alkaline gold related deposits (particularly Cripple Creek). In their study, lead isotope analyses for samples from an assortment of COMB deposits show a less radiogenic, more mantle like Pb signature. Data from the Allard stock plot along the same trend as the other alkaline Au-Te telluride districts (i.e. Boulder County) in the COMB. However several

samples lie outside of the scale of Kelly and Ludington's (2002) plot, but the trend is maintained. $^{206}Pb/^{204}Pb$ and $^{207}Pb/^{204}Pb$ compositions of all the alkaline rocks (Fig. 66) are consistent with a mantle Pb source (Zartman and Haines, 1988; Kelly and Ludington 2002). Lower crust input into the evolution of rocks in (plotting above the SK reference line) the northern part of the region could have been significant, as evidenced by the $^{208}Pb/^{204}Pb$ (Stein, 1985; Kelley et al., 1988). Post-subduction generated alkaline magmas could have likely assimilated with lower crustal material (Kelley and Ludington, 2002). Allard stock values plot below this line and show less crustal contamination than the rocks in the northern part of the COMB. La Plata district data fall in the general range of the San Juan Volcanics, roughly 56 km NW of the La Plata Mountains (Fig 1).

Relative to the 1.7 Ga reference isochron, all Allard stock lead isotope values appear to be rather unradiogenic and and fall along the general trend line, not above, as would be indicative of extensive crustal contamination of lead (Fig. 67). Plotting along the 1.7 Ga isochron indicates that source rock formation likely occurred during the formation of the Proterozoic Yavaipi Orogenic events. If crustal contamination did play a role in the tectonomagmatic and hydrothermal processes that created the Allard stock, it is minor, relative to magmatic lead input, but could be likely due to the overabundance of lead in crustal rocks. As is the case with the sulfur isotope values of the Allard stock, some crustal or wall rock contamination is evident, but is negligible relative to the overall mantle signature.

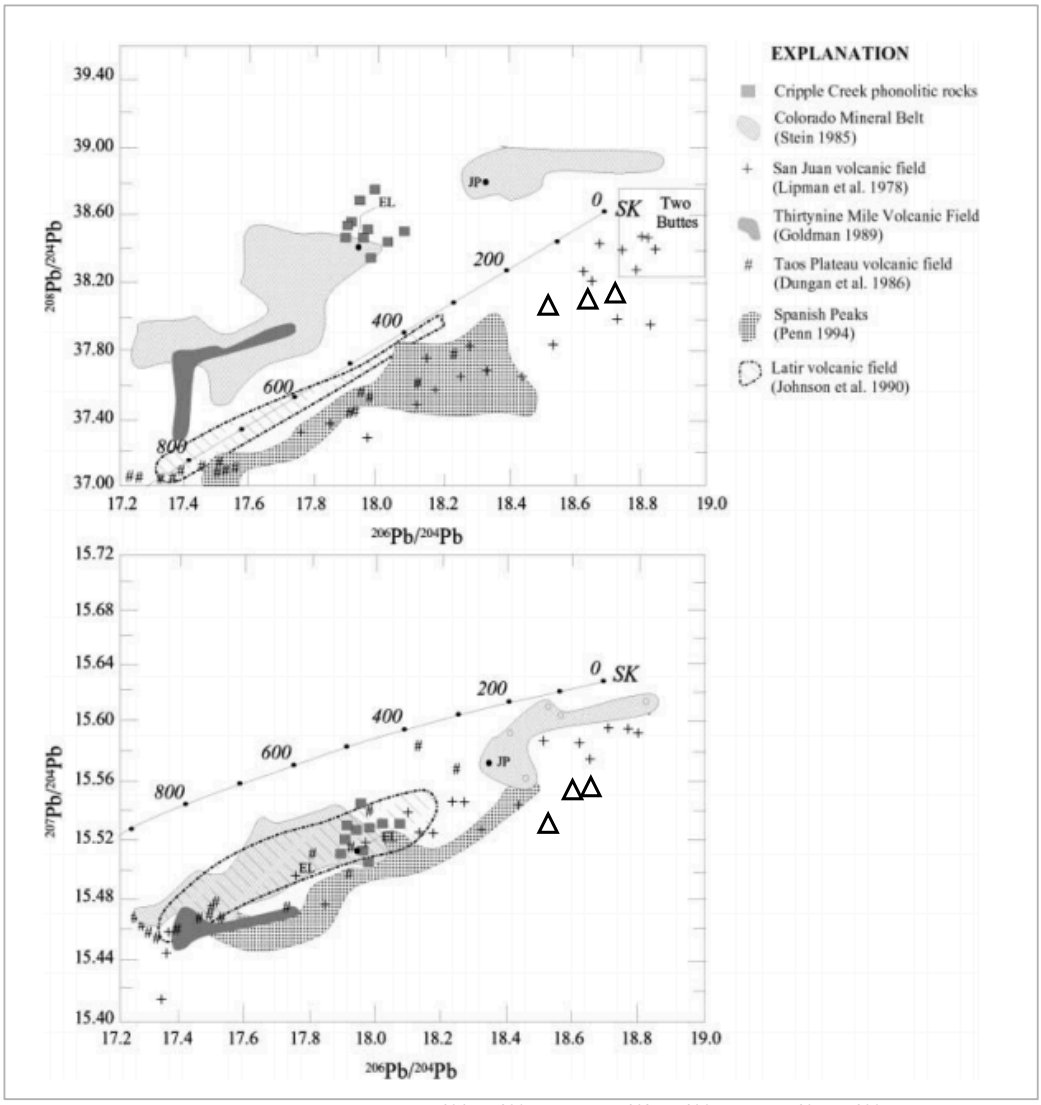

Fig. 66: Plots of lead isotope compositions ($^{206}Pb/^{204}Pb$ versus $^{208}Pb/^{204}Pb$, and $^{207}Pb/^{204}Pb$ versus $^{206}Pb/^{204}Pb$). Allard stock data indicated by the bold triangles. Plot modified from Kelley and Ludington (2002). Closed circles from the COMB are intrusions spatially associated with Au-Te mineralization in the Central City (Eldora Stock) and Boulder County district (Jamestown Porphyry). The SK line corresponds to the Stacey and Kramers (1975) growth curve, where tick marks show time in 100-million year intervals.

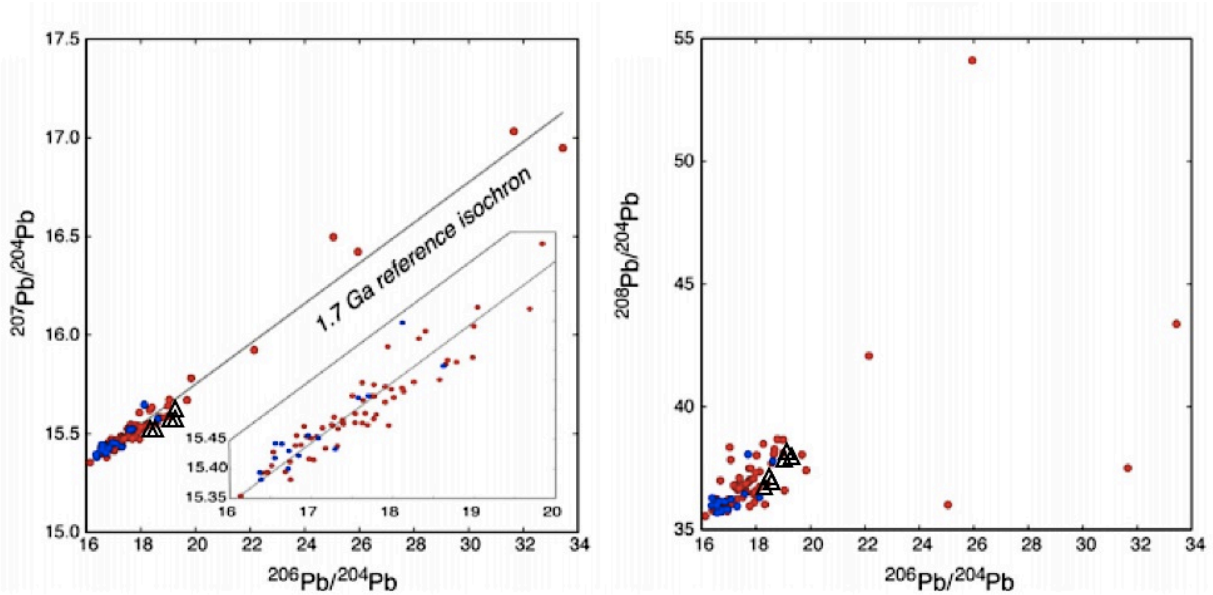

Fig. 67. Lead isotope composition graphs with Allard stock data (black triangles) superimposed on a graph from Bouchet et al (2014). Data plot along the 1.7 Ga reference isochron and show a relatively unradiogenic signature, likely that of mantle derived lead.

Four epithermal samples (2 from Bessie G and 2 from Cumberland) were analyzed for lead isotopes for comparison to the Allard stock porphyry Pb isotope values. While the porphyry values are less radiogenic, epithermal Pb values are more radiogenic and fall along a trend line relative to the porphyry samples (Fig. 68). Two scenarios are possible to explain this trend line for the La Plata district Pb isotopes. (1) The 1740±170 Ma calculated trend line is a real age for the Pb in the ores, meaning that the hydrothermal fluids that precipitated the mineralization in the La Plata district originally gathered the Pb from 1.7 By old basement rocks and recorded the basement Pb signature in the ores. (2) The "age" given is a coincidence and the trend line is simply a mixing line between an unradiogenic mantle Pb source (lower Pb ratios) and a more radiogenic crustal Pb source (higher Pb ratios). Both instances are plausible explanations for the lead isotope signature of the La Plata district.

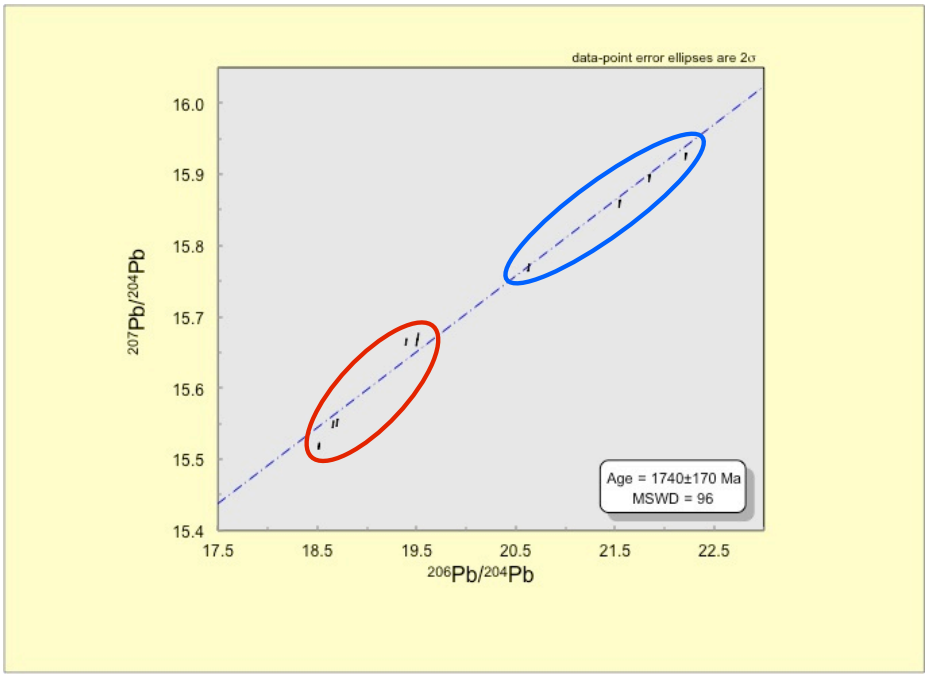

Fig. 68. Plot of lead isotope data for the La Plata district. Allard stock samples circled in red and epithermal samples circled in blue. Note slope difference and trend line.

5. Conclusions

1). Geochemical data from this study support a genetic link between porphyry and epithermal deposits in the La Plata mining district and between the hydrothermal fluids that deposited them, including Ag ± Au ± Cu ± Te ± Pt ± Pd.

2). Sulfur isotope data from this study yield a range of δ^{34}_{SVCDT} between -7.0 to +1.0‰, indicating a primarily magmatic source mixed with of ^{32}S enriched sulfur, likely from sediments the Allard stock intruded.

3). Copper isotope analyses also indicate a magmatic source of copper for the porphyry copper mineralization at the Allard stock. $\delta^{65}Cu$ values range from 0.956 to 2.7‰.

4). Samples of mineralization analyzed by two different techniques from the Copper Hill Glory Hole show several high values of > 1 ppm Pt and Pt. Most samples show >1.0% copper, 2.5 to 100 ppm Ag, and 0.1 to 1.4 ppm Au.

5). PGEs have been reported in the Allard stock as early as 1943, however no published analysis of phase occurrence exists. Using microprobe analyses based on selection by geochemical Pt and Pd compositions, Pt and Pd in the Allard stock occur in at least four phases: merenskyite, moncheite, sopcheite, and an unnamed Pd-Te

6). The possible new palladium telluride mineral has a formula of $PdTe_2$.

7). Lead isotope values indicate a mostly mantle Pb source, and Allard data follow the trend of much of the rest of the Colorado Mineral Belt and have the same lead values as the San Juan Volcanic Field.

8). The La Plata district fits the Saunders and Brueske (2012) model for Se, Te enrichment of the Western U.S. due to flat slab subduction. The La Plata district, abundant in Te, plots in the Te-enriched region on their proposed map.

9). General ore paragenesis from earliest to latest is as follows: pyrite, bornite, covellite, sphalerite, magnetite, acanthite, chalcopyrite, and Pt±Pd±Bi-tellurides.

10). High bismuth and tellurium content in both porphyry and epithermal deposits in the La Plata district further indicate a magmatic source for precious metals.

11). Further research in the district is needed to better characterize the geochemical signatures of the porphyry and epithermal ores. More sulfur, copper, and lead isotope analyses would help to verify the results of this study and make the Pb isotope interpretations for the area less ambiguous. More detailed microprobe analysis would ensure that all occurring PGE minerals are identified. A more detailed mapping of the Allard stock and any associated faulting could help to determine the presence or absence of other Cu-PGE rich mineralized areas.

6. REFERENCES

Anders, E., and Grevesse, N., 1989, Abundances of the elements: meteoritic and solar: Geochimica et Cosmochimica Acta, v. 53, p. 197–214.

Armstrong JT, 1988, Quantitative analysis of silicate and oxide materials: comparison of Monte Carlo, ZAF, procedures, in Newbury DE, ed., Microbeam Analysis p. 239-246

Arndt, N.T. Lesher, C.M., Czamanske, G.K., 2005, Mantle-derived magmas and magmatic Ni-Cu-(PGE) deposits: Economic Geology 100th Anniversary Volume, p. 5–24

Asael, D., Matthews, A., Bar-Matthews, M., and Halicz, L. 2007, Copper isotope fractionation in sedimentary copper mineralization (Timna Valley, Israel): Chemical Geology, v. 243, p. 238-254.

Asael, D., Matthews, A., Oszczepalski, S., Bar-Matthews, M., and Halicz, L. 2009, Fluid speciation controls of low temperature copper isotope fractionation applied to the Kupferschiefer and Timna ore deposits: Chemical Geology, v. 262, p. 147- 158.

Augé, T., Genna, A., Legendre, O., Ivanov, K.S., and Volchenko, Y.A., 2005, Primary platinum mineralization in the Nizhny Tagil and Kachkanar Ultramafic Complexes, Urals, Russia: A genetic model for PGE concentration in chromite-rich zones: Economic Geology, v. 100, p. 707-732.

Barnes, H. L. (Ed.). 1997, Geochemistry of hydrothermal ore deposits (2nd ed.). John Wiley & Sons.

Barnes, S.J. And Lightfoot, P.J., 2005, Formation of magmatic nickel sulfide deposits and processes affecting their copper and platinum group element contents: Economic Geology 100th Anniversary Volume, p. 179-213

Barr, D.A., Fox, P.E., Northcote, K.E. and Preto, V.A., 1976, The alkaline suite porphyry deposits: a summary; *in* Sutherland Brown, A., ed., Porphyry Deposits of the Canadian Cordillera, Canadian Institute of Mining and Metallurgy, Special Volume 15, p. 359-367.

Bethke, P.M., Rye, R.O., Stoffregen, R.E., and Vikre, P.G., 2005, Evolution of the magmatic-hydrothermal acid-sulfate system at Summitville, Colorado: Integration of geological, stable isotope, and fluid inclusion evidence: Chemical Geology, v. 215, p. 281-315.

Bonham, H.F. Jr., 1988, Models for volcanic-hosted precious metal deposits, *in* R.W., Cooper, J.J., and Vikre, P.G., eds., A review in Schafer, Bulk mineable precious metal deposits of the western United States, Reno: Geological Society of Nevada, p.259-271

Borrok, D. M., Nimick, D. A., Wanty, R. B., & Ridley, W. I., 2008, Isotopic variations of dissolved copper and zinc in stream waters affected by historical mining: Geochimica et Cosmochimica Acta, v.72, p. 329-344.

Bouchet, R. A., Blichert-Toft, J., Reid, M. R., Levander, A., & Albarède, F., 2014, Similarities between the Th/U map of the western US crystalline basement and the seismic properties of the underlying lithosphere: Earth and Planetary Science Letters, v. 391, p. 243-254.

Cabri, L. J., 2002, The platinum group minerals: Canadian Institure of Mining, Metallurgy and Petroleum Special Volume 54, p. 12-129

Cawthorn, R.G., Barnes, S.J., Ballhaus, C., Maltich, K.N., 2005, Platinum group elements, chromium, and vanadium deposits in mafic and ultramafic rocks: Economic Geology 100th Anniversary Volume, p. 215-249.

Christie, A. B., & Robinson, B. W., 1992, Regional sulphur isotope studies of epithermal Au–Ag–Pb–Zn–Cu deposits in the Hauraki Goldfield, South Auckland: New Zealand Journal of Geology and Geophysics, v. 35, p.145-150.

Christie, A. B., Simpson, M. P., Brathwaite, R. L., Mauk, J. L., and Simmons, S. F., 2007, Epithermal Au-Ag and related deposits of the Hauraki goldfield, Coromandel volcanic zone, New Zealand. Economic Geology, v.102, p. 785-816.

Crossey, L. J., Karlstrom, K. E., Springer, A. E., Newell, D., Hilton, D. R., and Fischer, T., 2009, Degassing of mantle-derived CO2 and He from springs in the southern Colorado Plateau region—Neotectonic connections and implications for groundwater systems: Geological Society of America Bulletin, v. 121, p. 1034-1053.

Eckel, E.B., 1949, Geology and ore deposits of the La Plata District, Colorado: USGS Professional Paper 219.

Eliopoulos, D.G., and Economou-Eliopoulos, M., 1991, Platinum-group element and gold contents in the Skouries porphyry copper deposit, Chalkidiki Peninsula, northern Greece: Economic Geology, v. 86, p. 740-749

Economou-Eliopoulos, M., 2005, Platinum Group element potential of porphyry copper deposits, *in* Mungall, J.E. ed., Exploration for deposits of Platinum Group Elements: Minearlogical Association of Canada, Short Course Notes 35, Chapter 10, p. 203-246.

English, J.M., Johnston, S.T., and Wang, K., 2003, Thermal modeling of the Laramide Orogeny: Testing the flat-slab subduction hypothesis: Earth and Planetary Science Letters, v. 214, p. 619-632

Gammons, C. H., and Williams-Jones, A. E., 1997, Chemical mobility of gold in the porphyry-epithermal environment: Economic Geology, v. 92, p. 45-59.

Gammons, C.H., and Bloom, M.S., 1993, Experimental investigation of the hydrothermal geochemistry of platinum and palladium: II. The solubility of PtS and PdS in aqueous sulfide solutions to 300°C: Geochimica et Cosmochimica Acta, v. 57, p. 2451-2467

Goncalves, Aaron, 2010, Metallogenesis of platinum-group elements in copper deposits of the Allard stock, La Plata County, Colorado, Unpublished B.S. thesis, Fort Lewis College, CO, 19 pgs.

Haest, M., Muchez, P., Petit, J. C., & Vanhaecke, F., 2009, Cu isotope ratio variations in the Dikulushi Cu-Ag deposit, DRC: of primary origin or induced by supergene reworking?: Economic Geology, v. 104, p. 1055-1064.

Hattori, K. H., & Keith, J. D., 2001, Contribution of mafic melt to porphyry copper mineralization: evidence from Mount Pinatubo, Philippines, and Bingham Canyon, Utah, USA. Mineralium Deposita, v.36, p. 799-806.

Hedenquist J.W., Lowenstern J.B., 1994, The role of magmas in the formation of hydrothermal ore deposits: Nature, v. 370, p. 519–527

Hedenquist, J. W., & Gulson, B. L., 1992, Intrusive and basement rock sources of lead in hydrothermal systems of the Taupo Volcanic Zone, New Zealand: Geochimica et Cosmochimica Acta, v. 56, p. 2821-2829.

Hedenquist, J.W., Arribas, A Jr, and Reynolds, T.J., 1998, Evolution of an intrusion-centered hydrothermal system: Far Southeast-Lepanto porphyry and epithermal Cu-Mo deposit, Phillipines: Economic Geology, v.93, p.372-404

Heinrich, C. A., Günther, D., Audétat, A., Ulrich, T., & Frischknecht, R., 1999, Metal fractionation between magmatic brine and vapor, determined by microanalysis of fluid inclusions: Geology, v.27, p. 755-758.

Heinrich, C.A., 2005, The physical and chemical evolution of low-salinity magmatic fluids at the porphry to epithermal transition; a thermodynamic study: Mineralium Deposita, v. 39, p. 864-889.

Heinrich, C.A., Driesner, T., Stefansson, A., Seward, T.M., 2004, Magmatic vapor contraction and the transport of gold from the porphyry environment to epithermal ore deposits: Geology, v. 32, p. 761-76

Henley, R. W., and McNabb, A., 1978, Magmatic vapor plumes and ground-water interaction in porphyry copper emplacement; Economic Geology, v.73, p. 1-20.

Humphreys, E., Hessler, E., Dueker, K., Farmer, G. L., Erslev, E., and Atwater, T., 2003, How Laramide-age hydration of North American lithosphere by the Farallon slab controlled subsequent activity in the western United States: International Geology Review, v. 45(7), p. 575-595.

Jensen, E.P., and Barton, M.D., 2000, Gold deposits related to alkaline magmatism: Reviews in Economic Geology, v. 13, p. 279–313

John, D.A. and Taylor, R.D., 2014, Byproducts of porphyry copper and molybdenum deposits, Economic Geology, In press, 66 pgs.

John, D.A., Ayuso, R.A., Barton, M.D., Blakely, R.J., Bodnar, R.J., Dilles, J.H., Gray, Floyd, Graybeal, F.T., Mars, J.C., McPhee, D.K., Seal, R.R., Taylor, R.D., and Vikre, P.G., 2010, Porphyry copper deposit model, chap. B of Mineral deposit models for resource assessment: U.S. Geological Survey Scientific Investigations Report 2010–5070–B, 169 p.

John, D.A., Hofstra, A.H., Fleck, R.J., Brummer, J.E., and Saderholm, E.C., 2003, Geologic setting and genesis of the Mule Canyon low-sulfidation epithermal gold-silver deposit, north-central Nevada: Economic Geology, v. 98, p. 425-464.

Jones, C. H., Farmer, G. L., Sageman, B., and Zhong, S., 2011, Hydrodynamic mechanism for the Laramide orogeny: Geosphere, v. 7, p. 183-201.

Kamenov, G. D., Mueller, P. A., and Perfit, M. R., 2004, Optimization of mixed Pb–Tl solutions for high precision isotopic analyses by MC-ICP-MS: Journal of Analytical Atomic Spectrometry, v. 19, p. 1262-1267.

Kamenov, G.D., Perfit, M.R., Jonasson, I.R., and Mueller, P.A., 2005, High-precision Pb isotope measurements reveal magma recharge as a mechanism for ore deposit formation: Examples from Lihir Island and Conical seamount, Papua New Guinea: Chemical Geology, v. 219, p. 131-148.

Kamenov, G.D., Saunders, J.A., Hames, W.E., Unger, D.L., 2007, Mafic Magmas as Sources for Gold in Middle Miocene Epithermal Deposits of the Northern Great Basin, United States: Evidence from Pb Isotope Compositions of Native Gold: Economic Geology, v. 102, p. 1191-1195

Kelley, K. D., Romberger, S. B., Beaty, D. W., Pontius, J. A., Snee, L. W., Stein, H. J., and Thompson, T. B., 1998, Geochemical and geochronological constraints on the genesis of Au-Te deposits at Cripple Creek, Colorado: Economic Geology, v. 93, p. 981-1012.

Kelley, K.D., and Ludington, S., 2002, Cripple Creek and other alkaline-related gold deposits of the southern Rocky Mountains, USA: influence of regional tectonics: Mineralium Deposita, v. 37, p. 38-60.

Kimball, B. E., Mathur, R., Dohnalkova, A. C., Wall, A. J., Runkel, R. L., and Brantley, S. L., 2009, Copper isotope fractionation in acid mine drainage: Geochimica et Cosmochimica Acta, v. 73, p. 1247-1263.

Larson, P. B., Maher, K., Ramos, F. C., Chang, Z., Gaspar, M., and Meinert, L. D., 2003, Copper isotope ratios in magmatic and hydrothermal ore-forming environments: Chemical Geology, v. 201, p. 337-350.

LeFort, D., Jacob Hanley, J., and Guillong, M., 2011, Subepithermal Au-Pd mineralization associated with an alkalic Porphyry Cu-Au Deposit, Mount Milligan, Quesnel Terrane, British Columbia, Canada: Economic Geology, v. 106, p. 781-808.

Lesher, C.M., and Keays, R.R., 2002, Komatiite-associated Ni-Cu-(PGE) deposits: mineralogy, geochemistry, and genesis, in L.J. Cabri (Ed.), The Geology, Geochemistry, Mineralogy, and Mineral Beneficiation of the Platinum-Group Elements, Canadian Institute of Mining, Metallurgy and Petroleum, Special Volume 54, p. 579-617

Li, X. H., Li, W. X., Wang, X. C., Li, Q. L., Liu, Y., Tang, G. Q., and Wu, F. Y., 2010, SIMS U–Pb zircon geochronology of porphyry Cu–Au–(Mo) deposits in the Yangtze River Metallogenic Belt, eastern China: magmatic response to early Cretaceous lithospheric extension: Lithos, v. 119, p. 427-438.

Lonsdale, J.T., 1921, The geology and ore deposits of Bedrock Gulch, La Plata County, Colorado. Unpub MS thesis from the University of Iowa.

Maher, K. C., & Larson, P. B., 2007, Variation in copper isotope ratios and controls on fractionation in hypogene skarn mineralization at Coroccohuayco and Tintaya, Peru: Economic Geology, v. 102, p. 225-237.

Marini, L., Moretti, R., and Accornero, M., 2011, Sulfur isotopes in magmatic-hydrothermal systems, melts, and magmas: Reviews in Mineralogy and Geochemistry, v. 73, p.423-492.

Mason, M.S., 2014, Ore petrology and geochemistry of epithermal gold-silver veins on Florida Mountain, Silver City District, Idaho, Unpub MS thesis, in progress, Auburn University.

Mathur, R., & Schlitt, W. J., 2010, Identification of the dominant Cu ore minerals providing soluble copper at Cañariaco, Peru through Cu isotope analyses of batch leach experiments: Hydrometallurgy, v.101, p. 15-19.

Mathur, R., Dendas, M., Titley, S., and Phillips, A., 2010, Patterns in the copper isotope composition of minerals in porphyry copper deposits in southwestern United States: Economic Geology, v. 105, p. 1457-1467

Mathur, R., Jin, L., Prush, V., Paul, J., Ebersole, C., Fornadel, A., and Brantley, S., 2012, Cu isotopes and concentrations during weathering of black shale of the Marcellus Formation, Huntingdon County, Pennsylvania (USA): Chemical Geology, v. 304, p. 175-184.

Mathur, R., Ruiz, J., Titley, S., Liermann, L., Buss, H., & Brantley, S., 2005, Cu isotopic fractionation in the supergene environment with and without bacteria: Geochimica et Cosmochimica Acta, v. 69, p, 5233-5246.

Mathur, R., Titley, S., Barra, F., Brantley, S., Wilson, M., Phillips, A., and Hart, G. , 2009, Exploration potential of Cu isotope fractionation in porphyry copper deposits: Journal of Geochemical Exploration, v. 102, p. 1-6.

Mathur, R., Titley, S., Ruiz, J., Gibbins, S., and Friehauf, K., 2005, A Re–Os isotope study of sedimentary rocks and copper–gold ores from the Ertsberg District, West Papua, Indonesia: Ore Geology Reviews, v. 26, p. 207-226.

Meinert, L. D., 1992, Skarns and skarn deposits: Geoscience Canada, v. 19, p. 145-162

Mertie, J.B. Jr., 1969, Economic geology of the platinum metals: USGS Professional Paper 630, p. 97-99

Mirnejad, H., Mathur, R., Einali, M., Dendas, M., & Alirezaei, S., 2010, A comparative copper isotope study of porphyry copper deposits in Iran: Geochemistry Exploration, Environment, Analysis, v. 10, p. 413-418.

Muntean, J. L., and Einaudi, M. T., 2001, Porphyry-epithermal transition: Maricunga belt, northern Chile: Economic Geology, v. 96, p. 743-772.

Mutschler, F. E., and Mooney, T. C., 1993, Precious-metal deposits related to alkalic igneous rocks: provisional classification, grade-tonnage data and exploration frontiers. Mineral deposit modeling: Geological Association of Canada Papers, v. 40, p. 479-520.

Mutschler, F.E., 1997, Laccolithic complexes of southeastern Utah; Time of emplacement and tectonic setting; Recommendations for additional studies: U.S. Geological Survey Bulletin 2158, p. 253-254.

Mutschler, F.E., Larson, E.E., and Ross, M.L., 1997a, Potential for alkaline-igneous rock-related gold deposits in the Colorado Plateau laccolithic centers: U.S. Geological Survey Bulletin 2158, p. 233-252.

Mutschler, F.E., Larson, E.E., and Gaskill, D.L., 1997b, The fate of the Colorado Plateau—A view from the mantle: U.S. Geological Survey Bulletin 2158, p. 203-222.

Naldrett, A.J., 1999, World-class Ni-Cu-PGE deposits: Key factors in their genesis: Mineralium Deposita, v. 34, p. 227-240.

Neubert, J.T., 1992, Mineral Appraisal of San Juan National Forest, Colorado: U.S. Bureau of Mines Mineral Land Assessment. Dolores, Colorado: U.S. Bureau of Mines, MLA 2-92, p. 64-147

Palacios, C.M, Townley, B.C., Lahsen, A.A., Egana AM., 1993, Geological development andmineralization in the Atacama segment of the South American Andes, northern Chile (26°15'–27°25'S): Geologische Rundschau, v.82, p. 652–662

Pašava, J., Oszczepalski, S., & Du, A., 2010, Re–Os age of non-mineralized black shale from the Kupferschiefer, Poland, and implications for metal enrichment: Mineralium Deposita, v. 45(2), p. 189-199.

Pokrovsky, O. S., Viers, J., Emnova, E. E., Kompantseva, E. I., and Freydier, R., 2008, Copper isotope fractionation during its interaction with soil and aquatic microorganisms and metal oxy (hydr) oxides: Possible structural control: Geochimica et Cosmochimica Acta, v. 72, p. 1742-1757.

Richards, J.P., 1995. Alkalic-type epithermal gold deposits: A review. Turbidite - hosted gold deposits of Central Victoria, Australia: their regional setting, mineralisation styles and some genetic constraints. Ore Geology Reviews 13, 131–15, *in* Thompson, J.F.H. ed , Magmas, Fluids and Ore Deposits. Mineralogical Association of Canada, Short Course Series 23, p. 367–400.

Richards, J. P., 2003, Tectono-magmatic precursors for porphyry Cu-(Mo-Au) deposit formation: Economic Geology, v. 98, p. 1515-1533.

Richards, J. P., 2011, Magmatic to hydrothermal metal fluxes in convergent and collided margins: Ore Geology Reviews, v. 40, p. 1-26.

Richards, J.P., 2009, Postsubduction porphyry Cu-Au and epithermal Au deposits: Products of remelting of subduction-modified lithosephere: Geology, v. 37, p. 247-250.

Rouxel, O., Fouquet, Y., and Ludden, J. N., 2004, Copper isotope systematics of the Lucky Strike, Rainbow, and Logatchev sea-floor hydrothermal fields on the Mid-Atlantic Ridge: Economic Geology, v. 99, p. 585-600.

Rye, R. O., and Ohmoto, H., 1974, Sulfur and carbon isotopes and ore genesis: a review: Economic Geology, v. 69, p. 826-842.

Sakai, H., 1968, Isotopic properties of sulfur compounds in hydrothermal processes: Geochemical. Journal, v. 2, p. 29-49.

Saunders, J.A., 1991, Gold deposits of the Boulder County gold district, Colorado: U.S. Geological Survey Bulletin, 1857-I, p. 137-148.

Saunders, J.A., and Brueseke, M.E., 2011, Volatility of Se and Te during subduction-related distillation and the geochemistry of epithermal ores of the western United States: Economic Geology, v. 107, p. 165-172.

Saunders, J.A., and May, E.R., 1986, Bessie G: A high-grade epithermal gold telluride deposit, La Plata County, Colorado, *in* Macdonald, A.J., ed. GOLD '86, An International Symposium on the Geology of Gold: Toronto, 1986, p. 436-444.

Schiowitz, D. S., White, S., and Cary, J., 2008, GIS and Geostatistical Analysis of the La Plata Mining District: ESRI Proceedings Paper 1743, p. 1-25

Schroeter, T.G., Lund C., and Carter, G. 1989, Gold production and reserves in British Columbia: B.C. Ministry of Energy, Mines, and Petroleum Resources, Open File Report 1989-33, 86 pages.

Seal, R. R., 2006, Sulfur isotope geochemistry of sulfide minerals: Reviews in Mineralogy and Geochemistry, v. 61, p. 633-677

Seo, J. H., Guillong, M., and Heinrich, C. A., 2009, The role of sulfur in the formation of magmatic–hydrothermal copper–gold deposits: Earth and Planetary Science Letters, v. 282, p. 323-328.

Seo, J.H., Lee, S.K., Lee, I., 2007, Quantum chemical calculations of equilibrium copper (I) isotope fractionations in ore-forming fluids: Chemical Geology, v. 243, p. 225-237.

Shikazono, N., Utada, M., and Shimizu, M., 1995, Mineralogical and geochemical characteristics of hydrothermal alteration of basalt in the Kuroko mine area, Japan: implications for the evolution of a Back Arc Basin hydrothermal system: Applied Geochemistry, v. 10, p. 621-641.

Sillitoe, R. H., 1983, Enargite-bearing massive sulfide deposits high in porphyry copper systems: Economic Geology, v. 78, p. 348-352.

Silitoe, R.H., 2000, Gold-rich porphyry deposits: descriptive and genetic models and their role in exploration and discovery, SEG Reviews, v.13. p. 315-345.

Silitoe R.H., 2002, Some metallogenic features of gold and copper deposits related to alkaline rocks and consequences for exploration: Mineralium Deposita, v.34, p. 4-13.

Silitoe, R.H., 2005, Supergene oxidized and enriched porphyry copper and related deposits: Economic Geology 100th Anniversary Volume, p.723-768.

Sillitoe, R. H., 2010, Porphyry copper systems: Economic Geology, v. 105, p. 3-41.

Sillitoe, R.H. and Hedenquist, J., 2003, Linkages between volcanotectonic setting, ore-fluid, compositions and epithermal precious metal deposits: SEG Special Publication, v.10, p. 315-345.

Simon, A. C., Pettke, T., Candela, P. A., Piccoli, P. M., and Heinrich, C. A., 2006, Copper partitioning in a melt–vapor–brine–magnetite–pyrrhotite assemblage: Geochimica et Cosmochimica Acta, v. 7, p. 5583-5600.

Stein, H. J., & Hannah, J. L., 1985, Movement and origin of ore fluids in Climax-type systems: Geology, v. 13, p. 469-474.

Suarez, S., Prichard, H.M., Fisher, P.C,, McDonald, I., 2012, Platinum group-minerals in the gossan from the Key West Cu-Ni-Pt sulfide occurrence (Nevada, USA): Spanish Society of Mineralogy Reviews, v. 16, p. 242-243.

Thompson, J.F.H., Lang, J.R., and Stanley, C.R., 2001, Platinum group elements in alkaline porphyry deposits, Brittish Columbia: Exploration and Mining in British Columbia, Mines Branch, Part B. p. 57-64

Tosdale, R.M. and Richards, J.P., 2001, Magmatic and structural controls on the development of porphyry Cu±Mo±Au deposits: Reviews in Economic Geology, v. 14, p. 157-181.

Tweto, O., 1979, The Rio Grande rift system in Colorado, *in* Riecker, R. E., ed., Rio Grande Rift: Tectonics and Magmatism: American Geophysical Union, Washington, p. 33-56.

Tweto, O., 1980, Tectonic history of Colorado, in Kent, H.C. and Porter K., eds., Colorado Geology: Rocky Mountain Association of Geologists, p., 5-9.

Tweto, O., and Sims, P. K., 1963, Precambrian ancestry of the Colorado mineral belt: Geological Society of America Bulletin, v. 74, p. 991-1014.

Wegert, D., and Parker, D. F., 2011, Petrogenesis of the McDermott Formation trachyandesite, San Juan basin, Colorado and New Mexico: Rocky Mountain Geology, v. 46, p. 183-196.

Werle, J.L., Ikramuddin, M., and Mutschler, F.E., 1984, Allard stock, La Plata Mountains, Colorado—an alkaline rock-hosted porphyry copper-precious metal deposit: Canadian Journal of Earth Sciences, v. 21, p. 630-641.

Werle, James L., 1983, Allard Stock, La Plata Mountains, Colorado—An Enigmatic Porphyry Copper-Precious Metals Deposit: Unpublished M.S. thesis, Eastern Washington Univ., 62 p.

Williams-Jones, A. E., and Heinrich, C. A., 2005, 100th Anniversary special paper: vapor transport of metals and the formation of magmatic-hydrothermal ore deposits: Economic Geology, v. 100, p. 1287-1312.

Wilson, A. J., Cooke, D. R., Harper, B. J., & Deyell, C. L., 2007, Sulfur isotopic zonation in the Cadia district, southeastern Australia: exploration significance and implications for the genesis of alkalic porphyry gold–copper deposits: Mineralium Deposita, v. 42, p. 465-487.

Wiser, Edward, 1960, Relation of ore deposition to doming in the North American Cordilliera: Geological Society of America Memoirs, v. 77, p. 1-112.

Wood, S.A., Mountain, B.W., Pan, P., 1992, The aqueous geochemistry of Pt, Pd, Au; recent experimental constraint and a re-evaluation of theoretical predictions: Canadian Mineralogist, v. 30, p. 955-982.

Zartman, R. E., & Doe, B. R., 1981, Plumbotectonics-the model: Tectonophysics, v. 75, p. 135-162.

Zartman, R. E., and Haines, S. M., 1988, The plumbotectonic model for Pb isotopic systematics among major terrestrial reservoirs—a case for bi-directional transport: Geochimica et Cosmochimica Acta, v. 52, p. 1327-1339.

Zhang, X., and Spry, P.G., 1994, Calculated stability of aqueous tellurium species, calaverite, and hessite at elevated temperatures: Economic Geology, v. 89, p. 1152-1166.